Investigating the dark photon dark matter through an oscillating dilaton

BY

Pirzada

A dissertation submitted in partial fulfillment of the

requirements for the degree of

MASTER OF PHILOSOPHY

IN

PHYSICS

Department of Physics

Quaid-i-Azam University, Islamabad, Pakistan

September 6, 2023

Declaration

This is to certify that the research work presented in the thesis, entitled "**Investigating the dark photon dark matter through an oscillating dilaton**" was conducted by Mr. Pirzada under the supervision of Dr. Mansoor ur Rehman and accepted in present form by Department of Physics, Quaid-i-Azam University, Islamabad as satisfying dissertation requirement for the degree of

MASTER OF PHILOSOPHY IN PHYSICS

Supervisor

Dr. Mansoor ur Rehman
Professor

Submitted through

Prof. Dr. Kashif Sabeeh
Chairperson
Department of Physics
Quaid-i-Azam University
Islamabad, Pakistan

Abstract

A novel mechanism is introduced for the generation of ultralight dark photon dark matter in the early stages of the Universe using a dilatonlike scalar field, which is coupled to the kinetic term of the dark photon. In this framework, energy is primarily contained in the dilaton's condensate. As this condensate begins its oscillatory motion during the Universe's early stages, it resonantly produces dark photons. Distinct from axion-dark-photon coupling scenarios that necessitate large coupling coefficients to saturate the dark photon, the dilatonic coupling in our model exhibits a special condition where the dark photon's mass is half of the dilaton's. In this regime, significant dark photon production is achievable even with minimal dilaton oscillations. this model, compatible with cosmic microwave background observations, opens the door to ultralight vector dark matter candidates, potentially having masses as minuscule as 10^{-20} eV.

Acknowledgment

First and foremost, I extend my deepest appreciation to my parents, [**Pir Ahmad waqar**] and [**Parveen Bibi**], for their boundless love, endless sacrifices, and unwavering belief in my abilities. Your unwavering support throughout this academic endeavor has been the cornerstone of my success. Your guidance and wisdom have been a constant source of inspiration, and I am forever grateful for the values you instilled in me.

I would also like to extend my sincere gratitude to my dedicated supervisor, **Dr. Mansoor ur Rehman**. Your guidance, mentorship, and expertise have been indispensable in shaping the trajectory of this research. Your patience, insights, and unwavering commitment to excellence have not only enriched my academic journey but have also fostered personal and professional growth.

To myself, I extend a heartfelt acknowledgment. This journey has been an odyssey of self-discovery, resilience, and self-belief. The trials overcome and the boundaries pushed are a testament to the unwavering dedication and determination that have fueled this endeavor. It is with a sense of pride and fulfillment that I recognize the effort invested in bringing this thesis to fruition.

Last but not least, I want to thank my friends, who have provided unwavering support, laughter, and encouragement throughout this academic journey. Your camaraderie, late-night study sessions, and the moments of relaxation amidst the chaos have made this experience truly memorable. Your friendship has been a source of strength, and I am fortunate to have you by my side.

Contents

List of Figures

Chapter 1

Introduction

The concept of dark matter has presented an enduring enigma within the realm of theoretical physics and cosmology, ever since its deduction from astrophysical evidence. This issue remains unresolved to this day. Comprising nearly 85% of the matter content in the cosmos, the mysterious nature of this entity [1] has stimulated numerous theoretical frameworks, each striving to offer a coherent and verifiable explanation of its characteristics and beginnings.

Throughout history, the prevailing framework for dark matter candidates has been the WIMP (Weakly Interacting Massive Particles) paradigm [2]. The aforementioned candidates were hypothesized to be particles with substantial mass and weak interaction, similar to neutrinos but with a substantially greater mass. Nevertheless, with the increasing focus on terrestrial and astronomical investigations for Weakly Interacting Massive Particles (WIMPs) yielding inconclusive results, it has become evident that a comprehensive analysis of the wider range of potential dark matter viable candidates is necessary.

Ultralight scalar and vector fields have recently emerged as potentially viable candidates for dark matter[3]. The wave-like characteristics shown by these entities at the galactic level can give rise to unique cosmological and astrophysical indications. These indications have the ability to address observational irregularities that cannot be explained by the WIMP paradigm[4]. Researchers have been captivated by dark photons, which are a vectorial counterpart to conventional photons, due to their exquisite simplicity and extensive phenomenology, among the options available for ultralight candidates.

Nevertheless, a perplexing dilemma persists. In order for dark photons to possess the requisite cosmic abundance to function as dark matter, it is vital to have an effective generating

mechanism during the early stages of the Universe. Axions, along with their axion-like counterparts, have conventionally served as precursors for the generation of dark photons [5]. The oscillations present in the early Universe have the potential to act as generators for dark photons. However, recent research has indicated that this scenario requires substantial coupling coefficients between the axion and dark photon, which may conflict with current observational limitations.

In this inquiry, we venture onto an alternative trajectory, drawing inspiration from the domain of string theory and its diverse scalar fields. The primary area of interest lies in the dilaton, which is a scalar field that exhibits universal coupling with all types of matter and radiation. The utilization of a dilaton as an intermediate in the generation of dark photons is a relatively unexplored research direction.

Through the establishment of a theoretical framework that establishes a direct coupling between the dilaton and the kinetic term of the dark photon[6], a multitude of intricate processes inside the early Universe are revealed. One noteworthy finding from our research is the identification of a certain scenario wherein the dark photon's mass is halved compared to the dilaton's . This configuration results in a significant increase in the creation of dark photons, even when the dilaton exhibits minor amplitude oscillations. This particular scenario not only facilitates the production of ultralight vector dark matter, which can potentially have masses as low as 10^{-20} eV, but also accomplishes this feat while effectively addressing the challenges posed by cosmic microwave background restrictions.

The parts that follow will examine the mathematical foundations of this mechanism, analyze its implications for the cosmological development of the Universe, and examine the possible observational indicators that can confirm or question this paradigm. By undertaking this endeavor, our aim is to broaden our comprehension of dark matter and its intricate interactions within the early Universe.

In this thesis, we embark on a comprehensive exploration of the enigmatic realm of dark matter, employing a structured approach to dissect and understand its various facets. The foundational groundwork begins with an introduction that outlines the overarching research question and its significance. We then establish a robust theoretical framework, elucidating the fundamental concepts and equations that underpin our investigation. Within this framework, we delve into the Ultralight Bosonic Dark Matter (UBDM) theory, a pivotal theoretical construct, and lay the groundwork for our subsequent analysis.

The heart of this thesis revolves around the meticulous investigation of dark photon dark matter, a promising yet elusive aspect of the broader dark matter puzzle. We examine the nature and relevance of dark photon dark matter, intertwining it with the concept of an oscillating dilaton. This exploration is conducted through an in-depth analysis, unveiling the results obtained through meticulous methodology, data collection, and computational models. These findings are then synthesized in the conclusion, offering a concise summary of our contributions to the field and proposing avenues for future research. throughout the chapters we have used natural units i.e h , c and G equal to one.

Chapter 2

Theortical framework.

2.1 Background

Numerous discoveries throughout the history of sciencehave already disclosed unknown types of matter, like the moons of Jupiter glimpsed by Galileo along with the neutron discovered by Chadwick. Scientists including Kelvin, Poincaré, Opik, Kapteyn, and Oort made early attempts that laid the foundation for the concept of "dark matter" as we know it today. They sought to determine the proportion of the Milky Way's visible matter mass (stars) to its overall mass [7]. These preliminary calculations demonstrated that stars greatly contributed to the mass in our immediate area.

Zwicky's study [8] of galaxy clusters contributed to our knowledge of dark matter. He found that there appeared to be a sizable amount of "dark matter" that was not generating light on bigger scales, beyond individual galaxies. He concentrated on the Coma cluster, which was made up of about a thousand galaxies and had a radius of R approximately 106 light-years. The virial theorem is used to compute the anticipated velocity dispersion of galaxies, which predicts the distribution of galaxies' velocities inside a cluster.

$$v \approx \sqrt{\frac{GM_{\text{tot}}}{R}}. \tag{2.1}$$

He discovered a sizable mismatch between the predicted and observed velocity dispersion. Despite taking into account the fact that the galaxy cluster contains hot gas.The moons of Jupiter identified by Galileo and the neutron discovered by Chadwick are only two examples of discoveries throughout the history of science that have revealed previously unrecognized forms of matter. They sought to calculate the mass of visible matter (stars) in relation to

the total mass of the Milky Way. These preliminary calculations demonstrated that stars played a considerable role in the mass of our neighborhood.

Galaxy cluster observations by Zwicky led to his contribution to the knowledge of dark matter. Beyond individual galaxies, he observed that there appeared to be a sizable amount of "dark matter" that was not generating light on bigger scales. He concentrated on the Coma cluster, which had roughly 1,000 galaxies in a sphere with a radius of R approximately 106 light-years. The discrepancy persisted after calculating the galaxies' expected velocity dispersion using the virial theorem, which predicts the velocity dispersion of galaxies in a cluster. This suggested the existence of extra invisible mass, which he called "dunkle Materie" or "dark matter."

Galaxies' rotational velocities were investigated depending on how far the galaxy is from its center by astronomers including Vera Rubin and Kent Ford [9]. They discovered that the rotation curves remained flat at greater distances from the center, defying expectations based solely on observable matter. In other words, stars at this distances were moving more quickly than would be expected based on their apparent mass. This difference suggested that there was a significant discrepancy with the observed velocity dispersion. This discrepancy indicated the presence of more mass than what was accounted for by visible matter. Theoretical predictions based solely on visible matter didn't match the observed behavior, which led to the idea of an invisible mass component or dark matter.

2.1.1 Gravitational lensing

Einstein's theory of general relativity predicts phenomena called gravitational lensing, in which the light is bent by large objects. The distribution of mass throughout the universe has been studied using this effect. Dark matter was strongly supported by the Bullet Cluster (1E0657-558) [fig. 1] [10]. The visible matter, which is dominated by hot gas, clashed and heated up during a galaxy cluster merger, but the dark matter scarcely interacted because of its weak interaction. Studies using gravitational lensing revealed that the Bullet Cluster's mass distribution did not match that of visible matter, supporting the idea that dark matter exists as a separate substance in the universe.

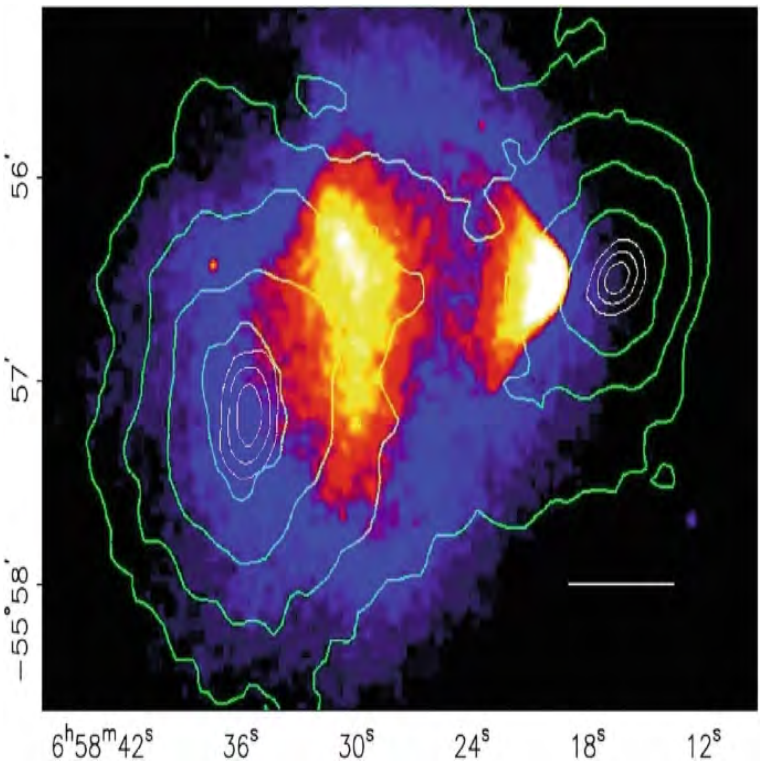

Figure 2.1: Image of the Bullet Cluster (1E0657-558), adapted from Ref. [11], comparing x-ray emission from hot gas [the bakground color map with increasing x-ray intensity scaling from blue (low) to yellow/white (high)] to the mass distribution deduced from gravitational lensing (green contour plot, where the outermost contour represents low mass density and the innermost contours are highest density). The white horizontal line in the lower right represents a distance of 200 kpc at the position of the Bullet Cluster. The mass distribution is clearly different from the gas distribution.

2.1.2 Cosmic Microwave Background (CMB)

Radiation from the early cosmos is still present in the cosmic microwave background (CMB). In a time when the universe was much denser and hotter, it offers a glimpse of the world. The CMB's consistency across the sky baffles me. If just visible stuff were taken into account, density fluctuations would increase as the cosmos grew.

$$\frac{\delta\rho_m}{\rho_m} \propto a. \tag{2.2}$$

Due to the fact that baryonic matter density variations would have been too slight to account for galaxies forming, it would not be able to explain the observed uniformity. However, the existence of cold dark matter, which gathered in large quantities early in the history of the universe, can account for these variations and the galaxies' observable patterns.Since recombination, density variations have multiplied by an order of magnitude of . $\frac{\delta\rho_m}{\rho_m} \approx 10^3$[11].

The presence of cold dark matter with significant density variations explains uniform CMB and galaxy formation.CDM fluctuations $>$ Baryonic fluctuations .Galaxy clusters, galactic rotation curves, with studies from gravitational lensing and the cosmic microwave background observations all provide evidence for the presence of dark matter. These findings imply the existence of a sizeable invisible mass that doesn't emit light and interacts with the cosmos through gravity to influence its structure and behavior.

2.2 Ultralight Bosonic Dark Matter

Dark matter particles are very different from Ultralight Bosonic Dark Matter (UBDM), which has a completely different nature. While the masses of WIMPs and sterile neutrinos are much more than 10 eV, with detection techniques designed to record individual interactions of these particles, UBDM uses bosons with masses much lower than 10 eV (therefore categorized as ultralight). The method for detecting UBDM differs because coherent effects caused by UBDM waves are the main emphasis.

This discrepancy in detection methods results from a critical factor: ultralight bosons typically have high numbers of modes occupied [12], which is necessary In order to align reported density of dark matter. As a result, treating UBDM as a classical field and taking use

of its coherent wavelike characteristics becomes the obvious choice. Using radio waves as an example, It is clear that a more efficient detection method than single photon detection entails coherent monitoring of the current of electrons induced by radio waves employing an antenna. The frequency of oscillation of the UBDM field is in alignment with the Compton frequency when observed from the UBDM reference frame [13].

$$\omega_c = m\cdot \tag{2.3}$$

The standard halo model (SHM), postulates that dark matter particles in the Milky Way are virilized within the galaxy's gravitational potential well. This results in a random distribution of boson velocity. This distribution has a characteristic width throughout the Milky Way of about triangle $\triangle v \approx 10^{-3}c$, which is roughly comparable to the speed of the solar system relative to the galactic rest frame. The observable UBDM field comes from the interference of a huge number of bosons with different velocities, which causes frequency dispersion due to the variable boson velocities.

The visible UBDM field develops from the interaction of bosons with random velocities, assuming that ultralight bosonic dark matter (UBDM) follow the standard halo model (SHM). As a result, this field's properties show stochastic changes with the recognizable τ_{coh} time scale and L_{coh} length scale.

Figure 2.2 illustrates a simulated virialized UBDM field evolving over multiple coherence times. While amplitude of the UBDM field remains in comparison constant for time intervals $\triangle t \ll \tau_{coh}$

it undergoes random fluctuations on longer time scales. The Rayleigh distribution well describes the random variation in this amplitude, which also characterizes the statistical behavior of thermal (chaotic) light.

For experiments conducted over a time span $\triangle t \gg \tau_{coh}$ On the basis of typical dark matter characteristics, the results may be understood. But for extremely small mass bosons, measuring over durations longer than τ_{coh}

becomes impractical. Consider "fuzzy dark matter," for instance, characterized by a boson mass $m_b c^2 \approx 10^{-22} eV$, resulting in $\tau_{coh} \gg 10^{13} s$. In such scenarios, experimental interpretations must incorporate the stochastic nature of UBDM.

It is crucial to acknowledge that the spatial arrangement of (UBDM) within the Milky Way

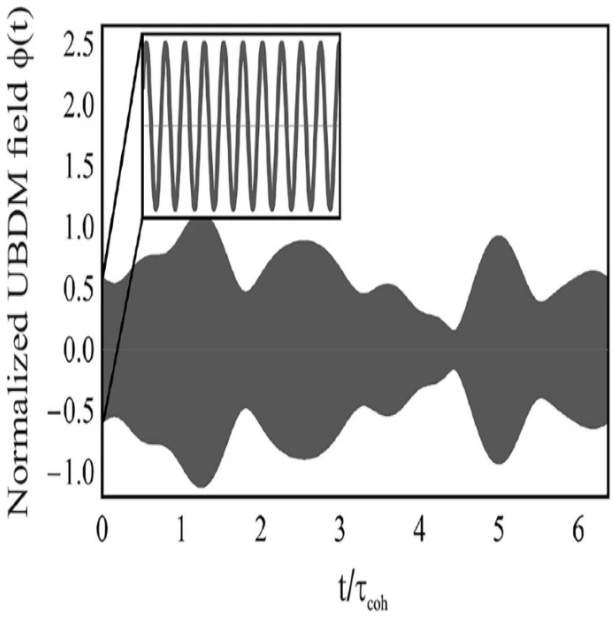

Figure 2.2: Simulated virialized UBDM field $\phi\,(t)$. The inset shows the coherent oscillations of the UDM field over a time scale $\ll \tau$coh.

galaxy may exhibit deviations based on projections of the standard halo model (SHM) in multiple respects. The occurrence of local variations in density can be attributed to the emergence of clusters or currents. Likewise, the UBDM field's self-interactions or topological characteristics may give rise to the emergence of larger composite objects like condensates, clusters, and boson stars or domain barriers. It can be reasonably assumed that the motion and distribution of such structures conform to (SHM). On the other hand, it is possible for a portion of (UBDM) to be gravitationally bound by the Earth or Sun, resulting in the formation of a localized halo characterized by an increased density of UBDM. The ambiguity pertaining to the quantity of dark matter at the local level constitutes a pivotal element in the interpretation of terrestrial studies aimed at detecting (UBDM).

2.3 Candidates

2.3.1 Spin 0 bosons

The axion is considered to be one of the most persuasive contenders for the (UBDM) theory. Axions are a theoretical concept that originates from a proposed solution to the strong CP problem, a theoretical issue pertaining to the existence of CP-violating terms within the framework of quantum chromodynamics. Axions provide a potential resolution to this

problem by their capacity to undergo dynamic evolution and naturally approach a value close to zero. There exist numerous mechanisms that give rise to the production of axions that are consistent with the observed abundance of dark matter. Furthermore, there is a common occurrence of ultralight spin-0 bosons in numerous theories that extend outside the framework of the Standard Model. Axion-like particles (ALPs) manifest in theoretical frameworks that incorporate flavor symmetry breaking, chiral lepton symmetry breaking, and even quantum gravity theories. Axions and Axion-Like Particles (ALPs) are theoretical entities that arise within the framework of string theory. They manifest as quantum field excitations that penetrate spatiotemporal dimensions that have been compactified. The masses of these particles span a range from around $m_a c^2 \approx 10^{-33} ev,$ to $10 \approx Mev$.

Axions also have a significant function within an alternate theoretical framework associated with cold dark matter (CDM) [14]. This framework shows potential in elucidating the source of dark matter and addressing several other unresolved mysteries. The enigmas encompass several intriguing phenomena within the field of cosmology, such as the baryon asymmetry of the Universe, the approximate equivalency in abundance between luminous and dark matter, and the abnormalities discovered in the abundance of lithium throughout the process of big bang nucleosynthesis . According to this theoretical framework, the composition of dark matter is postulated to consist of compact entities referred to as "nuggets." These nuggets are comprised of an estimated quantity of around 10^{25} quarks, which are densely arranged at nuclear densities. The binding force responsible for maintaining the structural integrity of these nuggets is attributed to a "axion domain wall." The axion-quark-nugget model postulates the coexistence of nuggets composed of quarks and "anti-nuggets" composed of antiquarks. This configuration guarantees a near-equilibrium state between the overall quantities of quarks and antiquarks in the cosmos, so efficiently addressing the enigma surrounding the lack of symmetry between matter and antimatter. The axion-quark nuggets has a characteristic radius of around 10^{-5} cm. In contrast to numerous alternative dark matter models, the interactions between these nuggets and ordinary matter are not characterized by weak strength. As an example, the cross-sectional area for proton annihilation falls within the magnitude of 3×10^{-10} cm². The underlying cause for the "darkness" observed in these nuggets can be attributed to their notably low ratio of cross-sectional area to mass.

2.3.2 Spin 1 boson

A distinct category of (UBDM) candidates is constituted by spin-1 bosons . The SM encompasses a collection of twelve fundamental spin-1 bosons, which comprise the photon, the W± and Z bosons, as well as the eight gluons. The emergence of a massless spin-1 boson can often be attributed to the presence of an unbroken $U(1)$ gauge symmetry. Paraphotons, denoted as γ', refer to newly discovered bosons with a spin of 1 and zero mass. These particles are akin to photons, which arise from the $U(1)$ gauge symmetry in the context of electromagnetism. Exotic spin-1 bosons with nonzero mass, similar to the Z boson in the Standard Model, are particularly pertinent when considering potential candidates for dark matter. The Z' boson, in a hypothetical scenario, has the potential to get a non-zero mass by means of the breakdown of a novel $U(1)$ gauge symmetry. Numerous theoretical frameworks postulate the presence of novel Z´ bosons, with theoretical projections encompassing a broad spectrum of mass values and interactions with quarks and leptons. The Z' bosons, which do not have direct interactions with particles in the Standard Model, are often referred to as hidden photons due to their presence in the hidden sector. Similar to axions and axion-like particles (ALPs), it is plausible that The production of boson ultralight spin-1 may be sufficient to explain the presence of dark matter.

2.4 Connection to SM

Ultralight bosons demonstrate associations with particles and fields within the Standard Model through multiple unique paths. A bosonic field with spin-0, denoted as ϕ, has the ability to form direct connections with fermions through two conceivable mechanisms:either a pseudoscalar vertex or a scalar vertex .When it comes to nonrelativistic physics, which deals with circumstances in which fermions have little momentum transfer and velocity, , the interaction between a fermion and the field ϕ can be described by a scalar vertex, which exhibits monopole-like behavior. Alternatively, an interaction involving a pseudoscalar vertex can be understood as a dipole-like phenomenon. The concept of differentiation may be comprehended by considering that within the context of the particle's center of mass frame of reference, there are just two vectors that can be utilized to construct a scalar or pseudoscalar number. These vectors are the spin S as well as the momentum vector P, under the assumption that the field ϕ is a scalar. As a result, the vertex can either remove the

variable S, leading to monopole coupling, or include both S and P, indicating the presence of a parity-odd, pseudoscalar term. As a result, the presence of the pseudoscalar interaction related to the field ϕ gives rise to new dipole interactions, which manifest themselves through spin-dependent changes in energy. Conversely, the scalar interaction is responsible for generating observable oscillations in basic constants. It is possible for spin-0 fields to establish linkages with the electromagnetic field .Many studies utilize this combination to explore the phenomena of axion-to-photon conversion in the presence of strong magnetic fields. The axion, which is grounded in the Peccei-Quinn resolution to the strong CP issue, posits that axions exhibit interactions with the gluon field and have the capacity to induce electric dipole moments (EDMs) that align with the direction of spin [15]. Spin-1 bosons, like to photons, possess the capability to induce modifications in energy that are contingent upon spin, and may possibly engage in interactions that involve the electromagnetic field via mixing.

2.5 Dark photons (DPs)

Previos and upcoming Section delves into the examination of (UBDM) through the utilization of axions, (ALPs), and hidden photons, focusing specifically on their electromagnetic couplings. This section centers its attention on hidden photons, which are classified as ultralight bosons.Hidden sectors, which are characterized by the presence of additional $U(1)$ symmetries beyond those seen in the Standard Model, are frequently observed in theoretical frameworks such as string theory. Although they possess intricate characteristics, the observable impacts of these entities can be elucidated through the utilization of effective operators that establish connections between them and the particles as well fields of the SM [16]. One methodology entails the utilization of direct couplings, wherein particles as well as fields of the SM are linked to the concealed sector [17]. Another potentiality that may be considered is the occurrence of kinematic mix between the recently introduced $U(1)$ symmetry along with electromagnetism, leading to the formation of a hidden photon.

The physics of the hidden photon may be described in a straightforward manner from a conceptual standpoint.It possesses a non-zero mass, denoted as $m_{\gamma'}$.The primary mode of interaction of the entity under consideration with charged particles is predominantly facilitated by its amalgamation with the "real" photon field, which is symbolized by the kinetic

mixing factor κ.

2.5.1 Lagrangian

The Lagrangian that characterizes both photons and hidden photons is formulated in the "mass basis" as shown:

$$\mathcal{L} = -\frac{1}{4}\left(F_{\mu\nu}F^{\mu\nu} + \mathcal{F}_{\mu\nu}\mathcal{F}^{\mu\nu}\right) + \frac{m_{\gamma'}^2}{2}\mathcal{X}_\mu\mathcal{X}^\mu - J^\mu(A_\mu + \kappa\mathcal{X}_\mu). \tag{2.4}$$

In this context, A_μ , $F_{\mu\nu}$ represent the electromagnetic gauge potential with field strength tensor respectively, which are associated with the ordinary photon field. On the other hand both, X_μ, $F_{\mu\nu}$ are related to the hidden photon's potential along with field strength. The symbol $J\mu$ is employed to represent the electromagnetic current, with Gaussian (cgs) units being utilized consistently. Significantly, in the case where the mass of the hidden photon, denoted as $m_{\gamma'}$, tends towards zero $(m_{\gamma'} \rightarrow 0)$, The correspondence between the visible photon and hidden photon fields should be taken into account. The consequence is that a combination that is linear can be redefined. $A_\mu + \kappa\mathcal{X}_\mu$. The aforementioned combination is associated with the electromagnetic current J_μ, although the electromagnetically inactive component $\mathcal{X}_\mu - \kappa A_\mu$ exists. In essence, this suggests that interactions involving hidden photons experience a substantial suppression, specifically by a power of small limitations, denoted as $m_{\gamma'}^2$. The act of suppressing these phenomena plays a crucial role in mitigating a range of astrophysical limitations associated with concealed photons [18].

The wave equation governs the behavior of the hidden photon field in a vacuum.

$$\left(\frac{\partial^2}{\partial t^2} - \nabla^2 + m_{\gamma'}^2\right)\mathcal{X}_\mu = 0. \tag{2.5}$$

and it is assumed that the constraint $\partial_\mu\mathcal{X}^\mu = 0$ is satisfied, which is analogous to the Lorenz gauge condition.

2.5.2 Properties

The unique characteristics of hidden photons, which include having a non-zero mass and exhibiting weak interactions with particles in the Standard Model due to their kinetic mixing with photons, give rise to three noteworthy consequences:

- The fact of nonzero mass allows hidden photons to potentially demonstrate attributes that make them good candidates for acting as cold dark matter [19].
- The phenomenon of kinetic mixing between hidden photons and photons enables the hidden photons to exert relatively mild impacts on electromagnetic systems, hence eliciting tiny excitations.
- Due to their weak interaction with particles in the Standard Model and their comparatively long Compton wavelength at a macroscopic level, hidden photons possess the ability to effectively permeate conductors and superconductors.

The aforementioned outcomes highlight the captivating characteristics of DPs and their possible ramifications across diverse fields of physics.

2.5.3 Dark photon electrodynamics

In order to gain a comprehensive understanding of the impact of DPs on the field of electrodynamics, it is advantageous to reformulate the Lagrangian, as presented in Equation (2.5), inside the framework sometimes referred to as the "interaction basis." The aforementioned objective is accomplished by the implementation of substitutes.

$$\bar{A}_\mu = A_\mu + \kappa \mathcal{X}_\mu \quad , \tag{2.6}$$

$$\bar{\mathcal{X}}_\mu = \mathcal{X}_\mu - \kappa A_\mu \quad , \tag{2.7}$$

This result in a Lagrangian expressed as :

$$\mathcal{L} = [-\frac{1}{4}\left((\bar{F}_{\mu\nu}\bar{F}^{\mu\nu}) + (\bar{\mathcal{F}}_{\mu\nu}\bar{\mathcal{F}}^{\mu\nu})\right) + \frac{m_{\gamma'}^2}{2}\bar{\mathcal{X}}_\mu\bar{\mathcal{X}}^\mu - J\bar{A}_\mu + \kappa\frac{m_{\gamma'}^2}{2}\bar{\mathcal{X}}^\mu\bar{A}_\mu]. \tag{2.8}$$

The influence of hidden photons on particles inside the SM may be deduced by examining Equation (2.8), which reveals the existence of an effective current density.

$$\bar{\mathcal{J}}^\mu = -\kappa m_{\gamma'}^2\bar{\mathcal{X}}^\mu, \tag{2.9}$$

This leads to :

$$\mathcal{L} = -\frac{1}{4}\left(\bar{F}_{\mu\nu}\bar{F}^{\mu\nu} + \bar{\mathcal{F}}_{\mu\nu}\bar{\mathcal{F}}^{\mu\nu}\right) + \frac{m_{\gamma'}^2}{2}\bar{\mathcal{X}}_\mu\bar{\mathcal{X}}^\mu - \left(J^\mu + \bar{\mathcal{J}}^\mu\right)\bar{A}_\mu. \tag{2.10}$$

It is noteworthy , temporal component of the 4-potential, denoted as X^0, exhibits a reduced magnitude in contrast to the spatial component represented by vector potential X. The

relation between the average value of X (denoted asX^{-0}) and X is a direct result of its equivalence to Lorenz gauge condition.

$$\frac{\partial \bar{\mathcal{X}}^0}{\partial t} = \{\nabla \cdot \boldsymbol{\mathcal{X}}\}. \tag{2.11}$$

For a plane wave solution this goes as $\bar{\mathcal{X}}^\mu \propto e^{i(\mathbf{k}\cdot\mathbf{r}-\omega t)}$, Equation (2.11) leads to:

$$\bar{\mathcal{X}}^0 = -\frac{\mathbf{k}\cdot\boldsymbol{\mathcal{X}}}{\omega}\ . \tag{2.12}$$

Utilizing the connection between the wave vector k and the hidden photon's c velocity:

$$\mathbf{k} = m_{\gamma'}\mathbf{v}. \tag{2.13}$$

recognizing $\omega \approx m_{\gamma'}$, it follows that:

$$\bar{\mathcal{X}}^0 \approx -\boldsymbol{v}\cdot\boldsymbol{\mathcal{X}}. \tag{2.14}$$

As a result, the temporal part of the hidden photon's 4-potential is squeezed by a factor of approximately $[v/c]$, which is approximately 10^{-3} in comparison to the spatial component. Likewise, as a consequence of the identical factor, the spatial part of the concealed photon's 4-current experiences a reduction of about v/c in comparison to the current density, J, of the DP.

2.6 Hill's equation

Hill's equation is a second-order linear differential equation :

$$y''(t) + p(t)y(t) = 0. \tag{2.15}$$

where $p(t)$is a periodic function with period T, i.e.,$p(t+T) = p(t)$.A classical example is the Mathieu equation where

$$p(t) = 2\lambda + 2\mu\cos(2t). \tag{2.16}$$

2.6.0.1 Floquet Theory

Given the periodic coefficient $p(t)$, According to Floquet theory, the solutions to Hill's equation can be expressed as

$$y(t) = e^{i\rho t}u(t). \tag{2.17}$$

where ρ is a constant and $u(t)$ is a function that shares the same period as $p(t)$, meaning $u(t+T) = u(t)$. The variable ρ represents the Floquet exponent, with its imaginary component denoting the Bloch wave number.

2.6.0.2 Floquet Transition Matrix

Given initial conditions for $y(t)$ and $y'(t)$at $t = 0$, the values of $y(t)$ and $y'(t)$ at $t = T$ can be determined using a linear relationship:

$$\begin{pmatrix} y(T) \\ y'(T) \end{pmatrix} = M \begin{pmatrix} y(0) \\ y'(0) \end{pmatrix}.$$

M is a 2×2 matrix called the Floquet transition matrix.

2.6.0.3 Eigenvalues and Stability

The Floquet multipliers, which are the eigenvalues of matrix M, play a crucial role in determining the stability of solutions to Hill's equation. If the absolute value of both eigenvalues is equal to 1, the solution can be considered stable. In the event when the magnitude of at least one eigenvalue deviates from unity, the solution can be deemed as unstable.

2.7 The Mathieu Equation

$$\frac{d^2y}{dt^2} + (a - 2q\cos(2t))y = 0. \tag{2.18}$$

The solution of interest, denoted as $y(t)$, is the subject under consideration.The variables a and q are constants. The periodicity of the coefficient of y is π.

The aforementioned equation is prevalent across various domains of physics, including but not limited to quantum mechanics and the examination of pendulum motion under specific circumstances.

2.7.1 Floquet Theory Introduction

Floquet theory is a fundamental tool in the analysis of differential equations having periodic coefficients. According to the given information, the solution to this particular differential equation can be represented as the multiplication of an exponential function and a periodic function.

The solution is provided in a formal manner as follows:

$$y(t) = e^{i\mu t}P(t). \tag{2.19}$$

The function $P(t)$ is a periodic function that has the same period as the coefficient. The symbol μ is commonly referred to as the Floquet exponent.

The utilization of Floquet Theory in the analysis of the Mathieu Equation

In order to examine the functionality of this solution form, we will proceed by substituting it into the Mathieu equation.

Starting with:

$$y(t) = e^{i\mu t}P(t), \tag{2.20}$$

Differentiating once:

$$y'(t) = i\mu e^{i\mu t}P(t) + e^{i\mu t}P'(t), \tag{2.21}$$

Differentiating again:

$$y''(t) = -\mu^2 e^{i\mu t}P(t) + 2i\mu e^{i\mu t}P'(t) + e^{i\mu t}P''(t), \tag{2.22}$$

Now, substituting it into the Mathieu equation:

$$e^{i\mu t}[-\mu^2 P + 2i\mu P' + P'' + (a - 2q\cos(2t))P] = 0, \tag{2.23}$$

For this to hold for all t, the term in the square brackets must be zero:

$$-\mu^2 P + 2i\mu P' + P'' + (a - 2q\cos(2t))P = 0. \tag{2.24}$$

This is the governing equation for$P(t)$ and μ. finding an explicit solution can is tough.

2.7.2 Solutions and Periodicity

Step 1:

Formulating the Solution We begin by postulating the solution $z(t) = e^{\mu t}P(t)$. Substituting this into the Floquet equation yields:

$$e^{\mu t}\left(\frac{d^2P}{dt^2} + (a - 2q\cos(2t) - \omega^2)P\right) = 0. \tag{2.25}$$

Since $e^{\mu t}$ is non-zero, we obtain:

$$\frac{d^2P}{dt^2} + (a - 2q\cos(2t) - \omega^2)P = 0. \tag{2.26}$$

This ordinary differential equation characterizes the behavior of $P(t)$ under the influence of the periodic modulation.

Step 2:

Analyzing the Periodic Component , Solving the equation for $P(t)$ requires capturing its periodic characteristics. Let's delve into the mathematical intricacies of this process.

The equation

$$\frac{d^2P}{dt^2} + (a - 2q\cos(2t) - \omega^2)P = 0. \tag{2.27}$$

contains the term $2q\cos(2t)$, which is periodic with a period of π. This prompts us to consider solutions in the form of a Fourier series:

$$P(t) = \sum_{n=-\infty}^{\infty} c_n e^{in(2t)}, \tag{2.28}$$

where c_n are complex coefficients to be determined. Substituting this series into the differential equation leads to:

$$\sum_{n=-\infty}^{\infty} \left(-c_n(2n)^2 + (a-\omega^2)c_n\right) e^{in(2t)} - \sum_{n=-\infty}^{\infty} 2qc_n \frac{e^{i(n+1)2t} + e^{i(n-1)2t}}{2} = 0, \tag{2.29}$$

This results in a collection of equations, each corresponding to a different n :

$$-c_n(2n)^2 + (a-\omega^2)c_n - qc_{n+1} - qc_{n-1} = 0. \tag{2.30}$$

Solving this system of equations for the coefficients c_n provides the periodic function $P(t)$.

2.7.2.1 Floquet Exponent

After the resolution of the equation for $P(t)$, the remaining equation reveals that the behavior of the solution is determined by the complex constant \mu. This phenomenon reveals the stability and resonance properties of the system.

The Floquet exponent, denoted as μ, is calculated based on the roots of the characteristic equation that is linked to the differential equation governing the function $P(t)$.

$$\mu^2 + (a-\omega^2) - 4q\cos(2t) = 0. \tag{2.31}$$

The roots, denoted as μ_1 and μ_2, are the real and imaginary components that elucidate the system's reaction to the periodic modulation. If the real components of these roots are greater than zero, the system demonstrates exponential development.

2.7.2.2 Formulating the Resonance Condition

The resonance condition is

$$\frac{a-n^2}{2} = \pm nq. \tag{2.32}$$

The critical threshold is a significant factor in determining the resonance of the system with the periodic modulation. This phenomenon offers valuable insights into the correlation between resonance order, modulation strength (q), and the constant (ω).

By substituting the expression $a = (n^2)/2 + nq$ into the Floquet exponent equation, we obtain:

$$\mu^2 - n^2 - 2nq - \omega^2 = 0. \tag{2.33}$$

This equation encapsulates the intricate interplay between the parameters and reveals the resonance-induced instability regime.

2.7.2.3 Evaluating the Floquet Exponent at Resonance

In order to examine the consequences of the resonance condition, it is necessary to assess the Floquet exponent μ under said circumstance. The present study aims to investigate the impact of the system's response to periodic modulation on its stability.

Setting $\mu^2 = n^2 + 2nq + \omega^2$, we attain the equation:

$$\mu^2 = n^2 + 2nq + \omega^2. \tag{2.34}$$

The real part of μ is crucial in determining the system's behavior. If $\mathrm{Re}(\mu) > 0$, the system exhibits a tendency for exponential growth, signifying instability. Conversely, if $\mathrm{Re}(\mu) \leq 0$, the system remains stable.

The dynamic connection between resonance and instability is revealed by the relationship that exists between the resonance state and the Floquet exponent. By assessing the value of μ under the resonance condition, we may determine if the system exhibits amplification of disturbances, resulting in instability, or if it maintains stability.

2.7.2.4 Beyond Instability:

Once the system surpasses the crucial threshold of instability, the resonance condition and the behavior of the variable μ provide insights into the intricate dynamics that unfold. The elaborate patterns governing the system's response are generated by the interaction of resonance orders, modulation strengths, and the constant ω.

By examining various permutations of a, q, and ω, it is possible to generate a stability chart, commonly known as an Arnold tongue diagram. The presented chart provides a visual representation of the regions characterized by stability and instability, effectively illustrating the impact of resonance orders on the behavior of the system.

The Arnold tongue diagram exhibits complex patterns, wherein the presence of overlapping tongues signifies the existence of places where different instabilities and stabilities

compete with each other. Through the examination and analysis of these patterns, a more profound understanding may be obtained of the complex and interconnected relationship among resonance, stability, and the dynamics of the Hill's equation.

2.7.2.5 Determining Regions of Stability:

It is a customary procedure to delineate regions of stability in the $a - q$ plane while analyzing the Mathieu equation. The proposed "stability chart" will consist of distinct bands, commonly referred to as "tongues," that represent stable zones, whereas areas of instability will be observed between these bands.

The delineation of these zones can be ascertained through, Given a predetermined set of values for variables a and q. The governing equation given above can be solved to obtain the expressions for $P(t)$ and μ. Examining the characteristics of solutions in order to ascertain their boundedness. Iterating across a range of values in order to systematically delineate stability areas.

2.8 Dilaton field

Role and Definition

The dilaton is a scalar field, which implies that it possesses a single value at every spatial position, in contrast to vector or tensor fields that exhibit numerous components. The subject matter pertains to the dimensions that have been compactified in accordance with the principles of string theory, specifically in relation to their size and shape.The dilaton field is a scalar field that emerges in specific theoretical frameworks within the study of theoretical physics, most notably in the context of string theory. The term "dilatation" is used to denote its association with scaling transformations.

2.8.1 Dilaton in gravity

The dynamics of the cosmos in dilaton gravity are significantly influenced by the presence of the dilaton field ϕ, which works in conjunction with the metric tensor. The cosmological implications become apparent when attempting to reconcile the concepts derived from string theory (or theories incorporating the dilaton) with the observed macroscopic arrangement of the cosmos [20].

The action. The expression for a common action in dilaton gravity, which is derived from string theory, can be formulated as follows:

$$S = \int d^4x\sqrt{-g}e^{-2\phi}\left(R + 4(\nabla\phi)^2 - V(\phi)\right), \tag{2.35}$$

Where as R is the Ricci scalar, g is the determinant of the metric tensor, and $V(\phi)$ is the potential of the dilaton field. This action describes the dynamics of both the metric and the dilaton field in the universe.
Given the Friedmann-Lemaître-Robertson-Walker (FLRW) metric:

$$ds^2 = -dt^2 + a(t)^2\left(\frac{dr^2}{1-kr^2} + r^2d\theta^2 + r^2\sin^2\theta d\phi^2\right), \tag{2.36}$$

For a spatially flat universe, the Einstein tensor components are given as folow:

$$G_{00} = 3\left(\frac{\dot{a}}{a}\right)^2, \tag{2.37}$$

$$G_{ij} = -\left(2\frac{\ddot{a}}{a} + \left(\frac{\dot{a}}{a}\right)^2\right)g_{ij}, \tag{2.38}$$

Varying the action gives the Einstein field equations (EFE):

$$3\left(\frac{\dot{a}}{a}\right)^2 = e^{2\phi}\left(2\dot{\phi}^2 - 4\dot{a}\dot{\phi}/a\right), \tag{2.39}$$

The equation for the evolution of the dilaton in an expanding universe is:

$$\ddot{\phi} + 3\frac{\dot{a}}{a}\dot{\phi} = 0, \tag{2.40}$$

If we introduce a potential $V(\phi)$ for the dilaton, its dynamics will change with it

2.8.2 Field Equations

From the action, we can derive the field equations using the variation principle. The resulting equations are:

$$R_{\mu\nu} + 2\nabla_\mu\nabla_\nu\phi = 0, \tag{2.41}$$

$$\nabla^2\phi - 2(\nabla\phi)^2 + \frac{V(\phi)}{2} = 0, \tag{2.42}$$

The determination of precise solutions for these equations is contingent upon the specific functional form of the dilaton potential $V(\phi)$. Nevertheless, under certain constraints or for particular potential forms, it is possible to obtain cosmological solutions that depict the

dynamics of the cosmos while accounting for the existence of the dilaton field.

Dilaton cosmology gives rise to a multitude of observable repercussions. Certain solutions propose the possibility of a time-dependent gravitational constant G or a time-dependent fine-structure constant α as a consequence of the evolution of the dilaton field. By juxtaposing these predictions with astronomical measurements, it is possible to establish limitations on the characteristics and progression of the dilaton field within the cosmos.

2.9 Dilaton-like field coupled to A_μ

coupling a dilaton-like scalar field ϕ to a vector field A_μ introduces a rich structure to the dynamics of the system. Let's consider the action for this system:

$$S = \int d^4x\sqrt{-g}\left[\frac{1}{2}\nabla^\mu\phi\nabla_\mu\phi - \frac{1}{4}e^{-\lambda\phi}F^{\mu\nu}F_{\mu\nu} - V(\phi)\right], \tag{2.43}$$

In this instance,The initial term corresponds to the kinetic term associated with the scalar field.

The second term in the equation reflects the kinetic term associated with the vector field A_μ. Here,$F_{\mu\nu} = \nabla_\mu A_\nu - \nabla_\nu A_\mu$ denotes the field strength tensor. The exponential factor $e^{-\lambda\phi}$ represents the interaction between the dilaton field and the vector field.

The third term, denoted as $V(\phi)$, corresponds to the potential energy associated with the scalar field. The symbol λ represents a coupling constant in this context. The determinant of the metric tensor is denoted by g.

2.9.1 Field Equations

To derive the field equations, we need to vary the action with respect to both the vector field and the scalar field.

Varying with respect toA^μ :

$$\delta S = -\frac{1}{4}\int d^4x\sqrt{-g}e^{-\lambda\phi}\delta F^{\mu\nu}F_{\mu\nu}, \tag{2.44}$$

implies

$$\delta S = -\frac{1}{2}\int d^4x\sqrt{-g}e^{-\lambda\phi}\nabla_\nu\left(F^{\mu\nu}\right)\delta A_\mu, \tag{2.45}$$

From the above, we get the equation:

$$\nabla_\nu\left(e^{-\lambda\phi}F^{\mu\nu}\right) = 0, \tag{2.46}$$

Varying with respect to ϕ:

$$\delta S = \int d^4x\sqrt{-g}\left[\nabla^\mu\phi\nabla_\mu\delta\phi + \frac{1}{4}\lambda e^{-\lambda\phi}F^{\mu\nu}F_{\mu\nu}\delta\phi - V'(\phi)\delta\phi\right]. \tag{2.47}$$

Combining the terms, we get:

$$\nabla^2\phi - \frac{1}{4}\lambda e^{-\lambda\phi}F^{\mu\nu}F_{\mu\nu} + V'(\phi) = 0. \tag{2.48}$$

2.9.2 Interpretation

The aforementioned equations provide the Euler-Lagrange equations corresponding to the provided action, which provide insight into the system's dynamics.

The equation resulting from the variation with respect to (A^μ) is the equation of motion for the vector field, which is altered as a result of its interaction with the dilaton. The equation derived by differentiating with respect to ϕ provides the dynamics of the scalar field, commonly known as the dilaton. This dynamics is impacted not only by the potential of the scalar field, but also by its coupling to the vector field A^μ.

2.9.2.1 Implications

The interaction between the dilaton-like field and the vector field implies that the dynamics of one field can be influenced by the existence of the other. In specific circumstances, the presence of a robust vector field can initiate changes in the scalar field, and conversely, the scalar field can also influence the dynamics of the vector field.

This framework is frequently utilized in theories that aim to integrate several forces or in situations that necessitate moduli stabilization. The inclusion of the coupling term can give rise to complex dynamics and may have significant ramifications in the fields of cosmology, particle physics, and black hole physics.

2.9.2.2 The Dilaton and Its Significance in Field Theory

The notion of a dilaton emerges from the framework of string theory and represents a scalar field that is postulated to govern the magnitude of string interactions, analogous to the role played by the Higgs field in determining particle masses within the standard model. In non-string theory contexts, the dilaton can be seen as a scalar field possessing specific characteristics.

The symbol ϕ represents the dilaton-like scalar field in our study. The symbol A_μ is used in academic contexts to represent a mathematical quantity. The provided expression denotes a four-vector, encompassing one temporal and three spatial components, which characterizes the potential of a dark photon. This potential bears resemblance to the electromagnetic potential found inside the standard model.

The Lagrangian density denoted as $\mathcal{L}_\phi$ that describes a scalar field is commonly expressed

as:

$$\mathcal{L}_\phi = \frac{1}{2}\partial^\mu\phi\partial_\mu\phi - V(\phi). \tag{2.49}$$

The Lagrangian density for the vector A_μ exhibits similarities to that of electromagnetism. The Lagrangian density for a gauge field A is given by

$$\mathcal{L}_A = -\frac{1}{4}F^{\mu\nu}F_{\mu\nu}, \tag{2.50}$$

where $F^{\mu\nu}$ represents the field strength tensor . The equation provided is the expression for the electromagnetic field tensor, $F^{\mu\nu}$ in terms of the vector potential, A^μ. The aforementioned phrase denotes the tensor that characterizes the strength of the field.

The introduction of the dilaton ϕ into the kinetic term of A_μ gives rise to the interaction Lagrangian

$$\mathcal{L}_{int} = -\frac{1}{4}W(\phi)F^{\mu\nu}F_{\mu\nu}. \tag{2.51}$$

The function $W(\phi)$ denotes the scalar field's coupling to the kinetic term of the vector field, hence affecting the propagation and interactions of the vector field.

The Equations of Motion

In order to get the equations of motion for the fields, it is necessary to apply the E-L equations by taking the variation of the total Lagrangian with respect to each field.

The equation of motion obtained from the Euler-Lagrange equation is expressed as

$$\frac{\partial\mathcal{L}}{\partial\phi} - \partial_\mu\left(\frac{\partial\mathcal{L}}{\partial(\partial_\mu\phi)}\right) = 0. \tag{2.52}$$

where $\mathcal{L}$ represents the Lagrangian density that is dependent on the field $\phi(x)$ and its spacetime derivatives $\partial_\mu\phi(x)$.In the context of this discussion, the dilaton scalar field ϕ is of primary interest.

The scalar Lagrangian, denoted as $\mathcal{L}_\phi$, is expressed as follows:

$$\mathcal{L}_\phi = \frac{1}{2}\partial^\mu\phi\partial_\mu\phi - V(\phi). \tag{2.53}$$

The Euler-Lagrange equation can be expressed as follows:

$$\partial^\mu\partial_\mu\phi + \frac{dV}{d\phi} = 0. \tag{2.54}$$

Regarding the vector field A_μ

Given the presence of the interaction term, the Lagrangian density denoted as $\mathcal{L}_A$ can be expressed as $-\frac{1}{4}W(\phi)F^{\mu\nu}F_{\mu\nu}$. The expression

$$F^{\mu\nu} = \partial^\mu A^\nu - \partial^\nu A^\mu. \tag{2.55}$$

represents the electromagnetic field tensor, where \(\partial^\mu\) denotes the partial

derivative with respect to the coordinate μ and A^ν represents the electromagnetic potential. The equation governing A_μ, known as the Euler-Lagrange equation, can be expressed as follows:

$$\partial_\nu(W(\phi)F^{\nu\mu}) = 0. \tag{2.56}$$

The Process of Coupling to the Dark Photon:

The presence of the dark photon introduces a coupling between the dilaton and the vector field, resulting in a modification of the equation of motion governing the behavior of the dilaton.

$$\frac{\partial \mathcal{L}_{int}}{\partial \phi} = -\frac{dW(\phi)}{d\phi} F^{\mu\nu}F_{\mu\nu}. \tag{2.57}$$

There will be a term in the dilaton's equation of motion which arises from the variation of the interaction term with respect to ϕ.

The revised equation of motion for the dilaton incorporates the following term:

$$\partial^\mu\partial_\mu\phi + \frac{dV}{d\phi} + \frac{dW(\phi)}{d\phi} F^{\mu\nu}F_{\mu\nu} = 0. \tag{2.58}$$

the solutions or consequences may vary depending on the precise mathematical forms of $V(\phi)$ and $W(\phi)$), as well as the beginning or boundary conditions.

2.10 Python code for numerical simulations

2.10.1 Essence

This script's complexity and depth demonstrate a great deal of effort and knowledge in both coding and physics. Let's examine some of the initiatives presented:

Knowledge Integration: The incorporation of intricate mathematical operations and physical notions into a computer model is one of the first things that jumps out. This calls for a thorough understanding of the underlying physics as well as the capacity to translate that understanding into code, which is a difficult challenge in and of itself.

Numerical Techniques: The application of numerical techniques, particularly the method of integrating differential equations (solve_ivp), highlights the difficulties in comprehending and foreseeing dynamic systems. Mathematical problems that cannot be solved analytically can sometimes be approximated using computing approaches known as numerical methods. Understanding the mathematics behind them as well as the numerical idiosyncrasies that come with approximating real-world phenomena are necessary for implementation.

Parameter Sweep:

In [1]:
```
import numpy as np
import matplotlib.pyplot as plt
import cmasher as cmr
from scipy.integrate import solve_ivp

m_phi = 1.0
M = 1.0

def dilaton(t):
    return phi_0 * np.cos(m_phi * t)

def dilaton_derivative(t):
    return -phi_0 * m_phi * np.sin(m_phi * t)

def dilaton_double_derivative(t):
    return -phi_0 * m_phi**2 * np.cos(m_phi * t)

def floquet_rhs_1(t, X, k, m_gamma_prime):
    A0, dA0 = X
    phi_bar = dilaton(t)

    d2A0 = -(k**2 + (m_gamma_prime**2) / np.exp(phi_bar / M)) * A0

    return [dA0, d2A0]

def floquet_rhs_2(t, X, k, m_gamma_prime):
    A0, dA0 = X
    phi_bar = dilaton(t)
    dphi_bar = dilaton_derivative(t)
    ddphi_bar = dilaton_double_derivative(t)

    d2A0 = -(k**2 + (m_gamma_prime**2) / np.exp(phi_bar / M) - (ddphi_bar / (2 * M)) - (dphi_bar / (2 * M))**2) * A0
```

Figure 2.3: Python code used in the simulation of my graphs used in chapter 6

```
    return [dA0, d2A0]

phi0_values = np.linspace(0.01, 6, 530)
k_values = np.linspace(0.01, 3, 530)

Re_mu_grid_1 = np.zeros((len(phi0_values), len(k_values)))
Re_mu_grid_2 = np.zeros((len(phi0_values), len(k_values)))

m_gamma_prime = 0.5 * m_phi

T = 2 * np.pi / m_phi
t_eval = np.linspace(0, 10 * T, 1000)

for i, phi_0 in enumerate(phi0_values):
    for j, k in enumerate(k_values):
        initial_conditions = [1.0, 0.0]

        sol_1 = solve_ivp(floquet_rhs_1, (0, 10 * T), initial_conditions, args=(k, m_gamma_prime), t_eval=t_eval, method='RK45')
        final_A0_1 = sol_1.y[0][-1]
        Re_mu_1 = (1 / (10 * T)) * np.log(np.abs(final_A0_1 / initial_conditions[0]))
        Re_mu_1 = np.maximum(0, Re_mu_1)
        Re_mu_grid_1[i, j] = Re_mu_1

        sol_2 = solve_ivp(floquet_rhs_2, (0, 10 * T), initial_conditions, args=(k, m_gamma_prime), t_eval=t_eval, method='RK45')
        final_A0_2 = sol_2.y[0][-1]
        Re_mu_2 = (1 / (10 * T)) * np.log(np.abs(final_A0_2 / initial_conditions[0]))
        Re_mu_2 = np.maximum(0, Re_mu_2)
        Re_mu_grid_2[i, j] = Re_mu_2

k_grid, phi0_grid = np.meshgrid(k_values / m_phi, phi0_values / M)

fig, axs = plt.subplots(1, 2, figsize=(12, 6))

cs1 = axs[0].contourf(k_grid, phi0_grid, Re_mu_grid_1, levels=100, cmap=cmr.ocean_r)
axs[0].set_title("Real part of Floquet exponent ('$A_0$')")
axs[0].set_xlabel('$k/m_{\phi}$')
axs[0].set_ylabel('$\phi_0/M$')
cs2 = axs[1].contourf(k_grid, phi0_grid, Re_mu_grid_2, levels=100, cmap=cmr.ocean_r)
axs[1].set_title("Real part of Floquet exponent ('$A_+-$')")
axs[1].set_xlabel('$k/m_{\phi}$')
axs[1].set_ylabel('$\phi_0/M$')
plt.tight_layout()
plt.show()
```

Figure 2.4: Python code used in the simulation of my graphs used in chapter 6

The scientific method's foundation—a thorough research under various conditions to understand a system's behavior—is reflected in the nested loops, which are a brute force method of evaluating a system over a variety of settings. This careful technique, however costly computationally, guarantees a thorough grasp of the dynamics at work.

Data visualization:

The script's culmination in the generation of contour plots indicates a desire to not only comprehend but also to convey this comprehension. By itself, visualization is both an art and a science. The selection of contour plots, levels, and colormaps reveals knowledge and a comprehension of the value of transparent, perceptive depiction of complex data.

Working Theory:

The main focus of the story is on how a certain quantum field or wave changes as a result of an oscillating dilaton field. Cosine functions are used to depict the dilaton's behavior in order to capture its oscillating nature over time.The Floquet theory, a mathematical framework used to examine the behavior of differential equations with periodic coefficients, is the important idea in this case. Simply said, Floquet theory aids in determining whether and how solutions to a system's equations can increase or deteriorate over time when it is driven periodically (as is the case with the oscillating dilaton). This increase or decline is measured by the Floquet exponent, which is computed in the script.

This script takes into account two separate sets of equations of motion (floquet_rhs_1 and floquet_rhs_2), each of which incorporates the dilaton's effect in a unique way. The script creates a detailed picture of the system's behavior in the presence of an oscillating dilaton by solving these equations for a variety of initial conditions and constants.In conclusion, the script's main idea is to use the Floquet theory's mathematical tools to comprehend how an oscillating dilaton interacts with a quantum field while looking for patterns, stabilities, or resonances in their interaction.

In retrospect, creating such a script—integrating complex mathematical ideas, computing methods, and showing the results—is no easy task. It is evidence of the synergy between sophisticated scientific investigation and the strength of computational techniques.

2.10.2 Breakdown of code

For two separate differential equations in the setting of dilaton physics, this code calculates as well as shows the real part of the Floquet exponent. The stability of periodic solutions to

the differential equations can be examined using the Floquet exponent. Here is a thorough breakdown of the code:

Imports and Constants:

Imported are necessary libraries like matplot.lib, sci.py.integrate, and num.py. [21][22]

For sophisticated colormap usage, the cmasher library is imported. The variables m_phi and M are established Dilaton Activities:

Dilation (t)

uses the cosine function to determine the value of the dilaton as a function of time t.

Dilaton_derivative(t),

calculates the dilaton's first time derivative.

The function **dilaton_double_derivative(t)** calculates the dilaton's second time derivative.

Right-side (RHS) functions

The right-hand sides of two differential equations are computed, respectively, using the floquet_rhs_1 and floquet_rhs_2 functions. dX/dt = f(t, X, k, m_gamma_prime), where X = [A0, dA0], is a function created for the system.

Parameter Room

The arrays phi0_values and k_values, respectively, show several values for phi_0 and k. The computed real sections of the Floquet exponents of both of the differential equations will be stored in Re_mu_grid_1 and Re_mu_grid_2, which have initialization values of zero.

Loop of Integration

The differential equations are solved across a time domain using SciPy's solve_ivp function and the Runge-Kutta method **('RK45')** for each combination of phi_0 and k values. The solution at the time domain's end is used to compute the real part of the Floquet exponent, which is then calculated and placed in the appropriate grid (Re_mu_grid_1 or Re_mu_grid_2).

Visualization:

The x and y axes for the contour plot are constructed from a meshgrid using the k_values and phi0_values. Using the ocean_r colormap from cmasher, two contour plots are produced for Re_mu_grids_1 and 2. Plots for both differential equations in the parameter space show the real part of the Floquet exponent. For two differential equations involving the dilaton function, this code essentially assesses how the real part of the Floquet exponent fluctuates

with respect to various phi_0 and k values. The contour plots make it easier to see areas of the parameter space where the system might be stable or unstable.

Chapter 3

Theory of (UBDM)

3.1 Properties of dark matter

The concept of dark matter (DM) arose due to the inadequacy of the gravitational pull from visible matter to explain the early-stage clustering of matter in universe. At that time, scientists speculated whether this phenomenon was caused by an undiscovered particle or merely unobservable ordinary matter.One possible explanation considered was black holes. These objects don't emit light but exert gravitational attraction and are detectable through gravitational lensing. Various types of Machos (massive compact halo objects), such as brown dwarfs, were also contemplated [23]. These Machos, residing in a galaxy's halo, possess substantial mass but emit minimal light. However, the number of Machos wasn't sufficient to explain the required amount of dark matter.Neutrinos were deemed as potential candidates. Similar to dark matter, neutrinos pass through matter without interaction[24]. However, they are too light to account for the gravitational effects of (DM) and are excessively fast. Their velocity would have hindered the formation of cosmic structures, resulting in collapsing density fluctuations on larger scales. According to the Top-Down Scenario, galaxy clusters would have formed initially, followed by galaxies and stars.

Following the exclusion of standard model particles as possible candidates, scientists speculate that dark matter is a novel, exotic particle possessing specific physical attributes[25]:

1. strong gravitational pull
2. Mild particle-to-particle interactions

3. Absence of electricity

4. For it to continue exist today, it must be stable on the cosmic time scale.

5. When combined, one or more candidates must possess the necessary relic density.

6. Given what we know, the baryonic type cannot make up a sizable portion of the mixture of the dark matte.

7. There was no display of the color force

WIMPs (weakly interacting massive particles) are the focus of the current popular understanding of dark matter. The mass of these particles ranges from 10 GeV to a few TeV.

However, there are a number of opposing ideas regarding the makeup of dark matter particles, such as the Modified Newtonian Dynamics (MoND) [26]. For problems like the galactic rotation issue, MoND suggests modifying Newton's law of gravity.

3.2 UBD matter theory.

This section explores the hypothesis that the primary constituent of dark matter consists of ultralight bosons. In this study, we examine the theoretical underpinnings of the (UBDM) theory and the hypothesis that can be tested that arise from it. Throughout our analysis, we provide relevant examples to support our arguments. At the outset, a number of inquiries automatically emerge:

- if we were to postulate that DM is composed of a bosonic field, what theoretical approaches can be employed to gain a deeper understanding of this concept?

- What is the reasoning behind the concept that these bosons would possess a "ultralight" nature, with masses considerably less than $1eV/c^2$?

- In what manner could ultralight bosonic matter potentially form connections with the established particles and fields inside the framework of the Standard Model?

- What factors contribute to the anticipation of the existence of bosons that have not yet been discovered, in addition to those that have already been identified.

- What are the potential mechanisms that could have resulted in the generation of ultralight bosons during the early stages of the universe, with quantities significant enough to compensate the measured density of DM in the present era?

The following inquiries function as initial prompts for our investigation into the idea surrounding ultralight bosonic dark matter. Our aim is to explore into its theoretical underpinnings and its ramifications.

3.3 Bosonic Field Lagrangians

Both classical and quantum field theory often start by building the Lagrangian (or more accurately, its Lagrangian density L) for the associated field in order to explain the physics of a novel particle. The subsequent parts heavily rely on Quantum Field Theory (QFT) textbooks, namely references [27] [28], which offer a more thorough understanding and in-depth elucidation of the fundamental principles under consideration.

Let us commence by making the initial assumption that we are working with a scalar field denoted as $\phi(r,t)$. In this context, it is understood that the quantum excitations of this scalar field, represented by $\phi(r,t)$, possess the characteristic of being spin-0 bosons. The primary motivation for including this particular excerpt is in its inherent simplicity. Additionally, it is worth noting that many noteworthy contenders for dark matter, namely axions and axion-like particles (ALPs), are classified as spin-0 bosons. Additionally, the detection of the Higgs boson (references 6 and 7) provides further impetus for the examination of scalar fields, thereby confirming the presence of elementary spin-0 bosons in the physical realm. [29]

The scalar field is defined by the Lagrangian L . comprises the temporal derivative of ϕ, $\partial_0\phi$= $\frac{\partial\phi}{\partial t}$, as well as the spatial derivative of ϕ with space coordinates $\nabla\phi$. In order to preserve Lorentz invariance, the Lagrangian is formulated by using the four-derivative of the field variable, denoted as ϕ.

$$\partial_\mu\phi = \frac{\partial\phi}{\partial x^\mu} = \left(\frac{\partial}{\partial t}, \boldsymbol{\nabla}\right)\phi, \tag{3.1}$$

$$\partial_\mu\phi = \frac{\partial\phi}{\partial t}, \frac{\partial\phi}{\partial x}, \frac{\partial\phi}{\partial y}, \frac{\partial\phi}{\partial z}, \tag{3.2}$$

The preservation of Lorentz invariance is expressly maintained by this construction.

In the subsequent discussion, we will utilize the standard Einstein summation norms, which involves the use of repeating indices denoted by Greek letters such as μ, spanning from 0 to 3. In this context, the number 0 represents the temporal component, and indices 1, 2, and 3 correspond to the spatially components. In the context of flat spacetime, the metric tensor is defined by:

$$g_{\mu\nu} = \begin{pmatrix} 1 & 0 & 0 & 0 \\ 0 & -1 & 0 & 0 \\ 0 & 0 & -1 & 0 \\ 0 & 0 & 0 & -1 \end{pmatrix} = diag\left[1, -1, -1, -1\right], \tag{3.3}$$

The connection between contravariant indices and covariant indices is established as $x_\mu = g_{\mu\nu x\nu}$.

In order to prioritize simplicity our objective is to find a formulation of L which encompasses the minimal number of derivatives. Given that L is a scalar and $\partial_\mu\phi$ is a 4-vector, it is necessary to consider the scalar product of the 4-derivatives of ϕ as a minimal condition. Therefore, our preliminary selection for the variable L is:

$$\mathcal{L} = \frac{1}{2}\partial^\mu\phi\partial_\mu\phi = \frac{1}{2}\left(\partial_\mu\phi\right)^2, \tag{3.4}$$

$$= \frac{1}{2}\frac{\partial^2\phi}{\partial t^2} - \frac{1}{2}\left(\boldsymbol{\nabla}\phi\right)^2, \tag{3.5}$$

The incorporation of a factor of $1/2$ is employed in order to streamline subsequent computations, and the metric for a flat spacetime is utilized. Similar to the $\mathcal{L}$ in classical mechanics that characterizes particles. the expression $[(1/2)(\partial_\mu\phi)^2]$ is frequently linked to the "kinetic" energy of the field.

Based on the given formulation of L , what conclusions can be derived regarding the features of ϕ?

By substituting Equation (3.4) into the E-L equation,

$$\left\{\frac{\partial\mathcal{L}}{\partial\phi} - \partial_\mu\left(\frac{\partial\mathcal{L}}{\partial\left(\partial_\mu\phi\right)}\right) = 0,\right\} \tag{3.6}$$

considering this:

$$\left[\frac{\partial\mathcal{L}}{\partial\phi} = 0\right], \tag{3.7}$$

$$\left[\frac{\partial\mathcal{L}}{\partial\left(\partial_\mu\phi\right)} = \partial^\mu\phi,\right] \tag{3.8}$$

we deduce from Equation (3.6)

$$\partial_\mu\partial^\mu\phi = \frac{\partial^2\phi}{\partial t^2} - \nabla^2\phi = 0 \tag{3.9}$$

The wave equation for the scalar field ϕ implies that the current$j_\mu = \partial_\mu \phi$ is preserved as a result of the equation $[\partial_\mu j^\mu = 0]$.The principle of current conservation arises from the persistent shift symmetry exhibited by the Lagrangian subjected to transformations. $\phi \rightarrow \phi + constant$, which is a direct outcome of Noether's theorem [30].

The solution to eq (3.9) can be obtained by employing solutions in the form of:

$$\left[\phi(\boldsymbol{r}, t) = \varphi_o e^{i(\boldsymbol{k}\cdot\boldsymbol{r} - \omega t)}\right], \tag{3.10}$$

The sign φ_0 represents the amplitude of a certain mode that corresponds to the scalar field being studied. The variable ω represents frequency, while k represents wave vector. Within the framework of natural units , symbol ω represents the energy E associated with the field ϕ. Using the energy operator yields this energy . $\left(\hat{E} = i(\partial/\partial t)\right)$ to the function $\phi(\boldsymbol{r}, t)$. In a similar vein, the wave vector k can be associated with the momentum P of the field ϕ. This association is established by using the momentum operator $(P = -i\nabla)$ to the field $\phi(\boldsymbol{r}, t)$.

Upon substitution, Eq (3.10) in Eq (3.9), dispersion relation can be obtained.

$$\omega^2 = |k|^2, \tag{3.11}$$

which is equivalent to:

$$E = |p|. \tag{3.12}$$

Among the fundamental principles in Quantum Field Theory is the idea that quantum excitations may be understood as particles originating from fields. According to the dispersion relation (3.12), it can be observed that the field denoted as ϕ possesses both zero momentum $(|p| = 0)$ and zero energy $(E = 0)$. This implies that the particles associated with ϕ possess a rest mass of zero $(m = 0)$. It is imperative to acknowledge that similar principles are applicable to classical domains as well. The determination of the "mass" of a classical field is established by the curvature of the dispersion relation in the vicinity of $(|k| = 0)$.

To conform toThe astrophysics observations that have been addressed in the previous chapters, it is necessary for the particles associated with φ to exhibit characteristics of cold dark matter, indicating that they cannot have zero mass. In order to develop a theoretical framework that incorporates particles with mass, it becomes necessary to make adjustments to the Lagrangian density (3.5) in order to incorporate an energy penalty associated with non-vacuum field values. The inclusion of a potential energy term that is dependent on the variable ϕ in the Lagrangian can lead to the attainment of this objective.

$$\mathcal{L} = \frac{1}{2}(\partial_\mu \phi)^2 - \frac{1}{2}m^2\phi^2, \tag{3.13}$$

The factor $m^2/2$ is selected to ensure suitable units and facilitate future outcomesThe rationale behind incorporating a negative sign in the potential energy component may be attributed to the definition of the Lagrangian, which is established as the disparity between

kinetic energy as well as potential energy. . Consequently, it follows that higher values of the field correspond to an increase in potential energy. In order to establish the validity of our theoretical framework in describing particles with significant mass, it is possible to re-derive the dispersion relation by incorporating the variable L from Equation (2.13). From this point forward:

$$\frac{\partial \mathcal{L}}{\partial \phi} = -m^2 \phi, \tag{3.14}$$

the E–L eq (3.6) yields:

$$\left(\partial_\mu \partial^\mu + m^2\right)\phi = 0 \tag{3.15}$$

known as the K–G equation. Solutions of the K–G eq (3.15) take the form as:

$$\phi(\boldsymbol{r}, t) = \varphi_0 e^{-i(Et - \boldsymbol{p}\cdot\boldsymbol{r})}. \tag{3.16}$$

The dispersion relation is expressed as:

$$E^2 = |\boldsymbol{p}|^2 + m^2. \tag{3.17}$$

The eq (3.17) demonstrates that in the case when the field ϕ possesses zero momentum, denoted as $|p| = 0$, it possesses energy that is of a similar magnitude to the rest mass of the associated particle, represented as $E = m$. Therefore, the Lagrangian equation presented in Eq (3.13) offers a straightforward framework for characterizing macroscopic particles, which might possibly encompass DM.

In Figure 2.1, a comparison study is shown, showcasing the dispersion relation for without mass particles as obtained from Eq (3.4), and the dispersion relation for large particles as determined from Eq (3.13). . One notable characteristic of the scalar field, which will be further discussed in this text, is its behavior as a nonrelativistic bosonic field. In this context, when the magnitude of the momentum $(|p|)$ is significantly smaller than the mass (m), the field undergoes oscillations at a frequency known as the Compton frequency, approximately denoted as $\omega \approx m$.

3.3.1 Origin of an Ultralight-Bosonic Field

We investigate the phenomena of the explicit and spontaneous breakdown of a complex scalar field's $U(1)$ symmetry. . Through the presentation of an illustrative scenario, we want to provide insights into the development of an ultralight bosonic field together with these symmetry-breaking mechanisms . rather than taking into account two real scalar fields, denoted as α , β, we will now focus on a single complex scalar field φ. This complex scalar field can be related in the following manner:

$$\varphi = \alpha + i\beta. \tag{3.18}$$

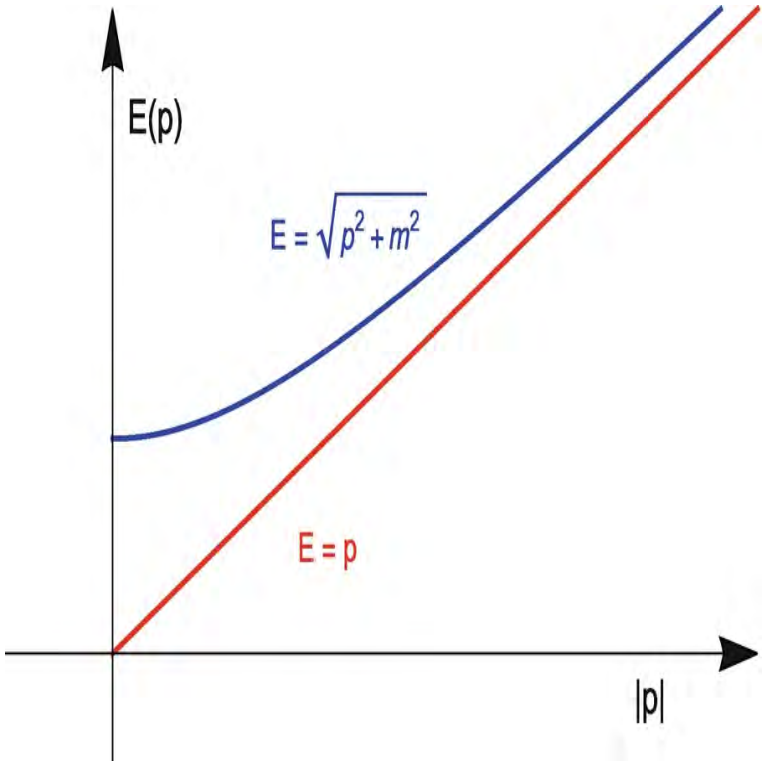

Figure 3.1: The dispersion relationship for a massless boson (red line) according to Eq. (3.12), along with the one of a massive boson (blue curve) according on Eq. (3.17), are plotted in comparison. The cost of energy for zero-momentum the excitations of the field, which is indicated by the positive intercept of the curve of dispersion on the energy axis, is a crucial characteristic of the massive boson.

with Lagrangian of the form

$$\mathcal{L} = \frac{1}{2}(\partial^{\mu}\varphi)^{\dagger}(\partial_{\mu}\varphi) + \frac{\mu^2}{2}\varphi^{\dagger}\varphi - \frac{\lambda}{4!}\left(\varphi^{\dagger}\varphi\right)^2, \tag{3.19}$$

Subsequently, by utilizing polar coordinates to re-parameterize the complex field:

$$\varphi = \rho e^{i\theta}, \tag{3.20}$$

we arrive at an alternative Lagrangian form (3.19):

$$\mathcal{L} = \frac{1}{2}(\partial_{\mu}\rho)^2 + \frac{1}{2}\rho^2(\partial_{\mu}\theta)^2 + \frac{\mu^2}{2}\rho^2 - \frac{\lambda}{4!}\rho^4 \tag{3.21}$$

It is noteworthy to mention that the Lagrangian expressed in the above equations shows a global $U(1)$ symmetry with respect to the variable φ. The $U(1)$ symmetry indicates that a global transformation, where the field φ is replaced by φ multiplied by the complex exponential of θ', does not affect the Lagrangian L. The notation $U(1)$ denotes the one-dimensional unitary group, which is a mathematical representation of complex numbers that have a magnitude equal to 1. As a result, the $U(1)$ symmetry can be interpreted as representing rotations within the complex plane.

In a manner akin to the situation with the real valued fields α and β, the potential demonstrates formation of minima that arrange themselves with a ring of a radius denoted as $\left[\rho = \rho_0 = \sqrt{6}\mu^2/\lambda\right]$. It is postulated that the $U(1)$ symmetry undergoes spontaneous breaking, resulting in the transformation of ρ to $\rho_{_0}$ and θ to 0.The Lagrangian is described in terms of $\rho = \rho - \rho_0$ and performing algebraic operations, we can derive the following expression:

$$\mathcal{L} = \frac{1}{2}(\partial_{\mu}\bar{\rho})^2 + \frac{1}{2}\rho_0^2(\partial_{\mu}\theta)^2 - \mu^2\bar{\rho}^2 - \frac{\lambda}{6}\rho_0\bar{\rho}^3 - \frac{\lambda}{24}\bar{\rho}^4 + \left(\frac{\bar{\rho}^2}{2} + \rho_0\bar{\rho}\right)(\partial_{\mu}\theta)^2, \tag{3.22}$$

Here, we have omitted constant terms that do not influence the physics. In Equation (3.22), terms that are free of dependence on θ and linearity in ρ^{-} cancel out. Focusing on second-order or lower terms in ρ^{-} and θ, we approximate:

$$\mathcal{L} \approx \frac{1}{2}(\partial_{\mu}\bar{\rho})^2 + \frac{1}{2}\rho_0^2(\partial_{\mu}\theta)^2 - \mu^2\bar{\rho}^2, \tag{3.23}$$

This can be compared to Equation (3.32). The relationship between the variables $\theta, \beta,$ and ρ_0 in Equation 3.23) can be expressed as $\theta = \beta/\rho_0 \approx \beta/f$, where f represents the scale of spontaneous symmetry breaking as given in Equation (3.43).

proceeding to implement explicit symmetry breaking by introducing a tilt to the potential in the Lagrangian (3.21) at an angle of ε towards the direction of $\theta = 0$.The explicit symmetry breakdown can be parametrized and clearly depicted in Figure 2.6. The introduction of a tilt via the parameter ε introduces the reliance on the variable angle θ to the potential. When considering the complex number $\varphi = \rho_{_0}e^{i\theta}$, the real component of this field may be expressed as $Re(\varphi) = \alpha = \rho_{_0}cos\theta$. The low of the tilted potential is observed at $\theta = 0$,

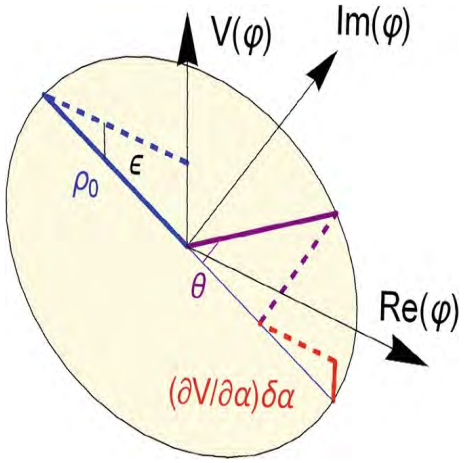

Figure 3.2: The accompanying figure presents a schematic representation of the impact of explicit symmetry breaking resulting from a tilt, characterized by an angle ϵ, in the quartic potential of the complex scalar field φ .In the given diagram, the solid purple radial line represents a specific value of $\varphi = \rho_0 e^{(i\theta)}$, where $\alpha = Re(\varphi)$, and the dashed red line illustrates the approximate deviation $\delta\alpha \approx \rho_0(cos\theta - 1)$. Additionally, the partial derivative of V with respect to α, denoted as $\partial V/\partial\alpha$, is equal to $-\varepsilon_\mu 2\rho_0$.

resulting in a shift in potential relative to the minimum.

$$\delta V(\theta) = \frac{\partial V}{\partial \alpha}\delta\alpha = \epsilon\mu^2\rho_0^2(1-\cos\theta), \tag{3.24}$$

Incorporating this term into the Lagrangian (3.23), we arrive at:

$$\mathcal{L} \approx \frac{1}{2}(\partial_\mu\bar{\rho})^2 + \frac{1}{2}\rho_0^2(\partial_\mu\theta)^2 - \mu^2\bar{\rho}^2 - \epsilon\mu^2\rho_0^2(1-\cos\theta), \tag{3.25}$$

using relations

$$|V_{\text{ min}}| \sim \frac{\mu^4}{\lambda^2} \sim f^4 \text{ , , } |V_\epsilon| \approx \epsilon\lambda\alpha_0^4 \sim \epsilon\frac{\mu^4}{\lambda} \sim \Lambda^4 \text{ .and } m_\beta^2 \sim \epsilon\mu^2 \sim \left(\epsilon\frac{\mu^4}{\lambda}\right) \times \left(\frac{\lambda}{\mu^2}\right) \sim \frac{\Lambda^4}{f^2} \text{ . , } \tag{3.26}$$

in to the previous approximation $\theta \approx \beta/f$, to express:

$$V(\beta) = m_b^2 f^2\left[1-\cos\left(\frac{\beta}{f}\right)\right] = \Lambda^4\left[1-\cos\left(\frac{\beta}{f}\right)\right], \tag{3.27}$$

Expanding $V(\beta)$ around $\beta = 0$ yields:

$$V(\beta) \approx \frac{1}{2}m_b^2\beta^2 \approx \frac{1}{2}\frac{\Lambda^4}{f^2}\beta^2. \tag{3.28}$$

This demonstrates that the β field has obtained a minor mass $\propto \sqrt{\epsilon}$ as a result of explicit symmetry breakdown.The symbol β is used to denote the ultralight bosonic field that is being sought for. The quantum excitations of this field are usually referred to as pseudo-Goldstone bosons or pseudo-Nambu-Goldstone bosons [31].

3.3.2 Relation of dark sector and SM

The primary inquiry we shall explore concerns the interaction among ultralight bosonic fields and particles within the SM[32], as well as fields that extend outside the realm of gravity. In order to enhance comprehension of these interactions, we will proceed to engage with the basic model of an ultralight bosonic field that was initially presented in the previous Section . Interactions across distinct fields under the framework of Quantum Field Theory (QFT) manifest themselves when the Lagrangian incorporates expressions that encompass both fields as multiplicative factors. This enables us to investigate the relationships between the α (or a¯) and β fields that were previously mentioned. The coupling constant "g" represents the constant coefficient before the terms. It serves as a measure of the strength of the field interactions, or in a scenario of the $\bar{a}^3$ term as self-interactions. The coupling constant can be mathematically represented in relation to the scale of spontaneous symmetry breaking denoted as "f".

$$g = \frac{\lambda\alpha_0}{6} = \frac{1}{\sqrt{6}}\frac{\mu^2}{f} \sim \frac{\mu^2}{f}. \tag{3.29}$$

Taking into account these interaction terms results in a new Lagrangian:

$$\mathcal{L} \approx \frac{1}{2}(\partial_\mu \bar{a})^2 + \frac{1}{2}(\partial_\mu \beta)^2 - \mu^2\bar{a}^2 - 3\epsilon\mu^2\beta^2 + \frac{1}{\sqrt{6}}\frac{\mu^2}{f}\bar{a}^3 + \frac{1}{\sqrt{6}}\frac{\mu^2}{f}\beta^2\bar{a}. \tag{3.30}$$

the above equations elucidate a noteworthy characteristic of ultralight bosonic fields, rendering them appealing contenders for dark matter: their interactions with other particles and fields typically exhibit a scaling behavior of $1/f$. When the symmetry breaking scale is chosen to be at a significantly high energy level, such as the (GUT) scale ($f \approx 10^{25}eV = 10^{16}GeV$) or the Planck scale ($f \approx 10^{28}eV = 10^{19}GeV$), the non-gravitational interactions involving ultralight bosons experience substantial suppression.

3.4 3.4 The Interplay of Ultralight Bosonic Fields and SM

In the subsequent section, an exploration will be conducted on the interplay between ultralight bosonic fields and particles within the framework of the Standard Model. By including terminology pertaining to particles, fields, and interactions inside the theory of the SM, together with the addition of terms representing bosonic fields of extremely low mass, a variety of interaction terms can be facilitated. The categorization of these interactions can be delineated into distinct phenomenological "portals" connecting the SM and dark sector. This classification is predicated on the observable consequences that would arise from the presence of (UBDM) in experimental settings. In order to gain a comprehensive understanding of various portals, we shall undertake an analysis of multiple interaction scenarios. This endeavor aims to offer valuable insights into the subject matter.

3.4.1 Axion photon interactions

To commence our analysis, we shall direct our attention towards a notably well-researched phenomenon pertaining to (UBDM), namely the interaction referred to as the axion-photon coupling [33]. process of turning axions or Axion-Like Particles (ALPs) into photons is considered crucial in the presence of intense magnetic fields. This idea serves as the foundation for several experimental methodologies, such as microwave cavity haloscopes, axion helioscopes that explore axion/ALP emissions originating from the Sun, "dark matter radios" that utilize lumped-element resonators, and light-shining-through-walls studies . $aF^{\mu\nu}\tilde{F}_{\mu\nu}$, which showcases an operator that encompasses a pseudoscalar axion (also known as an ALP) field denoted as "a," together with the electromagnetic field tensor (Faraday tensor) denoted as "$F_{\mu\nu}$,"and the dual field tensor denoted as"$\tilde{F}_{\mu\nu}$."The Faraday tensor, denoted as $F_{\mu v}$, is mathematically represented as:

$$F^{\mu\nu} = \partial^{\mu}A^{\nu} - \partial^{\nu}A^{\mu} \tag{3.31}$$

$$= \begin{pmatrix} 0 & -E_x & -E_y & -E_z \\ E_x & 0 & -B_z & B_y \\ E_y & B_z & 0 & -B_x \\ E_z & -B_y & B_x & 0 \end{pmatrix} \quad . \tag{3.32}$$

where "A_{μ}" is the four-potential, "E_i" and "B_i" are the Cartesian components of the electric and magnetic fields. The dual field tensor "$F_{\alpha\beta}$" is given by:

$$\tilde{F}_{\alpha\beta} = \frac{1}{2}\varepsilon_{\alpha\beta\mu\nu}F^{\mu\nu}. \tag{3.33}$$

where "$\varepsilon_{\alpha\beta\mu\nu}$" is the antisymmetric tensor. The operator responsible for the interaction between axions and photons demonstrates a distinct structure, characterized by the presence of one instance of the ultralight bosonic field "a" and bi instances of photon field. The structure in question has resemblance to the interaction terms, a similarity that becomes more evident when expressed in terms of the 4-potential "A_{μ}".

$$aF^{\mu\nu}\tilde{F}_{\mu\nu} = a\epsilon^{\mu\nu\alpha\beta}(\partial_{\mu}A_{\nu}\partial_{\alpha}A_{\beta}). \tag{3.34}$$

It is evident that the term denotes an exchange between an axion and two photons.

The Lagrangian includes a component that represents the interaction between the axion and photon.

$$\mathcal{L}_{a\gamma\gamma} = \frac{g_{\gamma}}{4}\frac{\alpha}{\pi}\frac{a}{f_a}F^{\mu\nu}\tilde{F}_{\mu\nu} = \frac{g_{a\gamma\gamma}}{4}aF^{\mu\nu}\tilde{F}_{\mu\nu}. \tag{3.35}$$

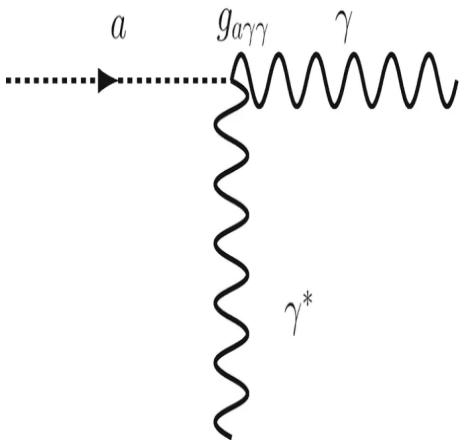

Figure 3.3: This feynman diagram depicts the inverse Primakoff effect, which showcases the conversion of an axion particle (a) into a real photon (γ) by its interaction of a virtual photon ($\gamma*$) generated by a magnetic field.

The symbol "g_γ" represents a dimensionless coupling factor that relies on the specific model being considered. The variable "α" denotes the fine structure constant, while "f_a" represents the scale at which spontaneous symmetry breaking occurs for the axion or ALP field. Additionally, the axion-photon coupling constant reads as "$g_{a\gamma\gamma} = g_\gamma \alpha/(\pi f_a)$". The inverse proportionality between the axion and photon coupling and the parameter "f_a" is a notable observation.The Lagrangian may be formulated in relation to the electric field "E" with magnetic field "B" in the following manner.

$$\mathcal{L}_{a\gamma\gamma} = \left(g_\gamma \frac{\alpha}{\pi} \frac{a}{f_a} \boldsymbol{E} \cdot \boldsymbol{B} \approx g_{a\gamma\gamma} a \boldsymbol{E} \cdot \boldsymbol{B} \right). \tag{3.36}$$

In experimental settings, the magnetic field denoted as "B" is commonly produced by techniques such as the application of electric current through a superconducting coil. Electric field denoted as "E" signifies the field that arises from the photons produced by the axion. The phenomenon in which axions are transformed into photons in the presence of a magnetic field is often named as the inverse Primakoff effect[34] . This process can be represented as Feynman diagram depicted in Figure 2.7.

In order to determine the measurable results arising from the interplay between axions and photons, the Euler-Lagrange equation is utilized on the combined Lagrangian that characterizes both electromagnetism and the axion-photon interaction, as described in Equation

$$\mathcal{L} = \left(-\frac{1}{4} F^{\mu\nu} F_{\mu\nu} \right) - (J^\mu A_\mu) + \left(\frac{g_{a\gamma\gamma}}{4} a F^{\mu\nu} \tilde{F}_{\mu\nu} \right). \tag{3.37}$$

The symbol "J_μ" is used to denote the electromagnetic current, whereas "A_μ" symbolizes the gauge potential. The inclusion of an axion field necessitates the modification of Maxwell's equations, leading to a revised formulation[35]

$$\boldsymbol{\nabla} \cdot \boldsymbol{E} = \rho + g_{a\gamma\gamma} \boldsymbol{B} \cdot \boldsymbol{\nabla} a, \tag{3.38}$$

$$\boldsymbol{\nabla} \cdot \boldsymbol{B} = 0 \ , \tag{3.39}$$

$$\boldsymbol{\nabla} \times \boldsymbol{E} = -\frac{\partial \boldsymbol{B}}{\partial t} \ , \tag{3.40}$$

$$\boldsymbol{\nabla} \times \boldsymbol{B} = \frac{\partial \boldsymbol{E}}{\partial t} + \boldsymbol{J} + g_{a\gamma\gamma}\bigg(\boldsymbol{E} \times \boldsymbol{\nabla} a - \frac{\partial a}{\partial t}\boldsymbol{B}\bigg). \tag{3.41}$$

where "$\boldsymbol{\rho}$" and "$\boldsymbol{J}$" has the chrage and electric density respectively.

In this analysis, we assume the spatial derivative of the axion field (∇a) could be omitted $(\nabla a \approx 0)$. In the given circumstances, when distinguishing between the overall magnetic field denoted as "B" and the induced fields "E" , "B" arising from the interplaybetween axions and photons (i.e., "$B = \boldsymbol{B_0} + B$"), and assuming that B_0 is significantly greater than B, the modified Maxwell's equations can be simplified as follows:

$$\boldsymbol{\nabla} \cdot \boldsymbol{E} = \boldsymbol{0}, \tag{3.42}$$

$$\boldsymbol{\nabla} \times \boldsymbol{\mathcal{B}} = 0, \tag{3.43}$$

$$\nabla \times \boldsymbol{E} = -\partial \boldsymbol{B}/\partial t, \tag{3.44}$$

$$\boldsymbol{\nabla} \times \boldsymbol{\mathcal{B}} = \frac{\partial \boldsymbol{\mathcal{E}}}{\partial t} - g_{a\gamma\gamma}\frac{\partial a}{\partial t}\boldsymbol{B}_0. \tag{3.45}$$

By applying the curl operator to Equation 3.44 and utilizing the provided identity,

$$\boldsymbol{\nabla} \times (\boldsymbol{\nabla} \times \boldsymbol{\mathcal{B}}) = \boldsymbol{\nabla}(\boldsymbol{\nabla} \cdot \boldsymbol{\mathcal{B}}) - \nabla^2 \boldsymbol{\mathcal{B}}. \tag{3.46}$$

along with Eq.(3.42) , (3.43), leads to:

$$-\nabla^2 \boldsymbol{\mathcal{B}} = \frac{\partial}{\partial t}\bigg(-\frac{\partial \boldsymbol{\mathcal{B}}}{\partial t}\bigg) - g_{a\gamma\gamma}\frac{\partial a}{\partial t}(\boldsymbol{\nabla} \times \boldsymbol{B}_0) = -\frac{\partial^2 \boldsymbol{\mathcal{B}}}{\partial t^2}, \tag{3.47}$$

where$\nabla \times \boldsymbol{B_0} = 0$. A similar procedure leads:

$$-\nabla^2 \boldsymbol{\mathcal{E}} = -\frac{\partial^2 \boldsymbol{\mathcal{E}}}{\partial t^2} + g_{a\gamma\gamma}\frac{\partial^2 a}{\partial t^2}\boldsymbol{B}_0, \tag{3.48}$$

resulting in the wave equations:

$$\bigg(\nabla^2 \boldsymbol{\mathcal{B}} - \frac{\partial^2 \boldsymbol{\mathcal{B}}}{\partial t^2}\bigg) = 0 \quad , \tag{3.49}$$

$$\nabla^2 \boldsymbol{\mathcal{E}} - \frac{\partial^2 \boldsymbol{\mathcal{E}}}{\partial t^2} = -g_{a\gamma\gamma}\frac{\partial^2 a}{\partial t^2}\boldsymbol{B}_0 \quad . \tag{3.50}$$

axions as dark matter manifestation may be observed as a field that undergoes oscillations at a Compton frequency denoted as m_a. since they are nonrelativistic. Given the long coherence time of the axion field, an appropriate initial model for the axion field is:

$$a(\boldsymbol{r},t) = \left\{ a_0 e^{i(\boldsymbol{k}\cdot\boldsymbol{r} - m_a t)} \right\}. \tag{3.51}$$

using cylidrical symmetry with $r = R$ and eq.3.48 and 3.49 leads to wave solutions as

$$\boldsymbol{\mathcal{E}}(\boldsymbol{r},t) = \left\{ g_{a\gamma\gamma} a_0 e^{-i\boldsymbol{m_a t}} \boldsymbol{B}_0 \left(1 - \frac{J_0(m_a x)}{J_0(m_a X)} \right) \right\} \quad , \tag{3.52}$$

$$\boldsymbol{\mathcal{B}}(\boldsymbol{r},t) = \left\{ i g_{a\gamma\gamma} a_0 e^{-i\boldsymbol{m_a t}} B_0 \hat{\boldsymbol{\phi}} \left(\frac{J_1(m_a x)}{J_1(m_a X)} \right) \right\} \quad . \tag{3.53}$$

where "$\boldsymbol{J}_{n(}x)$"is Bessel function . For "$m_a x \leq m_a X \ll 1$," it can approximated by taylor expansion

$$\boldsymbol{\mathcal{E}}(\boldsymbol{r},t) \approx \left[g_{a\gamma\gamma} a_0 e^{-i\boldsymbol{m_a} t} \boldsymbol{B}_0 \left(m_a^2 R^2 - m_a^2 x^2 \right) \right], \tag{3.54}$$

$$\boldsymbol{\mathcal{B}}(\boldsymbol{r},t) \approx \left[i g_{a\gamma\gamma} a_0 e^{-i\boldsymbol{m_a t}} B_0 \hat{\boldsymbol{\phi}}(m_a x) \right]. \tag{3.55}$$

It is worth mentioning , in the given particular scenario, the magnitude of the induced E field is significantly diminished in comparison to B field, with a factor of approximately $m_a X$ being much smaller than 1.

Upon careful examination of the study conducted, it becomes apparent that the axion field possesses the potential to function as a source term with the ability to produce quantifiable electromagnetic energy via the inverse Primakoff effect.

Chapter 4

Dark photon production mechanism

Dark Photon Production Mechanism

Dark photons, also known as DPs, provide a compelling opportunity to investigate novel aspects of physics. They represent a minimal expansion of the Standard Model (SM) by serving as the gauge boson associated with an extra U(1) symmetry [36]. The field of DP dark matter (DPDM) has gained attention due to recent proposals introducing new mechanisms for its generation. These proposals specifically examine the extent of polarization that these mechanisms can imprint on the remnant DPDM. The significance of this particular component, which is sometimes overlooked in scholarly works, holds great importance in the prospective identification of these phenomena. It is crucial to acknowledge that the polarization of dipole moments (DPs) exhibits variations in comparison to the isotropy of the stress-energy tensor linked to the field. Moreover, these variations are dependent on the particular production process utilized.

One of the most straightforward approaches to manufacture Dark Photon Dark Matter (DPDM) involves the utilization of the misalignment mechanism [37], which has resemblance to the widely employed method employed for axion generation. In contrast to axions, the attainment of the appropriate relic abundance for dark photons necessitates the inclusion of a nonminimal coupling to the Ricci scalar, in addition to the gravitational interaction. The connection between variables, although it maintains the desired abundance, leads to instability in the longitudinal mode of DPs. As a result, further theoretical considerations are required to ensure consistency. The aforementioned situation, commonly

known as the fixed polarization scenario, results in the presence of relic dark photon dark matter (DPDM) with a persistent polarization confined within the cosmic horizon. Another method that might be considered equivalent is the formation of Dark Photon Dark Matter (DPDM) through quantum fluctuations that occur during the inflationary period[38]. This mechanism exhibits a power spectrum that is concentrated at intermediate wavelengths, thereby avoiding certain constraints.

Another fascinating situation arises from the occurrence of tachyonic instabilities. This phenomenon occurs when dipole moments (DPs) interact with a misaligned axion,[39] leading to the transfer of energy from the axion field to both transverse and longitudinal components of the DPs. These methods primarily generate a distinct helicity in the produced DP, which suggests that the relic DPs would also possess the same helicity, but there may be a potential reduction due to scatterings. Additional scenarios propose even greater levels of polarization, which may persist even after scatterings. However, further investigation of these models requires the use of lattice simulations.

The phenomenon of (DPDM) may also arise as a result of the decay of topological defects, such as a network composed of nearly-global, Abelian-Higgs cosmic strings[40]. The observed scenario exhibits a preference for longitudinally polarized dipole moments (DPs) as a result of the inhibition of interactions involving transversely polarized DPs. The growth of the network encompasses both finite closed loops and infinite strings. It is possible that there exists a tendency for polarization alignment to occur among extended strings, while the convergence of smaller closed loops may eventually reduce this alignment. When dual-polarized (DP) systems do not possess a singular polarization, this circumstance is commonly denoted as the random polarization situation.

4.1 UBDM from Extra Dimensions

The framework of string theory, which seeks to unite fundamental forces and provide a comprehensive description of the universe's structure, holds significant implications for our comprehension of physics, particularly in relation to scenarios involving ultralight bosonic dark matter (UBDM). In the present context, string theory postulates the existence of a universe that surpasses the conventional four dimensions of spacetime, including a total of ten dimensions. The deviation from the normal four-dimensional spatial framework presents

both challenges and opportunities in the realm of physics, particularly in the exploration of exotic phenomena such as candidates for Beyond the Standard Model (UBDM).

Within the theoretical framework of string theory, it is postulated that the geometry of additional dimensions should be described by unique functions embedded within the metric tensor [41]. These functions, in turn, are influenced by both spatial and temporal factors. In addition, the gravitational significance of the curvature in these additional dimensions plays a role in contributing to the overall energy content of the cosmos. In order to ensure the compatibility of the theory with empirical facts, it is imperative that these additional dimensions possess a level of compactness that has hitherto evaded detection. Nevertheless, the possible gravitational impact of differences in the curvature of these dimensions over space cannot be disregarded. This mechanism facilitates the emergence of UBDM (Ultralight Bosonic Dark Matter) from string theory, resulting in the production of scalar moduli and pseudoscalar axions.

In order to elucidate this concept, we shall analyze a straightforward illustration that emerges not alone in the realm of string theory, but also in theories encompassing supplementary dimensions of spacetime, Kaluza-Klein theory, Randall-Sundrum theory, and theories of supergravity in higher-dimensions [42] [43]. Let us examine a spacetime characterized by D dimensions, consisting of $(3+1)$ dimensions of flat Minkowski space labeled as M4, which possesses the customary coordinates, together with an additional compact dimension represented by the manifold $S1$. The manifold $S1$ is topologically similar to a circle, and its coordinate θ wraps around it. Within the context of general relativity, the metric corresponding to the present circumstance is expressed as follows:

$$ds^2 = \left(-dt^2 + dx^2 + \rho(x,\theta,t)^2 L^2 d\theta^2\right). \tag{4.1}$$

The value of ρ is subject to variation when θ traverses the circumference of the circle. Furthermore, its determination is contingent upon the spatial and temporal dimensions within the framework of Minkowski space that we are accustomed to. The scalar field denoted by ρ is commonly referred to as the radion in academic literature.

In order to enhance comprehension of this notion, one may employ a metaphorical visualization wherein space is likened to a unidimensional tightrope, while ρ serves as a means to characterize the alterations in the tightrope's cross-sectional area along its longitudinal extent. Although the changes in ρ may not be readily apparent to human observers while

traversing the tightrope, it is plausible that a diminutive organism such as an ant may discern these variations by circumnavigating the rope. Although direct detection of changes in ϱ may not be possible, it is conceivable that alterations in attributes such as the thickness or texture of the rope could be observed indirectly.

Within the given framework, the physics of the theory is elucidated by the Einsteins-Hilbert action.

$$S = \frac{M_D^{D-2}}{2} \int \left(dt d^3x L d\theta \sqrt{-g_D} \mathcal{R}_D \right). \tag{4.2}$$

In the above setting, the symbol D denotes the overall count of dimensions in spacetime.M represents the reduced Planck mass in a D-dimensional space, while g_D signifies the determinant of the metric in D dimensions. Lastly, $\mathcal{R}_D$ denotes the Ricci scalar in a D-dimensional spacetime.

The procedure of integrating over the compact coordinate θ gives rise to a phenomenon referred to as "dimensional reduction," wherein the outcome is an action which exhibits 2nd-order derivatives of scalar fields ρ_n. The introduction of θ derivatives the Ricci scalar results in the inclusion of terms that are proportional to n^2. These terms effectively confer mass properties to the scalar fields ρ_n. The significance of these components increases when we consider higher modes inside the Kaluza-Klein tower, characterized by bigger values of n. However, in the context of low-energy physics, it is common practice to neglect higher modes and instead concentrate on the lowest mode, represented by $n = 0$. In this particular state, the scalar field denoted as ρ_0 demonstrates characteristics of a massless scalar field, serving as a representation of our perception of the variation in the size of the additional dimension as we traverse across spacetime.

Moreover, by adopting additional principles from physics, it is possible for the scalar field ρ_0 to gain a slight mass. This can occur due to causes that are analogous to the ones outlined in the context of tiny "explicit symmetry breaking." [44]The current configuration creates a conducive atmosphere for the formation of UBDM candidates. In more complex situations, it is conceivable to imagine additional dimensions exhibiting varied topologies that extend beyond the elementary S1 circle. In instances of this nature, a diverse array of fields denoted as ϱ are important for characterizing the compact space, and these fields are commonly known as moduli. By including other principles from physics, such as various string theory phenomena and symmetries, the theoretical framework is broadened to incorporate

not just scalar particles but also pseudoscalar axion-like particles (ALPs) and a diverse range of other unconventional fields.

String theory provides a rich platform for investigating ultra-high energy cosmic ray candidates. It showcases how these candidates might emerge organically from the study of higher-dimensional spacetime and the interplay of diverse fields within this theoretical framework.

4.2 Non-thermal Production of UBDM

the ultralight bosonic dark matter (UBDM) candidates' having incredibly low masses, breaking out of thermal equilibrium is necessary to produce cold populations that can fully account for the universe's dark matter component. The kinetic energy of these particles, if they were created thermally [45], would be too great for them to be considered cold dark matter. A technique known as "vacuum misalignment" is used to produce cold UBDM populations [46]. This mechanism acts outside of equilibrium and has the potential to produce populations of UBDM that are subzero.

For vacuum misalignment, particular circumstances are needed. The UBDM field within our visible horizon is homogeneous during inflation. During this time, vacuum misalignment takes over as the main process producing UBDM particles. An additional factor comes into play, though, if the UBDM candidate develops as a result of a phase shift that takes place after the inflationary epoch. It is also necessary to consider how cosmic strings and domain walls can produce UBDM particles. This scenario basically comprises a different manifestation of the vacuum misalignment phenomenon, but this time with respect to the UBDM field as a whole. It is theoretically connected to vacuum misalignment.

4.2.1 Vacuum Misalignment

The difference between a field's initial value and the minimum of its potential, also known as its vacuum expectation value, is the core idea of the vacuum misalignment mechanism. This mechanism, which causes the field to fluctuate around the lowest of the potential, results in the energy density associated with the oscillatory field, which in the case of (UBDM) is the dark matter itself. . Vacuum misalignment is the phrase used to describe this process since the field's initial value is not aligned with the potential's lowest point.The isotropy,

homogeneity, and expansion of the Universe on huge cosmic scales can all be characterized by the (FLRW) metric. The EOM can be obtained for a scalar field denoted by and having an effective potential $V(\phi)$ by building Lagrangian L employing the FLRW metric rather than the flat spacetime metric. This produces the following equation, which represents a harmonic oscillator operating in a FLRW metric:

$$\left(\frac{\partial^2}{\partial t^2} + 3\frac{\dot{R}(t)}{R(t)}\frac{\partial}{\partial t} - \frac{1}{R^2(t)}\boldsymbol{\nabla}^2\right)\phi(t,\mathbf{x}) + \frac{\partial V}{\partial \phi} = 0. \tag{4.3}$$

When examining potential candidates for dark matter, such as the hidden photon, it becomes evident that the spatial components of the vector boson field adhere to an equation of this nature. the above eq. 4.3 provides a concise representation of the dynamics exhibited by a harmonic oscillator embedded in an expanding Universe. In scenarios characterized by a homogenous field across the pertinent scale, the spatial derivative in the equation can be disregarded. By introducing the $H(t) = \dot{R}(t)/R(t)$, which is linked to the energy density of radiation during the early stages of the Universe, this can be rendered in a simpler form.

$$\left(\frac{\partial^2}{\partial t^2} + 3H(t)\frac{\partial}{\partial t}\right)\phi(t,\mathbf{x}) + \frac{\partial V}{\partial \phi} = 0. \tag{4.4}$$

The field's behavior depends on whether specific conditions are met. as the following:

$$\left(\frac{3}{2}\right)H(t) \gg \sqrt{\left(\frac{1}{\phi}\frac{\partial V}{\partial \phi}\right)}. \tag{4.5}$$

When the system reaches a state of satisfaction, the field undergoes overdamping and ceases to exhibit oscillatory behavior. Put simply, the field is unable to oscillate because its wavelength is too large to fit within the observed horizon, causing it to become "frozen." Nevertheless, when the potential satisfies the specified criterion:

$$\left(\frac{3}{2}\right)H(t) \simeq \sqrt{\left(\frac{1}{\phi}\frac{\partial V}{\partial \phi}\right)}. \tag{4.6}$$

The wavelength of the field is such that it is able to fit within the confines of the horizon, thereby enabling it to undergo unrestricted oscillations. The energy associated with these oscillations is contingent upon the starting condition, which is indicative of misalignment of the field relative to the potential minima. with the angle denoted as θ_i in this context represents the starting angle, which is associated with a certain field value ϕ_i. Over a period of

time, the field has the ability to undergo relaxation, resulting in the gradual reduction of the root-mean-square value towards zero. This process ultimately leads to the reestablishment of the vacuum state.

4.2.2 Vector Field Misalignment

The generation of a cold population of hidden photons is a significant outcome in the context of a vector ultralight bosonic dark matter (UBDM) candidate resulting from kinetic mixing. This outcome is mostly attributed to the process of vacuum misalignment. The present analysis will commence by examining the scenario of concealed photons, which is chosen as a simpler instance, despite the initial discussion of this mechanism being centered around the axion. The earliest presentation of the concept that the spatial aspect of a low-mass vector boson can also fulfill the equation of motion as specified by given Equations , resulting in the creation of a cold population, was documented in Reference [19].

We can examine the hidden photon field, represented as $\mathcal{X}_\mu$, which is anticipated to exhibit uniformity at the scale of the observable horizon subsequent to the inflationary epoch. This field commences with an initial random value. The EOM can be obtained by supposing the spatial derivative term $\partial_i \mathcal{X}_\mu$ to be negligibly small, owing to its spatial homogeneity.

$$\left(\frac{\partial^2}{\partial t^2} + 3H(t)\frac{\partial}{\partial t}\right)\mathcal{X}_i(\mathbf{x}) + m_{\gamma'}^2 \mathcal{X}_i(\mathbf{x}) = 0. \tag{4.7}$$

The inclusion of the mass term $m^2{}_{\gamma'}$ in the equation creates an effective potential, which becomes significant when $m_{\gamma'} \neq 0$. When the requirement specified in Eq. 4.6 is met and the magnitude of $H(t)$ is about equal to $m_{\gamma'}$, the field undergoes oscillations, resulting in its behavior resembling that of cold dark matter.

One can obtain a direct limitation on the value of $m_{\gamma'}$ by imposing the condition that the Compton wavelength of the particle permits the creation of structures on kiloparsec scales [47]. The given condition, expressed as $1kpc < /(m_{\gamma'} v_{esc})$, and v_{esc} represents the escape velocity , establishes a minimum value for the quantity $m_{\gamma'} c^2 \geq 1.7 \times 10^{-24}$ eV. Further limitations can be derived by taking into account decay processes, interactions involving the DP and other particles, and empirical data.

Chapter 5

Dark photon in inflationary era

Production of Dark Photons during inflation

This section presents a description of experimental setup, which involves the inclusion of a dark photon with a significant mass [48]. The dark photon is observed to have a coupling with the inflaton and operates within the framework of an inflationary background. The primary aim of this research is to examine the manufacturing process of a light dark photon dark matter (DPDM) within the context of the inflationary period. To disrupt the conformal invariance of a non-massive DPs and amplify its generation, we investigate a direct approach that effectively produces low-mass vector bosons through a kinetic interaction with the inflaton field, denoted as φ.

5.1 DP and the inflaton field

The action of particular interest is as follows:

$$S = \int \mathrm{d}^4x\sqrt{-g}\left[\frac{M_{\mathrm{P}}^2}{2}R - \frac{1}{2}\nabla_\mu\varphi\nabla^\mu\varphi - V(\varphi) - \frac{I^2(\varphi)}{4}F'_{\mu\nu}F'^{\mu\nu} - \frac{m_{\gamma'}^2}{2}A'_\mu A'^\mu\right]. \tag{5.1}$$

In the context of the metric convention $(-+++)$, the symbol M_{Pl}, R and ∇_μ these quantities are defined in a manner that is consistent with the metric $g_{\mu\nu}$. The symbol $V(\varphi)$ represents the potential of the inflaton. The coupling between the DP field, written as A'_μ, and the field, φ, occurs through the kinetic term of the DP field, which involves a function of φ. The field-strength tensor of the DP field is represented as,

$$F'_{\mu\nu} \equiv \partial_\mu A'_\nu - \partial_\nu A'_\mu. \tag{5.2}$$

The incorporation of the Stueckelberg/Proca mass $(m_{\gamma'})$ into the DP enables its recognition as non-relativistic dark matter in the current era. While it is theoretically possible for $m_{\gamma'}$ to depend on φ, we choose to disregard this reliance for the purposes of our current study. The essential component of our DP production mechanism is the modification of the kinetic term, or the dark $U(1)$ charge, under the influence of (φ) field. The modulation is represented by the function $I(\varphi)$.

in the inflationary period, it is assumed that the vacuum expectation values (VEVs) for the φ and the DP field are as follows: the inflaton VEV is denoted as ($\langle\varphi\rangle$) and is defined as $\phi(t) \neq 0$, while the dark photon field VEV is denoted as $\left\langle A'_{\mu}\right\rangle$ and is equal to zero. the generation of dark photons within proposed this mechanism yields a spectrum that exhibits a pronounced concentration at scales beyond the horizon. This suggests that, when observed by those within the sub-horizon, it can be perceived as a uniform "background," although not necessarily exhibiting isotropy. It is crucial to acknowledge that we must maintain the insignificance of the energy density of the generated DP in relation to that of the inflaton φ . This ensures the coherence and validity of our perturbative approach in studying the dark photon field in proximity to its null state.

The vacuum expectation value (VEV) of the inflaton typically exhibits temporal variation. The form of the flat (FLRW) metric is employed to describe the background spacetime during inflation.

$$\mathrm{d}s^2 = a^2(\tau)\left(-\mathrm{d}\tau^2 + \delta_{ij}\mathrm{d}x^i\mathrm{d}x^j\right). \tag{5.3}$$

In this context, the symbol τ is used to describe the conformal time, which is connected to the physical time t by the equation $(\mathrm{d}\tau = \mathrm{d}t/\boldsymbol{a})$. Here ,$a(\tau)$ represents the scale factor, and i takes on values of 1, 2, or 3 to represent the space index. In the context of the pure de-Sitter background, the correlation between the scale factor a and the conformal time τ is expressed as $a = \frac{-1}{H\tau}$, and $H \equiv \left(\partial_\tau a/a^2\right)$ represents the physical Hubble parameter, which remains constant. As the temporal dimension advances, the phenomenon of inflation initiates at a point where τ approaches negative infinity and subsequently evolves until a point where τ approaches zero. In this study, we consider a conventional slow-roll inflation scenario, which is a solution that exhibits attractor behavior when the slow-roll conditions, namely the conditions of ϵ_V and η_V, are met. The aforementioned constraints pertain to the derivatives of the inflaton potential, denoted as $V(\phi)$, and signify that the inflaton undergoes a gradual evolution during the inflationary period.

$$\epsilon_V \equiv \frac{M_{\mathrm{P1}}^2}{2}\left(\frac{V_\varphi}{V}\right)^2 \ll 1, \eta \equiv M_{\mathrm{PI}}^2\frac{V_{\varphi\varphi}}{V} \ll 1. \tag{5.4}$$

The variation over time of the (VEV) of the inflaton field, denoted as $\phi(t)$, along the trajectory of inflation leads to a changing value of the coupling between the dark photon and the inflaton field, represented as $\langle I(\varphi)\rangle \equiv I(\phi)$. In order to permit a rigorous analytical analysis, it is necessary to provide an assumption regarding the temporal evolution of the quantity $I(\phi)$ during the inflationary period. It is postulated that the coupling undergoes modification within the range of $a_i < a < a_{\mathrm{end}}$, where $[a_i\,(a_{\mathrm{end}})]$ denotes the scale factor values at the initiation and termination of inflation. Although the coupling function $I(\phi)$ has the potential to be dependent on either time or the scale factor a, we suggest a simplified approach by considering the time dependency of the coupling during the inflationary period.

$$I(\phi) = \left(\frac{a}{a_{\mathrm{end}}}\right)^n \approx \left(\frac{\tau_{\mathrm{end}}}{\tau}\right)^n. \tag{5.5}$$

This assumption adequately encompasses the fluctuation in coupling that occurred over the pertinent period of inflation. It is crucial to acknowledge that this approximate relationship hold at the primary level in the slow-roll growth. The process of normalization for the variable I guarantees that its numerical value reaches 1 upon the conclusion of inflation, so reinstating the canonical kinetic term associated with the dark photon field.

In the interval $(a_i < a < a_{\text{end}})$, where a_i and a_{end} represent the scale factor values at start and end of inflationtionary period . we make the assumption that the time-dependent coupling $I(\phi)$ is a real number n. The symbol τ_{end} represents the conformal time at the conclusion of the inflationary period, and it is calculated as the reciprocal of the negative value of $\tau_{\text{end}} = -(Ha_{\text{end}})^{-1}$. The final approximation, denoted by the symbol $\approx$, is valid at the leading order when considering the slow-roll expansion framework. In order to establish a consistent approach to treatment, we employ a normalization procedure for the function I that ensures it attains a value of 1 upon the conclusion of inflation and remains constant thereafter. The process of normalizing guarantees the restoration of the canonical kinetic term for the field of the DP. In the framework of the slow-roll approximation, the temporal dependency of the function $(I(\phi))$ could be generated by the specific functional form of the coupling.

$$I(\varphi) \approx \mathrm{e}^{-\frac{n}{MM_{\mathrm{P1}}^2}\int_{\varphi_{\text{end}}}^{\varphi} d\varphi' \frac{V(\varphi')}{V_\varphi(\varphi')}}. \tag{5.6}$$

5.1.1 Modes

5.1.1.1 The transverse modes

The analysis will commence by investigating the transverse mode sector, which is symbolically represented as S_T. In order to get canonical normalization for the field $A_i'^T$, we introduce the definition $V_i \equiv I(\phi)A_i^T$, where $I(\phi)$ represents a classical quantity. By considering the dependence of the function φ simply on time, we may derive the expression for ST.

$$S_T = \frac{1}{2}\int \mathrm{d}\tau \mathrm{d}^3x \left[\partial_\tau V_i \partial_\tau V_i - V_i\left(-\partial^2 - \frac{\partial_\tau^2 I}{I} + \frac{a^2 m_\gamma^2}{I^2}\right)V_i\right]. \tag{5.7}$$

where as $\partial^2 \equiv \partial_i\partial_i$. Next, we decompose Vi into Fourier components and polarization modes as follows:

$$V_i(\tau, \boldsymbol{x}) = \sum_\sigma \int \left(\frac{\mathrm{d}^3k}{(2\pi)^{3/2}}\mathrm{e}^{i\boldsymbol{k}\boldsymbol{x}}\epsilon_i^T(\hat{k})\hat{V}_{*\boldsymbol{k}}(\tau)\right). \tag{5.8}$$

where$e_i^\sigma(\hat{k})$The orthonormality of polarization vectors are defined as vectors that are orthogonal to the momentum path, denoted as k, which is equivalent to k divided by its magnitude.The state of reality, denoted as V_i,

$$P^\sigma e_i^\sigma(\hat{k})\hat{V}_{\sigma,k}^\dagger = P^\sigma e_i^\sigma(-\hat{k})\hat{V}_{\sigma,-k}. \tag{5.9}$$

which leads to

$$S_T = \frac{1}{2}\sum_{\sigma}\int d\tau\, d^3k \left[\partial_\tau \hat{V}^\dagger_{\sigma,k}\partial_\tau \hat{V}_{\sigma,k} - \left(k^2 - \frac{\partial_\tau^2 I}{I} + \frac{a^2 m_\gamma^2}{I^2}\right)\hat{V}^\dagger_{\sigma,k}\hat{V}_{\sigma,k}\right]. \tag{5.10}$$

The system's parity invariance guarantees that the mode functions of both polarizations are equal. In addition, the background isotropy ensures that the mode function is only dependent on the magnitude of the momentum, denoted as $k \equiv |k|$. As a result, it is possible to represent the operator $\hat{V}_{\sigma,k}$ in terms of creation and annihilation operators.

$$\left(\hat{V}_{\sigma,k}(\tau) = (V_k(\tau)\hat{a}_{\sigma,k}) + \left(V_k^*(\tau)\hat{a}^\dagger_{\sigma,-k}\right)\right), \tag{5.11}$$

$$[\hat{a}_{\sigma,k}, \hat{a}^\dagger_{\sigma_0,k_0}] = \delta_{\sigma\sigma_0}\delta^{(3)}(\mathbf{k}-\mathbf{k}_0). \tag{5.12}$$

and we can also derive the EOM for the mode function as:

$$\partial_\tau^2 V_k + \left(k^2 - \frac{\partial_\tau^2 I}{I} + \frac{a^2 m_\gamma^2}{I^2}\right)V_k = 0. \tag{5.13}$$

we solve this equation using the explicit form of $I(\tau)$ presented earlier, ultimately allowing us to calculate the relic abundance of dark photon dark matter.

5.1.1.2 Longitudnal mode

The focus of our analysis now turns to the longitudinal mode sector, which is represented by the symbol S_L. In a manner akin to the preceding instance, a Fourier transform is conducted on the longitudinal mode denoted as χ.as

$$\chi(\tau, x) = \int \frac{d^3k}{(2\pi)^{3/2}} e^{ik\cdot x}\hat{X_k}(\tau).$$

The function $\hat{X_k}$ satisfies the reality condition $\hat{X_k}$= $\hat{X}_{-k}$. As a result, the quadratic action pertaining to the longitudinal sector is transformed.

$$S_L = \frac{1}{2}\int d\tau\, d^3k\, a^2 m_{\gamma'}^2 \left[\frac{I^2k^2}{I^2k^2 + a^2 m_{\gamma'}^2}\right]\left[\partial_\tau \hat{X_k}\partial_\tau \hat{X_{-k}} - k^2 \hat{X_k}\hat{X_{-k}}\right].$$

By canonical normalization $\hat{X_k}$ as

$$\hat{X_k}(\tau) = \hat{X_k}(\tau) z_k(\tau),$$

$$z_k(\tau) \equiv \frac{a m_{\gamma'} I_k}{\sqrt{I_k^2 k^2 + a^2 m_{\gamma'}^2}}, \tag{5.14}$$

we get

$$S_L = \frac{1}{2}\int d\tau\, d^3k \left[\partial_\tau X_k^\wedge \partial_\tau X_{-k}^\wedge - k^2\left(\frac{z_k}{z_k}\right)\hat{X_k}\hat{X_{-k}}\right], \tag{5.15}$$

We get the following expression for S_L

$$S_L = \frac{1}{2}\int d\tau\, d^3k \left[\partial_\tau \hat{X}_k \partial_\tau \hat{X}_k - \left(k^2 - \frac{\partial_\tau^2 z_k}{z_k} + \frac{a^2 m_{\gamma'}^2 I^2}{I_k^2 k^2 + a^2 m_{\gamma'}^2}\right)\hat{X}_k \hat{X}_k\right]. \tag{5.16}$$

up to terms that are total derivatives. Similar to the transverse modes, the mode function only depends on the magnitude of the momentum, $k \equiv |k|$. We further decompose $X_k^\wedge$ into the creation and annihilation operators:

$$\hat{X}_k(\tau) = \left(X_k(\tau)\hat{a}_{L,k} + X_k^*(\tau)\hat{a}_{L,-k}^\dagger\right), \tag{5.17}$$

$$[\hat{a}_{L,k}, \hat{a}_{L,k_0}^\dagger] = \delta^{(3)}(\mathbf{k} - \mathbf{k}_0). \tag{5.18}$$

We derive the EOM for the mode function X_k

$$\partial_\tau^2 X_k + \left(k^2 - \frac{\partial_\tau^2 z_k}{z_k} + \frac{a^2 m_{\gamma'}^2 I^2}{I_k^2 k^2 + a^2 m_{\gamma'}^2}\right) X_k = 0. \tag{5.19}$$

using this equation we can also calculate the relic abundance.

Chapter 6

Investigating the DPDM through an oscillating Dilaton

6.1 Overview

Ultralight dark photons, characterized as spin-1 vector bosons, offer a compelling prospect as a potential constituent of dark matter (DM) within our Universe [49] [50]. Comparable to scalar fuzzy dark matter , these ultralight dark photons exhibit wave-like characteristics on a broader range, reaching up to approximately 10 parsecs. This feature is particularly prominent for masses above 10^{-21}[51] . The existence of DPs has the potential to generate vector solitonic cores that exhibit similarities to those reported in scalar fuzzy dark matter. However, a noteworthy distinction can be observed in their intrinsic spin [52]. The inclusion of vector fields in the composition of these condensates presents the potential for the emergence of distinct high-energy solitonic structures like Proca stars, which are distinguished by radially oriented vector fields. The presence of self-interactions [53]among these dark photons gives rise to the formation of stable structures that bear resemblance to stars. The vector form of dark matter has distinct characteristics on smaller scales in comparison to its scalar counterpart, mostly due to its distinct mechanisms of formation. As a consequence, it often manifests a highly pronounced power spectrum at these scales. The presence of such a spectrum suggests the existence of complex, fine-grained structures, with a significant proportion of the energy density attributed to boson stars [54].

The examination of dynamical heating impacts on ultrafaint dwarf galaxies, with a focus on coherent fluctuations in fuzzy dark matter, has prompted a reevaluation of the mini-

mum mass range. This reevaluation proposes a lower threshold of $m_{fdm} > 10^{-19}eV$. [55] It is anticipated that the vector scenario will exhibit somewhat looser limitations due to the diminished interference of numerous polarization states. According to existing research [56], there is evidence supporting a minimum value of $m_{fdm} > 10^{-18}eV$ as a universal lower limit for dark matter when its origin is linked to a causal event occurring after the inflationary period. The superradiance limits associated with solar-mass black holes impose limitations on the mass ranges $(10^{-13} - 10^{-11}eV)$ of both scalar and vector fields[57] [58] . However, these limitations can be circumvented by incorporating vector field self-interactions, thereby allowing for a wider range of feasible masses.

Nonetheless, the production of DPDM inside the realm of ultralight masses continues to pose a significant obstacle. The initial models, which were initially inspired by the creation mechanisms of scalar dark matter[59], subsequently indicated the necessity of incorporating nonstandard couplings with the Ricci scalar [60]. The graviton-photon interactions may potentially violate unitarity at specific energy scales. During the slow-roll inflation phase, dark photons that exhibit little coupling to Einstein gravity, while remaining independent from other matter fields, are generated. However, the observed abundance of these dark photons is consistent with dark matter only when the mass of the dark photon, denoted as $m_{\gamma'}$, is on the order of $10^{-5}eV$. [61] The synthesis of ultralight dark photons with the requisite abundance of dark matter can be achieved using production procedures that involve an oscillating Higgs or an oscillating, misaligned axion [62]. Nevertheless, these models, which are firmly rooted in robust theoretical foundations, prompt relevant inquiries regarding the intrinsic naturalness and selection of couplings [63].

In this study, a novel methodology is presented centered around resonance phenomena to generate dark photon dark matter (DPDM) without relying on excessively huge couplings. In addition to the DP, this theoretical framework incorporates a scalar field, denoted as ϕ, which is dynamically connected to the DP by an interacting term in the Lagrangian density given by $L \supset W(\phi)F_{\mu\nu}F^{\mu\nu}/4$. Previous studies [64] have examined this particular form of interaction, wherein the variable ϕ has been utilized as the inflaton. In order to accurately determine the quantity of ultralight dark photons during slow-roll inflation, it is necessary to consider the effective dependency of the coupling on the (FLRW) scale factor. This dependence may be expressed as $W(\phi(a)) \propto a^{-n}$, where the exponent n is approximately equal to 4. Previous studies [65] have examined the role of the scalar field, denoted as φ, as a pas-

sive participant in the inflationary process, which subsequently resulted in the production of dark photons with significant spatial scales. Nevertheless, this methodology considers ϕ as a low-mass field that undergoes oscillations after the inflationary period, leading to the generation of vector dark matter by resonance.

Efficient dark photon creation is observed when the dilaton exhibits strong oscillations, resembling models incorporating axion couplings. Resonances of this nature tend to exhibit limited efficacy when subjected to oscillation amplitudes of minuscule magnitudes. However, in the context of dilatonic coupling, a significant instability arises at low momenta when the mass of the vector particle is equal to half the mass of the dilaton. This instability is particularly pronounced during periods of small amplitude oscillations. In this model, the function $W(\phi)$ is defined as the exponential of the ratio ϕ/M. However, principal findings primarily pertain to oscillations of modest amplitude that bear resemblance to the small amplitude oscillations $\phi/M \leq 1$ for which $W(\phi) \approx 1 + \phi/M + \mathcal{O}\left(\phi/M\right)^2$. this model is consistent with ultralight vector dark matter scenarios, satisfying constraints from the cosmic microwave background and inflation scales, with a mass scale of around $10^{17} GeV$. In contrast to other methods, the approach needs no significant connection between the DP and scalar, but relies on precise tuning of their respective masses.

The subsequent analysis of this thesis delves into the mathematical equations that govern the behavior of a massive vector when it is coupled to a dilaton. It further investigates the resonant production of a dark photon caused by the oscillations of the dilaton[66]. Finally, the study presents the resulting relic abundance and identifies the parameter space that is considered viable, taking into account different cosmological constraints. In our calculations, we have utilized a FLRW metric and adopted natural units, in accordance with the Einstein summation standard.
$ds^2 = -dt^2 + a(t)^2 \delta_{ij} dx^i dx^j$.

6.2 Model and dynamics

A scalar is explored that resembles a dilaton, represented by ϕ, linked to a vector A_μ through the action given by:

$$S = \int d^4x\sqrt{-g}\left(\frac{m_{\rm Pl}^2 R}{2} - \frac{1}{2}\partial_\mu\phi\partial^\mu\phi - \frac{m_\phi^2\phi^2}{2} - \frac{W(\phi)F_{\mu\nu}F^{\mu\nu}}{4} - \frac{m_{\gamma'}^2 A_\mu A^\mu}{2}\right). \tag{6.1}$$

Here, $F_{\mu\nu}$ is derived from A_μ . The kinetic term for the dark photon modulated by $W(\phi)$

implies a dependency on ϕ for the dark $U(1)$ coupling strength. Potential origins for the dark photon mass term include the Stueckelberg and Higgs mechanisms. While in some scenarios $m_{\gamma'}$ might depend on ϕ, this work assumes $m_{\gamma'}$ to be a constant.

1. **Variation with respect to** ϕ

For this variation, we'll isolate the Lagrangian terms dependent on ϕ :

$$\mathcal{L}_\phi = -\frac{1}{2}\partial_\mu\phi\partial^\mu\phi - \frac{m_\phi^2\phi^2}{2} - \frac{W(\phi)F_{\mu\nu}F^{\mu\nu}}{4}. \tag{6.2}$$

The Euler-Lagrange equations are:

$$\frac{\partial\mathcal{L}_\phi}{\partial\phi} - \partial_\mu\left(\frac{\partial\mathcal{L}_\phi}{\partial(\partial_\mu\phi)}\right) = 0, \tag{6.3}$$

$$\frac{\partial\mathcal{L}_\phi}{\partial\phi} = -m_\phi^2\phi - \frac{W'(\phi)F_{\mu\nu}F^{\mu\nu}}{4}, \tag{6.4}$$

$$\frac{\partial\mathcal{L}_\phi}{\partial(\partial_\mu\phi)} = -\partial^\mu\phi, \tag{6.5}$$

iii) The term:

$$\partial_\mu\left(\frac{\partial\mathcal{L}_\phi}{\partial(\partial_\mu\phi)}\right) = \nabla_\mu\nabla^\mu\phi, \tag{6.6}$$

Therefore, the equation for ϕ becomes:

$$0 = \nabla_\mu\nabla^\mu\phi + m_\phi^2\phi + \frac{W'(\phi)F_{\mu\nu}F^{\mu\nu}}{4}. \tag{6.7}$$

2. **Variation with respect to** A^μ

The Lagrangian terms dependent on A^μ are

$$\mathcal{L}_A = -\frac{W(\phi)F_{\mu\nu}F^{\mu\nu}}{4} - \frac{m_{\gamma 0}^2A_\mu A^\mu}{2}. \tag{6.8}$$

The Euler-Lagrange equation for A^μ is

$$\frac{\partial\mathcal{L}_A}{\partial A^\mu} - \partial_\nu\left(\frac{\partial\mathcal{L}_A}{\partial(\partial_\nu A^\mu)}\right) = 0. \tag{6.9}$$

i) The term:

$$\frac{\partial\mathcal{L}_A}{\partial A^\mu} = -m_{\gamma'}^2A^\mu. \tag{6.10}$$

ii) The term becomes:

$$\frac{\partial\mathcal{L}_A}{\partial(\partial_\nu A^\mu)} = -\frac{W(\phi)F^{\mu\nu}}{2}. \tag{6.11}$$

iii) The term leads:

$$\partial_\nu \left(\frac{\partial \mathcal{L}_A}{\partial(\partial_\nu A^\mu)} \right) = -\nabla_\nu [W(\phi) F^{\mu\nu}]. \tag{6.12}$$

Therefore, the equation for A^μ becomes:

$$0 = \nabla_\nu [W(\phi) F^{\mu\nu}] + m_{\gamma'}^2 A^\mu. \tag{6.13}$$

The Euler-Lagrange equations become:

$$0 = -\nabla_\mu \nabla^\mu \phi + m_\phi^2 \phi + \frac{W'(\phi) F_{\mu\nu} F^{\mu\nu}}{4}. \tag{6.14}$$

$$0 = -\nabla_\mu [W(\phi) F^{\mu\nu}] + m_{\gamma'}^2 A^\nu. \tag{6.15}$$

$$\nabla_\mu A^\mu = 0. \tag{6.16}$$

This last equation aligns with the Lorenz gauge choice, but here, it's a consistency-required constraint for the motion equations.

Standard For the FLRW spacetime metric:

$$ds^2 = -dt^2 + a(t)^2 \delta_{ij} dx^i dx^j. \tag{6.17}$$

For the Klein-Gordon equation

$$0 = -\nabla_\mu \nabla^\mu \phi + m_\phi^2 \phi + \frac{W'(\phi) F_{\mu\nu} F^{\mu\nu}}{4}, \tag{6.18}$$

The d'Alembertian operator is:

$$\nabla_\mu \nabla^\mu \phi = \partial_\mu \partial^\mu \phi - \Gamma^\alpha_{\mu\nu} \partial^\mu \phi \partial^\nu \phi, \tag{6.19}$$

Time-time component:

$$\partial_t^2 \phi - \Gamma^t_{tt} \dot{\phi}^2 - 2\Gamma^t_{ti} \dot{\phi} \partial^i \phi - \Gamma^i_{ij} \partial^j \phi \partial^i \phi = \ddot{\phi} + 3H\dot{\phi}, \tag{6.20}$$

Space-space component:

$$\frac{1}{a^2} \partial_i \partial_i \phi = \frac{1}{a^2} \nabla^2 \phi, \tag{6.21}$$

Thus, the Klein-Gordon equation becomes:

$$0 = \ddot{\phi} + 3H\dot{\phi} - \frac{1}{a^2} \nabla^2 \phi + m_\phi^2 \phi + \frac{W'(\phi) F_{\mu\nu} F^{\mu\nu}}{4}. \tag{6.22}$$

for the proca equation

The covariant derivative of a tensor $F_{\mu\nu}$ is given by:

$$\nabla_\lambda F^{\mu\nu} = \partial_\lambda F^{\mu\nu} + \Gamma^\mu_{\mu\alpha} F^{\alpha\nu} + \Gamma^\nu_{\mu\alpha} F^{\mu\alpha}. \tag{6.23}$$

where the Christoffel symbols $\Gamma^\mu_{\lambda\nu}$ are derived from the metric tensor.
Using the FLRW metric, the relevant Christoffel symbols are:

$$\begin{aligned} \Gamma^t_{tt} &= \dot{a} \\ \Gamma^t_{ij} &= a\dot{a}\delta_{ij} \\ \Gamma^i_{jt} &= \Gamma^i_{tj} = \frac{\dot{a}}{a}\delta^i_j \end{aligned} \quad . \tag{6.24}$$

For the $\nu = 0$component, this becomes:

$$\nabla_\mu F^{\mu 0} = \partial_\mu F^{\mu 0} + \Gamma^\mu_{\alpha\mu} F^{\alpha 0}, \tag{6.25}$$

Using the FLRW metric, the covariant derivative of $F^{\mu 0}$ is:

$$\nabla_\mu F^{\mu 0} = \partial_\mu F^{\mu 0} + \Gamma^t_{ij} F^{i0} + \Gamma^i_{ti} F^{00}, \tag{6.26}$$

Using $F^{i0} and, F^{00}$, and substituting the Christoffel symbols:

$$\nabla_\mu F^{\mu 0} = \partial_t F^{t0} + \partial_i F^{i0} + a\dot{a} F^{i0} + \frac{\dot{a}}{a} F^{00}. \tag{6.27}$$

From the definition of the field strength tensor:

$$F^{t0} = \dot{A}_0, \tag{6.28}$$

$$F^{i0} = \frac{1}{a^2}(\partial^i A_0 - \dot{A}^i). \tag{6.29}$$

Substituting these into our equation, we get:

$$\nabla_\mu F^{\mu 0} = \ddot{A}_0 + \frac{1}{a^2}\partial_i \partial^i A_0 - \frac{\dot{a}}{a^2}\partial_i \dot{A}^i + a\dot{a}\frac{1}{a^2}(\partial^i A_0 - \dot{A}^i). \tag{6.30}$$

Combining like terms and simplifying:

$$\nabla_\mu F^{\mu 0} = \ddot{A}_0 + 3H\dot{A}_0 + 3\dot{H}A_0 - \frac{1}{a^2}\partial_i \partial^i A_0 + \frac{2H}{a^2}\partial_i A^i. \tag{6.31}$$

Using our initial Proca equation:

$$0 = -\nabla_\mu [W(\phi) F^{\mu\nu}] + m^2_{\gamma'} A^\nu, \tag{6.32}$$

For $\nu = 0$:
Inserting our derived expression for $\nabla_\mu F^{\mu 0}$ and simplifying:

$$0 = \ddot{A}_0 + 3H\dot{A}_0 + 3\dot{H}A_0 - \frac{1}{a^2}\partial_i\partial^i A_0 + \frac{2H}{a^2}\partial_i A^i + \frac{m_{\gamma'}^2}{W(\phi)}A_0 - \frac{1}{a^2}\frac{\partial_i W(\phi)}{W(\phi)}(\partial^i A_0 - \dot{A}^i). \quad (6.33)$$

For the $\nu = i$ component, this gives:

$$\nabla_\mu F^{\mu i} = \partial_\mu F^{\mu i} + \Gamma^\mu_{\mu\alpha}F^{\alpha\nu} + \Gamma^i_{\mu\alpha}F^{\mu\alpha}. \quad (6.34)$$

Inserting our previously known Christoffel symbols:
For the $\nu = i$ component:

$$\nabla_\mu F^{\mu i} = \partial_t F^{ti} + \partial_j F^{ji} + a\dot{a}F^{ji} + \frac{\dot{a}}{a}F^{0i}. \quad (6.35)$$

From the definition of the field strength tensor:

$$F^{ti} = A^{i\cdot}\frac{1}{a^2}\partial^i A_0, \quad (6.36)$$

$$F^{ji} = \frac{1}{a^2}(\partial^j A^i - \partial^{i\cdot}A^j). \quad (6.37)$$

Substituting these into our expression for $\nabla_\mu F^{\mu i}$:

$$\nabla_\mu F^{\mu i} = \ddot{A}^i - \frac{1}{a^2}\partial^i\dot{A}_0 + \frac{1}{a^2}\partial_j\partial^j A^i - \frac{1}{a^2}\partial^i\partial_j A^j, \quad (6.38)$$

Combining terms and simplifying:

$$\nabla_\mu F^{\mu i} = \ddot{A}^i + H\dot{A}^i - \frac{1}{a^2}\partial_j\partial^j A^i + 2H\frac{1}{a^2}\partial^i A_0. \quad (6.39)$$

using

$$0 = -\nabla_\mu[W(\phi)F^{\mu\nu}] + m_{\gamma'}^2 A^\nu, \quad (6.40)$$

Inserting our derived expression for $\nabla_\mu F^{\mu i}$ and simplifying:

$$0 = \ddot{A}^i + H\dot{A}^i - \frac{1}{a^2}\partial_j\partial^j A^i + 2H\frac{1}{a^2}\partial^i A_0 + \frac{m_{\gamma'}^2}{W(\phi)}A^i - \frac{\partial^\mu W(\phi)}{W(\phi)}F_{\mu i}. \quad (6.41)$$

When considered in FLRW spacetime, the equations simplify to:

$$0 = \ddot{\phi} + 3H\dot{\phi} - \frac{1}{a^2}\partial_i\partial_i\phi + m_\phi^2\phi + \frac{W'(\phi)}{4}F_{\mu\nu}F^{\mu\nu}. \quad (6.42)$$

$$0 = \ddot{A}_0 + 3H\dot{A}_0 + 3\dot{H}A_0 - \frac{1}{a^2}\partial_j\partial_j A_0 + \frac{2H}{a^2}\partial_i A_i + \frac{m_{\gamma'}^2}{W(\phi)}A_0 - \frac{1}{a^2}\frac{\partial_i W(\phi)}{W(\phi)}\left(\partial_i A_0 - \dot{A}_i\right). \quad (6.43)$$

$$0 = \ddot{A}_i + H\dot{A}_i - \frac{1}{a^2}\partial_j\partial_j A_i + 2H\partial_i A_0 + \frac{m_{\gamma'}^2}{W(\phi)}A_i - \frac{\partial^\mu W(\phi)}{W(\phi)}F_{\mu i}. \tag{6.44}$$

6.2.1 Fourier decomposition

The vector expands in Fourier modes as:

our vector fields A_0 and $A_j$are expanded in Fourier modes. This is a common technique to solve partial differential equations in quantum field theory. By expanding in Fourier modes, we are expressing the fields as a superposition of plane waves, each labeled by a momentum vector k.

$$A_0(t,x) = \int \frac{d^3k}{(2\pi)^3} e^{ik\cdot x} A_0(t,k). \tag{6.45}$$

$$A_j(t,x) = \sum_{\lambda\in\{\pm,k\}} \int \frac{d^3k}{(2\pi)^3} e^{ik\cdot x} A_\lambda(t,k)\epsilon_j^\lambda(k). \tag{6.46}$$

Here $\epsilon_j^\lambda(k)$ are the polarization vectors, which essentially describe the orientation of the vector field for each Fourier mode.

Properties of Polarization Vectors:
Orthogonality

$$\delta_{mn}\epsilon_\lambda^m(\mathbf{k})\epsilon_{\lambda'}^n(\mathbf{k}) = \delta_{\lambda\lambda'}. \tag{6.47}$$

This equation states that different polarization vectors are orthogonal to each other

Transversality

$$i\delta_{mn}k^m\epsilon_\pm^n(\mathbf{k}) = 0. \tag{6.48}$$

This states that the transverse polarizations (often labeled by $\pm, \epsilon1, \epsilon2$) are orthogonal to the momentum vector k, i.e., they are transverse modes.

Complex Conjugate Relation

$$\epsilon_\lambda^m(\mathbf{k}) = \epsilon_\lambda^m(-\mathbf{k})^*. \tag{6.49}$$

This is essentially a reality condition which ensures that the physical fields remain real.

Longitudinal Mode

$$\delta_{mn}k^m\epsilon_k^n(\mathbf{k}) = k. \tag{6.50}$$

This defines the longitudinal polarization vector, which is parallel to $\boldsymbol{k}$.

Cross Product with Transverse Modes

$$\epsilon_{ijk}k^m\epsilon_\pm^n(\mathbf{k}) = \pm\epsilon_\pm^i(\mathbf{k}). \tag{6.51}$$

This is a defining relation for transverse polarization vectors, stating that the cross product of $\boldsymbol{k}$ and the transverse polarizations gives the polarizations themselves (up to a sign)

Cross Product with Longitudinal Mode

$$\epsilon_{ijk} k^m \epsilon_k^n(\mathbf{k}) = 0. \tag{6.52}$$

This states that the cross product of $\boldsymbol{k}$ and the longitudinal polarization is zero.

These properties of the polarization vectors are crucial for the Fourier decomposition of the vector fields and will be important when computing quantities like the propagator or the interactions in momentum space.

Similarly, the dilaton is expanded as:

$$\phi(t,x) = \bar{\phi}(t) + \int \frac{d^3k}{(2\pi)^3} e^{ik\cdot x} \delta\phi(t,k). \tag{6.53}$$

In cosmological perturbation theory, it is often useful to decompose fields into Fourier modes to study their behavior in an expanding universe. Let's assume that the fields can be Fourier-decomposed as:

$$A_i(t,\vec{x}) = \int \frac{d^3k}{(2\pi)^{3/2}} e^{i\vec{k}\cdot\vec{x}} A_i(t,\vec{k}). \tag{6.54}$$

$$A_0(t,\vec{x}) = \int \frac{d^3k}{(2\pi)^{3/2}} e^{i\vec{k}\cdot\vec{x}} A_0(t,\vec{k}). \tag{6.55}$$

Here $A_i(t,\vec{k})$ and $A_0(t,\vec{k})$ are the Fourier modes of $A_i(t,\vec{x})$ and $A_0(t,\vec{x})$ respectively.The differential operator $\partial_j\partial^j$ acting on a Fourier mode gives $-k^2$, when considering flat spatial sections.

Let's proceed to decompose the equation for A_i

$$0 = \ddot{A}_i + H\dot{A}_i - \frac{k^2}{a^2}A_i + 2Hk\frac{A_0}{a} + \frac{m_{\gamma'}^2}{W}A_i - \frac{\partial^\mu W}{W}F_{\mu i}. \tag{6.56}$$

We have linearized the equation, so all terms are to linear order in fluctuations. Now, let's focus on the term $\frac{\partial^\mu W}{W}F_{\mu i}$, Assuming $W = \bar{W}(t) \Rightarrow \frac{\partial^\mu W}{W} = \frac{\dot{\bar{W}}}{\bar{W}}$,

putting everything together we get

$$A_i 0 = \ddot{A}_i + \left(H + \frac{\dot{\bar{W}}}{\bar{W}}\right)\dot{A}_i + \left(\frac{k^2}{a^2} + \frac{m_{\gamma'}^2}{\bar{W}}\right)A_i + \left(\frac{\dot{\bar{W}}}{\bar{W}} - 2H\right)\frac{k}{a}A_0. \tag{6.57}$$

Since A_i can be circularly polarized, we can rewrite the equation for each polarization state $A_\pm$ and for each Fourier mode A_k.

as:

$$0 = \ddot{A}_{\pm} + \left(H + \frac{\dot{\bar{W}}}{\bar{W}}\right)\dot{A}_{\pm} + \left(\frac{k^2}{a^2} + \frac{m_{\gamma'}^2}{\bar{W}}\right)A_{\pm}. \tag{6.58}$$

$$0 = \ddot{A}_{k} + \left(H + \frac{\dot{\bar{W}}}{\bar{W}}\right)\dot{A}_{k} + \left(\frac{k^2}{a^2} + \frac{m_{\gamma'}^2}{\bar{W}}\right)A_{k} + \left(\frac{\dot{\bar{W}}}{\bar{W}} - 2H\right)kA_0. \tag{6.59}$$

the above equation are linearized to first order now.using the shorthand notation $\bar{W} = W(\bar{\phi})$. From the Lorenz constraint , we deduce :$kA_k/a^2 = \dot{A}_0 + 3HA_0$
The original equation for A_0 is

$$0 = \ddot{A}_0 + 3H\dot{A}_0 + 3\dot{H}A_0 - \frac{1}{a^2}\partial_j\partial_j A_0 + \frac{2H}{a^2}\partial_i A_i + \frac{m_{\gamma'}^2}{W(\phi)}A_0 - \frac{1}{a^2}\frac{\partial_i W(\phi)}{W(\phi)}\left(\partial_i A_0 - \dot{A}_i\right). \tag{6.60}$$

using lorentz constraint $\dot{A}_0 + 3HA_0$ replace kA_k/a^2 from this we have

$$kA_k/a^2 = \dot{A}_0 + 3HA_0. \tag{6.61}$$

The first terms in this equation are straightforward: they directly involve $\ddot{A}_0$,$\dot{A}_0$,A_0. We then have terms involving spatial derivatives of A_0, A_i given as $\partial_j\partial_j A_0$ and $\frac{2H}{a^2}\partial_i A_i$. In Fourier space, the spatial derivatives turn into $\frac{k^2}{a^2}A_0$ and $\frac{2H}{a^2}kA_k$ respectively . where k is the fourier wavenumber . the term $\frac{m_{\gamma'}^2}{W(\phi)}A_0$ can be kept as is because it already is a function of A_0 . the last term $\frac{1}{a^2}\frac{\partial_i W(\phi)}{W(\phi)}\left(\partial_i A_0 - \dot{A}_i\right)$ in fourier space simplifies to $\frac{1}{a^2}k\frac{\dot{W}}{W}A_k$.
Substitute into the original equation

$$\ddot{A}_0 + 3H\dot{A}_0 + 3\dot{H}A_0 - \frac{1}{a^2}k^2A_0 + \frac{2H}{a^2}kA_k + \frac{m_{\gamma'}^2}{W(\phi)}A_0 - \frac{1}{a^2}k\frac{\dot{W}}{W}A_k. \tag{6.62}$$

using lorentz constraint $\dot{A}_0 + 3HA_0$ replace kA_k/a^2

$$\ddot{A}_0 + 3H\dot{A}_0 + 3\dot{H}A_0 - \frac{1}{a^2}k^2A_0 + 2H(\dot{A}_0 + 3HA_0) + \frac{m_{\gamma'}^2}{W(\phi)}A_0 - \frac{1}{a^2}k\frac{\dot{W}}{W}A_k. \tag{6.63}$$

collecting like terms

$$0 = \ddot{A}_0 + 5H\dot{A}_0 + \left(\frac{k^2}{a^2} + \frac{m_{\gamma'}^2}{W(\phi)} + 3\dot{H} + 6H^2\right)A_0 - \frac{k}{a^2}\frac{\dot{W}}{W}A_k, \tag{6.64}$$

This, combined with starting equation, provides:

$$0 = \ddot{A}_0 + 5H\dot{A}_0 + \left(\frac{k^2}{a^2} + \frac{m_{\gamma'}^2}{\bar{W}} + 3\dot{H} + 6H^2\right)A_0. \tag{6.65}$$

Considering the dynamics of the transverse modes and A_0, it is more efficient to study the rescaled fields defined as:

$$A_\pm \equiv \sqrt{aW}\bar{A}_\pm, \tag{6.66}$$

$$A_0 \equiv a^{5/2}A_0. \tag{6.67}$$

yielding the following equations:

$$\ddot{A}_\pm = -\left(\frac{k^2}{a^2} + \frac{m_{\gamma'}^2}{\bar{W}} - \frac{\partial_t^2\sqrt{\bar{W}}}{\sqrt{\bar{W}}} - \frac{\dot{H}}{2} - \frac{H^2}{4}\right)A_\pm. \tag{6.68}$$

$$\ddot{A}_0 = -\left(\frac{k^2}{a^2} + \frac{m_{\gamma'}^2}{\bar{W}} + \frac{\dot{H}}{2} - \frac{H^2}{4}\right)A_0. \tag{6.69}$$

Generally, as ϕ diminishes with expansion ,$W(\phi)$ approaches 1 at late times. Consequently, $A_\pm$ and$\sqrt{a}A_\pm$ tend to coincide. Nonetheless, analyzing instability is more straightforward with the former field. Moreover, from Eq. (12), we have:

$$A_k = \frac{1}{\sqrt{ak}}\left(\dot{A}_0 + \frac{H}{2}A_0\right). \tag{6.70}$$

indicating that the dynamics in former equation can replace the study of the longitudinal mode due to its relative simplicity.

6.3 Stability analysis

recall that the d'Alembertian operator $\Box$ in Minkowski spacetime is given by:

$$\Box = -\partial_t^2 + \nabla^2, \tag{6.71}$$

where ∂_t is the partial derivative with respect to time t, and ∇^2 is the Laplacian operator acting on spatial coordinates on equation

Now, let's take the Laplacian of $\phi(t,x)$:

$$\nabla^2\phi(t,x) = \nabla^2\left(\bar{\phi}(t) + \int \frac{d^3k}{(2\pi)^3}e^{ik\cdot x}\delta\phi(t,k)\right). \tag{6.72}$$

Using the properties of the Laplacian and the exponential function, we can write:

$$\nabla^2\left(\int \frac{d^3k}{(2\pi)^3}e^{ik\cdot x}\delta\phi(t,k)\right) = \int \frac{d^3k}{(2\pi)^3}(-k^2)e^{ik\cdot x}\delta\phi(t,k). \tag{6.73}$$

Now, let's plug this result back into the equation for $\Box\phi(t,x)$):

$$\Box\phi(t,x) = -\partial_t^2\phi(t,x) + \nabla^2\phi(t,x). \tag{6.74}$$

Substitute the Laplacian result and notice that the partial derivative with respect to time only acts on the time-dependent factor $\bar{\phi}(t)$:

$$\Box\phi(t,x) = -\partial_t^2\bar{\phi}(t) + \int \frac{d^3k}{(2\pi)^3}(-k^2)e^{ik\cdot x}\delta\phi(t,k). \tag{6.75}$$

Since we are considering a Minkowski spacetime with no explicit time-dependent background, the partial derivatives with respect to time act only on $\bar{\phi}(t)$ and $\delta\phi(t,k)$, giving:

$$\Box\phi(t,x) = -\ddot{\bar{\phi}}(t) - \int \frac{d^3k}{(2\pi)^3}k^2e^{ik\cdot x}\delta\phi(t,k). \tag{6.76}$$

Now, substitute this result back into the equation for $\Box\phi(t,x)$ and equate it to zero:

$$-\ddot{\bar{\phi}}(t) - \int \frac{d^3k}{(2\pi)^3}k^2e^{ik\cdot x}\delta\phi(t,k) = 0. \tag{6.77}$$

To proceed, we can exchange the order of differentiation and integration since the operations are linear. We can also factor out constants from the integral, leading to:

$$-\ddot{\bar{\phi}}(t) - \frac{1}{(2\pi)^3}\int d^3k\, k^2 \int e^{ik\cdot x}\delta\phi(t,k). \tag{6.78}$$

The integral over d^3k is just a constant. Now, we can express the integral of the exponential term as a Dirac delta function:

$$\int e^{ik\cdot x}\delta\phi(t,k) = \delta^3(x)\delta\phi(t,k). \tag{6.79}$$

Substitute this back into the equation:

$$-\ddot{\bar{\phi}}(t) - \frac{1}{(2\pi)^3}\int d^3k\, k^2\delta^3(x)\delta\phi(t,k) = 0. \tag{6.80}$$

Perform the integration over d^3k to get rid of k :

$$-\ddot{\bar{\phi}}(t) - \int d^3x\, \delta^3(x)\delta\phi(t,k) = 0. \tag{6.81}$$

The integral of the Dirac delta function over all space gives 1:

$$-\ddot{\bar{\phi}}(t) - \delta\phi(t,k) = 0. \tag{6.82}$$

This simplifies to:

$$\ddot{\bar{\phi}}(t) + \delta\phi(t,k) = 0. \tag{6.83}$$

Since we are considering a homogeneous dilaton background, $\delta\phi(t,k)$ must be zero, and thus:

$$\ddot{\bar{\phi}}(t) = 0. \tag{6.84}$$

This means that the homogeneous component of the dilaton , $\bar{\phi}(t)$, evolves according to a

simple harmonic motion with zero acceleration. In this context, $\ddot{\bar{\phi}}$ represents the second time derivative of $\bar{\phi}(t)$, and m_ϕ represents the mass of the dilaton. Therefore, for the homogeneous component, we obtain the equation of motion:

$$\ddot{\bar{\phi}} + m_\phi^2 \bar{\phi} = 0. \tag{6.85}$$

It describes the evolution of the dilaton field as a simple harmonic oscillator with a mass term m_ϕ^2.

We first discuss the (in)stability of vector modes in a periodically oscillating dilaton background within Minkowski spacetime. In this approximation, the homogeneous dilaton evolves as:

$$\ddot{\bar{\phi}} + m_\phi^2 \bar{\phi} = 0, \tag{6.86}$$

which is solved by:

$$\bar{\phi}(t) = \phi_0 \cos(m_\phi t), \tag{6.87}$$

from the initial condition $\bar{\phi}(t) \to \phi_0 - and \dot{\bar{\phi}}(t) \to 0 \to when \to H(t) \gg m_\phi$.

Let's specify the function W as:

$$W(\phi) = e^{\phi/M}, \tag{6.88}$$

Differentiating with respect to t, we obtain:

$$\dot{\bar{\phi}}(t) = -\phi_0 m_\phi \sin(m_\phi t), \tag{6.89}$$

and once more:

$$\ddot{\bar{\phi}}(t) = -\phi_0 m_\phi^2 \cos(m_\phi t), \tag{6.90}$$

Given the condition $H(t) \gg m_\phi$, we can approximate:

$$\bar{\phi}(t) \approx \phi_0, \tag{6.91}$$

$$\dot{\bar{\phi}}(t) \approx 0. \tag{6.92}$$

Now, let's find $\frac{\partial_t^2 \sqrt{\bar{W}}}{\sqrt{\bar{W}}}$. Using the expression for $\bar{W}$ and differentiating

$$\sqrt{\bar{W}} = e^{\bar{\phi}/2M}, \tag{6.93}$$

$$\frac{\partial \sqrt{\bar{W}}}{\partial t} = \frac{\dot{\bar{\phi}}}{2M} e^{\bar{\phi}/2M}, \tag{6.94}$$

$$\frac{\partial^2 \sqrt{\bar{W}}}{\partial t^2} = \frac{\ddot{\bar{\phi}}}{2M} e^{\bar{\phi}/2M} + \left(\frac{\dot{\bar{\phi}}}{2M}\right)^2 e^{\bar{\phi}/2M}, \tag{6.95}$$

$$\frac{\partial_t^2 \sqrt{\bar{W}}}{\sqrt{\bar{W}}} = \frac{\ddot{\bar{\phi}}}{2M} + \left(\frac{\dot{\bar{\phi}}}{2M}\right)^2. \tag{6.96}$$

Given the condition $H(t) \gg m_\phi$, this means that the expansion rate of the universe, characterized by $H(t)$, is much faster than the oscillation of the field $\bar{\phi}$, In such scenarios, the field $\bar{\phi}$ can be approximated as being "frozen" since it changes very slowly compared to the rapid expansion of the universe. From the initial conditions, and $H(t) \gg m_\phi$, which means the field remains approximately constant at ϕ_0 and its time derivative is close to zero.neglecting the expansion terms $H(t) \gg m_\phi$ and Substituting the expressions for $\bar{W}$,$\dot{\bar{\phi}}$, and $\ddot{\bar{\phi}}$ into the equations , when expansion is overlooked, yield:

$$\ddot{A}_\pm = -\left[k^2 + \frac{m_{\gamma'}^2}{e^{\bar{\phi}/M}} - \frac{\ddot{\bar{\phi}}}{2M} - \left(\frac{\dot{\bar{\phi}}}{2M}\right)^2\right] A_\pm, \tag{6.97}$$

$$\ddot{A}_0 = -\left[k^2 + \frac{m_{\gamma'}^2}{e^{\bar{\phi}/M}}\right] A_0. \tag{6.98}$$

Given that $\bar{\phi}(t)$ is periodic, the above Hill's equation represent harmonic oscillators with fluctuating frequencies. According to the Floquet theorem, the solutions are:

$$P_+(t)e^{\mu t} + P_-(t)e^{-\mu t}, \tag{6.99}$$

where μ denotes the Floquet exponent and $P_\pm(t) = P_\pm(t+T)$ with T being the background's period. Modes with $\mathrm{Re}(\mu) \neq 0$ are unstable, growing exponentially over time. We proceed to explore the form of parametric instabilities in these equations.

6.3.1 Floquet theory solutions

To employ Floquet theory, we need to turn the second-order differential equations into a system of first-order differential equations. We'll begin with the $A_\pm$

equation and then move to the A_0

Transverse mode $A_\pm$

Define:

$$u_1 = A_\pm, \tag{6.100}$$

$$u_2 = \dot{A}_\pm, \tag{6.101}$$

The first-order system becomes:

$$\dot{u}_1 = u_2, \tag{6.102}$$

$$\dot{u}_2 = -\left[k^2 + \frac{m_{\gamma'}^2}{e^{\bar{\phi}/M}} - \frac{\ddot{\bar{\phi}}}{2M} - \left(\frac{\dot{\bar{\phi}}}{2M}\right)^2\right] u_1, \tag{6.103}$$

The matrix form is:

$$\frac{d}{dt}\begin{bmatrix} u_1 \\ u_2 \end{bmatrix} = \begin{bmatrix} 0 & 1 \\ -\left[k^2 + \frac{m_{\gamma'}^2}{e^{\bar{\phi}/M}} - \frac{\ddot{\bar{\phi}}}{2M} - \left(\frac{\dot{\bar{\phi}}}{2M}\right)^2\right] & 0 \end{bmatrix} \begin{bmatrix} u_1 \\ u_2 \end{bmatrix}. \tag{6.104}$$

Longitudnal mode A_0

Define:

$$v_1 = A_0, \tag{6.105}$$

$$v_2 = \dot{A}_0, \tag{6.106}$$

The first-order system becomes:

$$\dot{v}_1 = v_2, \tag{6.107}$$

$$\dot{v}_2 = -\left[k^2 + \frac{m_{\gamma'}^2}{e^{\bar{\phi}/M}}\right] v_1, \tag{6.108}$$

The matrix form is:

$$\frac{d}{dt}\begin{bmatrix} v_1 \\ v_2 \end{bmatrix} = \begin{bmatrix} 0 & 1 \\ -\left[k^2 + \frac{m_{\gamma'}^2}{e^{\bar{\phi}/M}}\right] & 0 \end{bmatrix} \begin{bmatrix} v_1 \\ v_2 \end{bmatrix}. \tag{6.109}$$

Both systems are linear and time-periodic due to the periodicity of $\bar{\phi}(t)$. According to Floquet theory, solutions to the above systems are of the form [67]:

$$\mathbf{y}(t) = P(t)e^{\mu t}. \tag{6.110}$$

Where: $\mathbf{y}(t)$ represents either $\begin{bmatrix} u_1(t) \\ u_2(t) \end{bmatrix}$ or $\begin{bmatrix} v_1(t) \\ v_2(t) \end{bmatrix}$. $P(t)$is a matrix with periodic functions of$t$ as its entries (with period$T$). μ is a Floquet exponent. To derive $P(t)$ and μ, you need to solve the eigenvalue problem of the monodromy matrix over one period T:

$$\Phi(T) = \mathbf{Texp}\left(\int_0^T A(t)dt\right), \tag{6.111}$$

Where $\Phi(T)$ is the so-called monodromy matrix and $Texp$ denotes the time-ordered exponential. The Floquet exponents μ are then given by the logarithm of the eigenvalues of the monodromy matrix divided by the period T. The matrix $P(t)$ can be found by solving the system using the fundamental matrix solution.

6.3.2 Floquet Exponents

Given the monodromy matrix $\Phi(T)$ (a matrix that describes the evolution of a system of

differential equations over one period T, the Floquet exponents μ are given by:

$$\mu_i = \frac{1}{T} \ln \lambda_i. \tag{6.112}$$

Where: λ_i are the eigenvalues of $\Phi(T)$. There are as many Floquet exponents μ_i as there are dimensions to the system of differential equations. These exponents give vital information about the stability of the periodic solutions. If any of the real parts of the Floquet exponents are positive, then the solution is unstable.

6.3.3 Fundamental Matrix Solution

A fundamental matrix solution $\Psi(t)$ of a time-periodic system of differential equations is a matrix whose columns are linearly independent solutions to the system. The relationship between the fundamental matrix solution and the matrix $P(t)$ from Floquet theory is given by:

$$\Psi(t) = P(t)e^{\mu t}. \tag{6.113}$$

Where: $P(t)$ is a periodic matrix with the same period as the coefficient matrix of the differential equations. It contains functions that capture the periodic nature of the solutions .$e^{\mu t}$ is a diagonal matrix with terms that capture the exponential growth or decay dictated by the Floquet exponents. Finding $P(t)$ often involves integrating the differential equations over one period while incorporating the behavior dictated by the Floquet exponents.

6.4 A Small-amplitude broad resonance

When considering massless dark photons, unstable solutions only emerge for sizable oscillation amplitudes, $(\phi_0 \gtrsim M)$. Massive dark photons, if not overly massive $(m_{\gamma'} \lesssim W/\dot{\bar{W}} \approx m_\phi)$, experience these instabilities. The mass term leads to a new, small-momentum $(k \ll m_\phi)$ instability in the small-amplitude$(\phi_0 \ll M)$ regime when$m_{\gamma'}/m_\phi = 1/2$. Recognizing this instability, and under this approximation with terms of order ϕ_0/M taken into account, above hills equations converge to the Mathieu equation:

$$\frac{d^2X}{dz^2} + [p - 2q\cos(2z)]X(z) = 0. \tag{6.114}$$

6.4.1 Longitudnal mode

Step 1: Start with the equation

$$\ddot{A}_0 = -\left[k^2 + \frac{m_{\gamma'}^2}{e^{\bar{\phi}/M}}\right] A_0, \tag{6.115}$$

Step 2: Introduce time-dependence for $\bar{\phi}$

$$\frac{m_{\gamma 0}^2}{e^{\phi_0 \cos(m_\phi t)/M}}, \tag{6.116}$$

Step 3: Taylor Expansion

$$e^{\phi_0 \cos(m_\phi t)/M} \approx 1 + \frac{\phi_0 \cos(m_\phi t)}{M}, \tag{6.117}$$

Continuing the approximation

$$\Rightarrow \frac{m_{\gamma'}^2}{e^{\phi_0 \cos(m_\phi t)/M}} \approx m_{\gamma 0}^2 - \frac{\phi_0 m_{\gamma'}^2 \cos(m_\phi t)}{M}, \tag{6.118}$$

Step 4: Substitution into the equation

$$\ddot{A}_0 + \left[k^2 + m_{\gamma 0}^2 - \frac{\phi_0 m_{\gamma'}^2 \cos(m_\phi t)}{M}\right] A_0 = 0, \tag{6.119}$$

Step 5: Change of variables

$$z = \frac{m_\phi t}{2}, \tag{6.120}$$

Define the variable transformation

$$z = \frac{m_\phi t}{2} \Rightarrow t = \frac{2z}{m_\phi}, \tag{6.121}$$

Derive dt/dz

$$\frac{dt}{dz} = \frac{2}{m_\phi} \Rightarrow \frac{d^2 t}{dz^2} = 0, \tag{6.122}$$

Chain rule for second derivatives in terms of z

$$\frac{d^2 A_0}{dt^2} = \frac{d^2 A_0}{dz^2} \times \left(\frac{dt}{dz}\right)^2 \ddot{A}_0 = \frac{d^2 A_0}{dz^2} \times \left(\frac{2}{m_\phi}\right)^2 \ddot{A}_0 = 4\frac{d^2 A_0}{dz^2}\frac{1}{m_\phi^2}, \tag{6.123}$$

The differential relation

$$\ddot{A}_0 = 4\frac{d^2 A_0}{dz^2}\frac{1}{m_\phi^2}, \tag{6.124}$$

Step 6: New equation

$$4\frac{d^2 A_0}{dz^2}\frac{1}{m_\phi^2} + \left[4\left(\frac{k}{m_\phi}\right)^2 + 4\left(\frac{m_{\gamma'}}{m_\phi}\right)^2 - 4\frac{\phi_0}{M}\left(\frac{m_{\gamma'}}{m_\phi}\right)^2 \cos(2z)\right] A_0 = 0. \tag{6.125}$$

Step 7: Match to Mathieu

$$p = 4\left(\frac{k}{m_\phi}\right)^2 + 4\left(\frac{m_{\gamma'}}{m_\phi}\right)^2. \tag{6.126}$$

$$q = \frac{2\phi_0}{M}\frac{m_{\gamma'}^2}{m_\phi^2}. \tag{6.127}$$

6.4.2 Transverse mode

for the second equation compute the derivative of

$$\bar{\phi}(t) = \phi_0 \cos(m_\phi t), \tag{6.128}$$

Differentiating with respect to t, we obtain:

$$\dot{\bar{\phi}}(t) = -\phi_0 m_\phi \sin(m_\phi t), \tag{6.129}$$

and once more:

$$\ddot{\bar{\phi}}(t) = -\phi_0 m_\phi^2 \cos(m_\phi t), \tag{6.130}$$

For $\frac{\bar{\phi}}{M}$ much smaller than 1, we can Taylor expand the exponential function:

$$e^{\frac{\bar{\phi}}{M}} \approx 1 + \frac{\bar{\phi}}{M}, \tag{6.131}$$

Thus, the term $\frac{m_{\gamma 0}^2}{e^{\bar{\phi}/M}}$ can be approximated as:

$$\frac{m_{\gamma'}^2}{e^{\bar{\phi}/M}} \approx m_{\gamma'}^2 \left(1 + \frac{\bar{\phi}}{M}\right)^{-1}, \tag{6.132}$$

Substituting $\bar{\phi}(t) = \phi_0 \cos(m_\phi t)$ into the above, we get:

$$\frac{m_{\gamma'}^2}{e^{\bar{\phi}/M}} \approx m_{\gamma'}^2 \left(1 + \frac{\phi_0 \cos(m_\phi t)}{M}\right)^{-1}, \tag{6.133}$$

Using the binomial expansion for small $\frac{\phi_0}{M}$, the expression further reduces

$$\frac{m_{\gamma'}^2}{e^{\bar{\phi}/M}} \approx m_{\gamma'}^2 \left(1 - \frac{\phi_0 \cos(m_\phi t)}{M}\right), \tag{6.134}$$

Plugging our earlier result into the differential equation for

$$\ddot{A}_\pm : \ddot{A}_\pm = -\left[k^2 + m_{\gamma'}^2 - \frac{\phi_0 m_{\gamma'}^2 \cos(m_\phi t)}{M} + \frac{\phi_0 m_\phi^2 \cos(m_\phi t)}{2M} + \frac{\phi_0^2 m_\phi^2 \sin^2(m_\phi t)}{4M^2}\right] A_\pm \quad . \tag{6.135}$$

Now, using the substitution:

$$z = \frac{m_\phi t}{2}, \tag{6.136}$$

We get the derivatives as:

$$\frac{dz}{dt} = \frac{m_\phi}{2}, \tag{6.137}$$

$$\frac{d^2 z}{dt^2} = 0, \tag{6.138}$$

Given this substitution, we have:

$$\cos(m_\phi t) = \cos(2z), \tag{6.139}$$

$$\sin(m_\phi t) = \sin(2z), \tag{6.140}$$

Substituting and changing the derivatives as discussed:

$$\left(\frac{dz}{dt}\right)^2 \frac{d^2A_\pm}{dz^2} = -\left[k^2 + m_{\gamma'}^2 - \frac{\phi_0 m_{\gamma 0}^2 \cos(2z)}{M} + \frac{\phi_0 m_\phi^2 \cos(2z)}{2M} + \frac{\phi_0^2 m_\phi^2 \sin^2(2z)}{4M^2}\right] A_\pm. \tag{6.141}$$

Where:

$$\left(\frac{dz}{dt}\right)^2 = \left(\frac{m_\phi}{2}\right)^2, \tag{6.142}$$

To reduce to Mathieu's equation, collect terms of $A_\pm$ and $\cos(2z)$. The $\sin^2(2z)$ term can be expressed in terms of $\cos(2z)$ using the trigonometric identity:

$$\sin^2(2z) = \frac{1 - \cos(4z)}{2}, \tag{6.143}$$

Given the equation:

$$\left(\frac{m_\phi}{2}\right)^2 \frac{d^2A_\pm}{dz^2} = -\left[k^2 + m_{\gamma'}^2 - \frac{\phi_0 m_{\gamma'}^2 \cos(2z)}{M} + \frac{\phi_0 m_\phi^2 \cos(2z)}{2M} + \frac{\phi_0^2 m_\phi^2 \sin^2(2z)}{4M^2}\right] A_\pm. \tag{6.144}$$

We expresssin$^2(2z)$ in terms of $\cos(2z)$ using the identity:

$$\sin^2(2z) = \frac{1 - \cos(4z)}{2}, \tag{6.145}$$

Substituting this in gives:

$$\left(\frac{m_\phi}{2}\right)^2 \frac{d^2A_\pm}{dz^2} = -\left[k^2 + m_{\gamma'}^2 + \frac{\phi_0^2 m_\phi^2}{8M^2} - \left(\frac{\phi_0 m_{\gamma'}^2}{M} - \frac{\phi_0 m_\phi^2}{2M} + \frac{\phi_0^2 m_\phi^2 \cos(4z)}{8M^2}\right)\cos(2z)\right] A_\pm. \tag{6.146}$$

Neglecting the higher-order term with $\cos(4z)$ and considering only terms up to order ϕ_0/M :

$$\left(\frac{m_\phi}{2}\right)^2 \frac{d^2A_\pm}{dz^2} = -\left[k^2 + m_{\gamma'}^2 - \left(\frac{\phi_0 m_{\gamma'}^2}{M} - \frac{\phi_0 m_\phi^2}{2M}\right)\cos(2z)\right] A_\pm. \tag{6.147}$$

Comparing with the Mathieu equation form:

$$\frac{d^2X}{dz^2} + [p - 2q\cos(2z)]X(z) = 0. \tag{6.148}$$

We identify:

$$p = \left(\frac{2k}{m_\phi}\right)^2 + \left(\frac{2m_{\gamma'}}{m_\phi}\right)^2, \tag{6.149}$$

$$q = \frac{2\phi_0}{M}\frac{m_{\gamma'}^2}{m_\phi^2}\left(1 - \frac{m_\phi^2}{2m_{\gamma'}^2}\right), \tag{6.150}$$

for both cases we have

$$z = \frac{m_\phi t}{2}. \tag{6.151}$$

$$p = \left(\frac{2k}{m_\phi}\right)^2 + \left(\frac{2m_{\gamma'}}{m_\phi}\right)^2. \tag{6.152}$$

$$q = \frac{2\phi_0}{M}\frac{m_{\gamma'}^2}{m_\phi^2} \times \begin{cases} 1, & \text{if } X = A_0, \\ 1 - \frac{m_\phi^2}{2m_{\gamma'}^2}, & \text{if } X = A_\pm. \end{cases} \tag{6.153}$$

The solution to the Mathieu equation is unstable for small q given that $p = n^2$. for an integer n. Specifically, for $n = 1$, which corresponds to $m_{\gamma 0} = m_\phi/2$ for modes $k \ll m_\phi$, there is an unstable solution in the small q (and thus small amplitude) limit. The Floquet exponent of the Mathieu equation in this situation is known analytically to be

$$\lim_{q\to 0} \mathrm{Re}(\tilde{\mu}_{n=1}) \approx \frac{|q|}{2}. \tag{6.154}$$

resulting in

$$\mathrm{Re}(\mu) \approx \frac{m_\phi \phi_0}{8M}.$$

for the solutions to hills equations when $\phi_0 \ll M$ and $k \ll m_\phi$.

The Floquet exponents for the transverse and longitudinal components are depicted in Figure 1, illustrating their dependence on the wave number of the vector and the amplitude of the dilaton's oscillation. In addition to the wide range of instability bands observed for substantial momenta and amplitudes, Figure 1 also illustrates the previously mentioned band for low (k/m_ϕ), which extends towards the limit of $(\phi_0/M \to 0)$. The band exhibiting instability does not attain very tiny amplitudes unless the value of $(m_{\gamma'})$ is precisely equal to half of m_ϕ. The magnitude of the difference between the first-order momentum eigenvalue and unity, denoted as $|p_{n=1} - 1|$, represents the width of the instability band in the wavevector space (k) for small values of the wavevector (q). When considering the case when $n = 1$, it can be shown that the Mathieu resonance parameters q for $A_\pm$ and A_0 exhibit contrasting signs while possessing equal magnitudes. Consequently, they provide

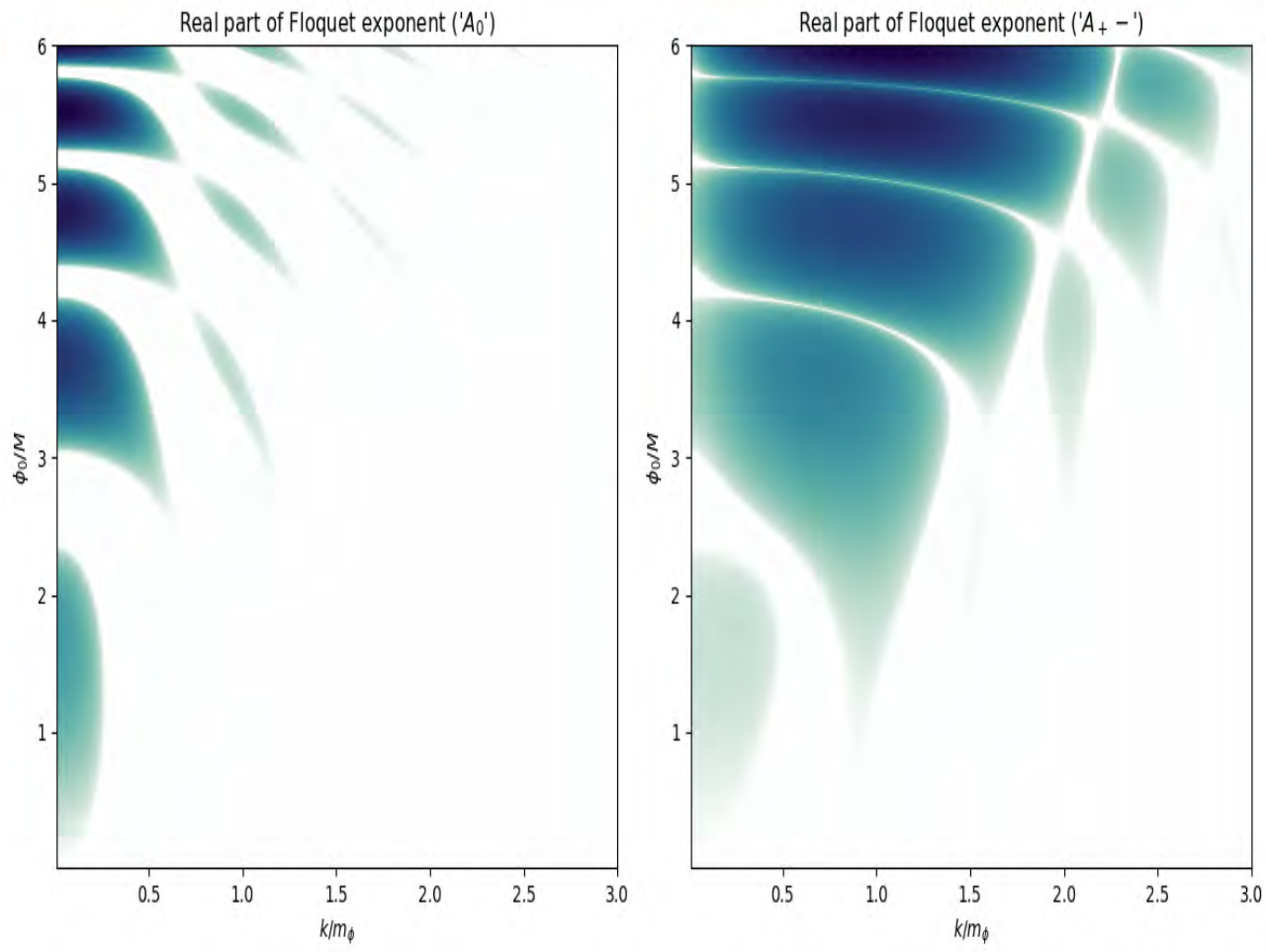

Figure 6.1: The real component of the Floquet exponent μ_k for solutions of the EOM associated with the transverse and the longitudinal domains is presented. For both domains, when $m_\phi = 2m_{\gamma'}$, there exists a domain where $\mathrm{Re}(\mu_k) > 0$. This can be extended to minimal values of ϕ_0/M and k/m_ϕ, as illustrated in the inset figures. The results are normalized by ϕ_0/M to aid in understanding within the context of FLRW spacetime.

the same Floquet exponent. The mass tuning can be defined as

$$\delta \equiv \left(\frac{m_{\gamma'}}{m_\phi}\right)^2 - \frac{1}{4}, \tag{6.155}$$

the width of the instability band becomes

$$\left|\frac{k}{m_\phi}\right|^2 + \delta \leq \frac{\phi_0}{8M}. \tag{6.156}$$

The instability band for low momentum disappears for $\phi_0/M < 8\delta. \rightarrow If \rightarrow \delta < 0$, a thin instability band remains down to very small ϕ_0/M, centered at $k = m_\phi\delta$ with width $\phi_0/8M$. We will discuss the mass tuning level this suggests for feasible dark photon dark matter models.

6.5 Parametric resonance in FLRW

The extrapolation of resonant instabilities in Minkowski spacetime to an expanding Universe involves the consideration of the redshifts of physical momenta k/a and the oscillation amplitude of the dilaton. In the context of a FLRW spacetime, the dilaton exhibits oscillatory behavior when the Hubble parameter at a given time, denoted as $H(t_i)$, approaches a value approximately equal to the mass of the dilaton, denoted as m_ϕ as $H(t_i) \approx m_\phi$. This oscillation is initiated with an initial amplitude denoted as ϕ_{0i}, which then undergoes a decrease in magnitude due to the redshifting effect.

$$\phi_0(t) \approx 1.5\phi_{0,i}\left(\frac{a(t)}{a_i}\right)^{-3/2}. \tag{6.157}$$

In the period characterized by dominance of radiation. The temporal variation of the coefficients in hill's equations which could cause them to deviate from the structure of Mathieu equation , can be considered insignificant when the oscillation frequency of the dilaton is significantly higher than the rate of expansion (during the radiation-dominated epoch, characterized by an evolution of the form $H \propto 1/a^2$). In this domain, the terms related to the Hubble rate in equations 6.58 and 6.59 can be considered insignificant. During the later stages, the amplitude of the dilaton's oscillation and the physical wave number of each mode remain relatively consistent throughout each oscillation. Hence, by substituting the fading amplitude from Eq.6.155 for the constant ϕ_0, the Minkowski-space Floquet exponent may accurately represent the instantaneous growth rate in FLRW spacetime.

In order for the dilaton's energy to diminish and result in a significant proportion of dark

matter being composed of dark photons, it is imperative that parametric resonance operates with a high level of efficiency. For a significant duration, it is necessary for the exponential growth rate to far exceed the Hubble rate ($\mathrm{Re}(\mu)/H \gg 1$). Significantly, during the radiation-dominated epoch, the rate of expansion decreases at a quicker rate compared to the amplitude of the dilaton's oscillation, . Hence, the ratio between the exponential growth rate, and the expansion rate may be represented as

$$\frac{\mathrm{Re}[\mu(t)]}{H} = \frac{1}{8}\left(\frac{3\phi_{0,i}}{2M}\right)\left(\frac{a(t)}{a_i}\right)^{1/2}. \tag{6.158}$$

As the expansion of the Universe occurs, there is an observed increase in the effectiveness of resonance. In addition, it is observed that the comoving width of the instability band increases over time. The maximum value of this width is determined by the inequality $k^2 \leq \frac{\phi_{0,i}}{8M}\left(\frac{a}{a_i}\right)^{1/2}$ [derived from Eq 6.154. Furthermore, the lower bound can be determined by considering the horizon scale, namely the ratio of the scalar field mass to the scale factor ratio.

Eq. 6.156 implies that even with a small initial oscillation amplitude, as the Universe expands by a factor $\propto (\phi_{0,i}/M)^{-2}$, particle production becomes efficient. Specifically, the vector's production concludes shortly after its energy density matches that of the dilaton. the energy density of the dilaton is$\rho_\phi \approx m_\phi^2\phi_{0,i}^2/(a/a_i)^3$. The vector becomes nonrelativistic at the moment of production, as it is generated considerably later than a_i and possesses a comoving wave number approximately equivalent to m_ϕ. The energy density can be approximated as

$$\rho_A(t) \approx \frac{m_{\gamma`}^2}{2(a/a_i)^3\overline{W}}\sum_\lambda \langle A_\lambda(t,x)^2\rangle.$$

where

$$\langle A_\lambda(t,x)^2\rangle = \int\left(d\ln k\frac{k^3}{2\pi^2}\langle|A_\lambda(t_i,k)|^2\rangle e^{2\int_{t_i}^t dt'\mathrm{Re}[\mu(t')]}\right). \tag{6.159}$$

Before production,A_λ is in the vacuum state, withA. Small-amplitude broad resonance

$$\langle|A_\lambda(t_i,k)|^2\rangle = \frac{1}{2\sqrt{(k/a)^2+m_{\gamma 0}^2}.}. \tag{6.160}$$

If we set the growth rate and assume the integral over wave number is populated by modes

with $k \sim m_\phi$, and acknowledge that $\overline{W} \approx 1$ at longer times, we get

$$\rho_A(t) \approx \frac{m_{\gamma'}^2 m_\phi^2}{(a/a_i)^3} \exp\left(\frac{3\phi_{0,i}}{4M}\left(\frac{a}{a_i}\right)^{1/2}\right). \tag{6.161}$$

.

When considering the dilaton and vector, they have nearly identical energy densities at a specific scale factor. We can represent this as:

$$\frac{a*}{a_i} = \left(\frac{3\phi_{0,i}}{4M}\right)^{-2} \ln\left(\frac{m_\phi^2 \phi_{0,i}^2}{m_{\gamma'}^2 m_\phi^2}\right)^2. \tag{6.162}$$

Given $\frac{\phi_{0,i}}{M} = 1$ and $m_{\gamma'} = 10^{-18}$ eV with $\phi_{0,i}$ aligned to the relic abundance of dark matter as mentioned .we find that $\frac{a*}{a_i}$ approx 7.1 $\times 10^4$. This value reduces by roughly a factor of 2.3 when $m_{\gamma'} = 10^{-6}$eV.

The validity of these conclusions is contingent upon the modes remaining inside the resonance region characterized by modest amplitudes. An instability has been reported in the case of small amplitude vectors, when the mass of the vector is precisely half that of the dilaton. Nevertheless, the phenomenon of resonance ceases prematurely in cases where the mass ratios are not properly aligned. Specifically, the $n = 1$ band needs a non-zero k width for a small enough value of $|q| \propto \frac{\phi_0}{M}$. To ensure low-momentum modes don't exit the instability area before resonance becomes effective, we deduce:

$$|\delta| < \frac{3\phi_{0,i}}{16M\left(\frac{a_*}{a_i}\right)^{3/2}} < 10^{-7}\left(\frac{\phi_{0,i}}{2M}\right)^4. \tag{6.163}$$

This is valid for mass values around $m_{\gamma'} \sim 10^{-18}$eV

There are other narrow-band resonances that can be observed when the mass ratio $m_{\gamma'}$ is somewhat smaller than $2m_\varphi$ or when the mass ratio is given by $nm_\varphi/2$. However, these resonances are placed at $K \neq 0$ values, unlike the low-momentum band with $n = 1$. Furthermore, the width of these resonances decreases as the amplitude of the dilaton decays. The phenomenon of redshifting of momenta in FLRW spacetime serves as a hindrance to the significant growth of any mode, hence preventing the depletion of the dilaton background's energy density in such scenarios.

6.6 Analysis of dark matter content

The objective is to investigate the various factors in order to identify specific scenarios in which dark photons are the sole constituents of dark matter. The generation of dark matter should occur prior to the point at which the scales of the cosmic microwave background (CMB) exhibit dynamic behavior, thereby suggesting that its emergence takes place during the early stages of the radiation-dominated epoch. When the dilaton initiates its oscillatory motion at a Hubble parameter approximately equal to the dilaton mass $H \approx m_\phi$, it retains a minuscule fraction of the overall energy content of the cosmos. Following a substantial transfer of energy from the dilaton to dark photons, an observable nonlinear trend is detected. To facilitate the examination , we make the assumption that a significant portion of the dilaton's energy is converted into DPs, hence limiting its impact on the overall dark matter composition. If dark photons possess nonrelativistic characteristics upon their initial formation, their present abundance can be mathematically represented as:

$$\frac{\Omega_{\gamma'} h^2}{0.12} \approx \left(\frac{m_{\gamma'}}{10^{-17}\text{eV}}\right)^{1/2} \left(\frac{\phi_{0,i}}{10^{16}\text{GeV}}\right)^2. \tag{6.164}$$

In this context, we consider the value of g_* to be 10.75, representing the effective amount of relativistic degrees of independence in the plasma during its creation phase.

The data of the (CMB) impose two additional constraints on the parameter space under consideration. To ensure the production of dark matter occurs prior to the re-entry of cosmic microwave background (CMB) scales into the horizon, a lower limit is established for the vector mass, namely when $m_{\gamma'} = \frac{m_\phi}{2}$. Considering the principle of entropy conservation and , the redshift of production, denoted as z_*, can be expressed $\frac{a_0}{a*} - 1$.

$$\frac{z_* + 1}{1.9 \times 10^5} = \left(\frac{\phi_{0,i}}{M}\right)^2 \left(\frac{m_{\gamma'}}{10^{-17}\text{eV}}\right)^{1/2}. \tag{6.165}$$

If the redshift of matter-radiation equality is about 3400, it is possible that dark photons with mass values less than or equal to $m_{\gamma'} \leq 10^{-17}\text{eV}$, might not have originated early enough if the ratio of the initial field value to the Planck mass is less than 1. However, it is possible to make adjustments for lighter masses by raising the amplitude, as the relationship between the initial phase $(\phi_{0,i})$ and the mass (M) may be expressed as $\frac{\phi_{0,i}}{M} \propto m_\gamma^{-1/4}$.

Furthermore, within the framework of this particular model, it is observed that the VEV

of the dilaton is generated as a consequence of quantum fluctuations occurring during the process of inflation. The emergence of an isocurvature perturbation occurs after the decay of DP, as the value of $\phi_{0,i}$ fluctuates across disconnected Hubble patches. The power equation utilized to describe the perturbation arising from inflation is given by $P_S = \frac{H_I^2}{(\pi\phi_{0,i})^2}$, and H_I represents the Hubble scale during inflation. Under the assumption that the energy density of the photon field $(\Omega_{\gamma'})$ is equal to the energy density of dark matter (Ω_{DM}), the limits imposed by the (CMB) on isocurvature perturbations impose a restriction on the Hubble scale of inflation.

$$H_I < 3 \times 10^{11}\text{GeV}\left(\frac{m_{\gamma'}}{10^{-17}\text{eV}}\right)^{-1/4}. \tag{6.166}$$

6.7 Discussions and conclusions

A distinctive decay mechanism has been identified in a large vector field that is dynamically connected to an oscillating scalar field. In addition to the commonly observed strong-coupling phenomenon in axion-dark photon models, the presence of an oscillating dilaton with a mass twice that of its corresponding dark photon can result in significant vector generation, even in cases where the amplitudes of the oscillations are minor. This method allows for the synthesis of DPDM across a wide range of masses, without requiring significant couplings. However, in order to achieve ideal parametric resonance in circumstances with low coupling, it is necessary to have a certain mass ratio of $m_{\gamma'}/m_{\varphi} = 1/2$. The inquiry arises over the fundamental ultraviolet (UV) model that could provide an explanation for the masses of both the dark photon and dilaton.

In the preceding section, we examined the implications of adhering to cosmic microwave background (CMB) data, which imposes constraints on the mass of vectors and the intensity of their couplings. It is noteworthy that the achievement of remarkably low masses in the range of $10^{-20}to10^{-18}$ eV requires relatively modest couplings. To obtain a thorough evaluation of the relic abundance of dark photons and dilatons, it is necessary to conduct complex computational simulations in a $3+1D$ framework, taking into account factors such as particle mass and starting field amplitude. The simulations conducted initially are consistent with the estimations presented in previous sections; however, a comprehensive investigation of the topic still has to be undertaken in future research.

The rapid advancement of vector modes, along with the non-linear dynamics observed during the closing of production, may potentially give rise to a gravitational wave background. This could provide an opportunity to thoroughly examine and evaluate the aforementioned model. While achieving accurate predictions would require a rigorous quantitative analysis, it is plausible that anticipated signals could resemble those generated by resonantly produced dark photons originating from a developing axion. However, it is worth noting that the amplitude of these signals may not be significantly high. The limitations of stochastic backgrounds are primarily determined by the energy composition of the cosmos and the relative scale of gravitational-wave wavelengths at the time of their emergence. In the model under consideration, it is shown that both the vector and dilaton exhibit characteristics of being heavy relics. The relative abundance of these particles is found to be influenced by the ratio of scale factors during their formation, as well as the shift from radiation to matter dominance. It is conceivable that the extended duration between the initiation of oscillation and the onset of the production phase could enhance the detectability of signals. However, the intricacies of gravitational dynamics indicate a contrasting perspective. The topic of discussion pertains to wave emission and the considerations related to modeling.

The emission of waves is consistently observed at comoving scales that are about comparable to m_{φ}. The scales in question are influenced by the factor of a/a_i, which results in a greater level of inclusion inside the horizon during the production phase. Interestingly, there is a delicate equilibrium between these two phenomena, indicating that the generation of gravitational waves, even if highly efficient, may not exceed the presently measured levels, which are estimated to be approximately $\Omega_{GW}, 0 \approx 10^{-15}$, as shown in previous research[68].

Although the precise source of the dark photon's mass remains undetermined, the potential association of this mass with the Higgs process raises concerns regarding the feasibility of DPDM due to the emergence of vortex patterns during its synthesis. Furthermore, as indicated by prior scholarly investigations[69], it has been observed that Stueckelberg masses within the domain of string theory exhibit a minimum threshold, implying that any mass below this threshold could potentially arise as a consequence of the Higgs mechanism. The imposition of vortex formation limitations appears to have a significant influence on the majority, if not all, suggested methods for the generation of ultralight DPDM. However, the small magnitude that have been illuminated could potentially circumvent these limitations.

The notable disparity between dilaton oscillations and the generation of dark photons may serve to maintain the energy density of the vector below the crucial threshold required for the development of vortices. Further investigation into the variations in vortex formation limits, as influenced by different parameters, and the consequences of interactions with the photon of the Standard Model and consequent affects on plasma, will be explored in forthcoming studies.

During the course of our deliberations, it has been proceeded on the premise that the mass of the DP remains independent of the variable φ. The aforementioned relationship, in conjunction with the kinetic coupling denoted as $W(\varphi)$, is influenced by the principles of higher-level physics, namely those pertaining to ultraviolet (UV) phenomena. Although this work does not delve into an in-depth analysis of a UV-centric theory,It is plausible that the respective kinetic & mass terms may be influenced by the variable φ, possibly due to phenomena such as radiative corrections. In order to provide more clarification, it should be noted that resonance at small amplitude remains present even when the coupling function $W(\varphi)$ alters the mass term rather than the kinetic term of the vector, as the dynamic equation components of both terms are equivalent. Interactions of this kind, in conjunction with dark photon self-interactions, have the potential to impact the efficiency of DP generation and the parameters governing DPDM. Subsequent examination of these intricacies will be undertaken in forthcoming research endeavors.

Bibliography

[1] Michael Klasen, Martin Pohl, and Günter Sigl. Indirect and direct search for dark matter. *Progress in Particle and Nuclear Physics*, 85:1–32, 2015.

[2] R Agnese, Alan J Anderson, M Asai, D Balakishiyeva, R Basu Thakur, DA Bauer, J Beaty, J Billard, A Borgland, MA Bowles, et al. Search for low-mass weakly interacting massive particles with supercdms. *Physical review letters*, 112(24):241302, 2014.

[3] D Antypas, A Banerjee, C Bartram, M Baryakhtar, J Betz, JJ Bollinger, C Boutan, D Bowring, D Budker, D Carney, et al. New horizons: scalar and vector ultralight dark matter. *arXiv preprint arXiv:2203.14915*, 2022.

[4] Howard Baer, Ki-Young Choi, Jihn E Kim, and Leszek Roszkowski. Dark matter production in the early universe: beyond the thermal wimp paradigm. *Physics Reports*, 555:1–60, 2015.

[5] Joerg Jaeckel, Mike Lamont, and Claude Vallée. The quest for new physics with the physics beyond colliders programme. *Nature Physics*, 16(4):393–401, 2020.

[6] Tony Gherghetta and Benedict Von Harling. A warped model of dark matter. *Journal of High Energy Physics*, 2010(4):1–25, 2010.

[7] Ernst Öpik. Selective absorption of light in space, and the dynamics of the universe. *Bull. de la Soc. Astr. de Russie*, 21(150):5, 1915.

[8] Fritz Zwicky. Die rotverschiebung von extragalaktischen nebeln. *Helvetica Physica Acta, Vol. 6, p. 110-127*, 6:110–127, 1933.

[9] Vera C Rubin and W Kent Ford Jr. Rotation of the andromeda nebula from a spectroscopic survey of emission regions. *Astrophysical Journal, vol. 159, p. 379*, 159:379, 1970.

[10] Douglas Clowe, Maruša Bradač, Anthony H Gonzalez, Maxim Markevitch, Scott W Randall, Christine Jones, and Dennis Zaritsky. A direct empirical proof of the existence of dark matter. *The Astrophysical Journal*, 648(2):L109, 2006.

[11] George R Blumenthal, SM Faber, Joel R Primack, and Martin J Rees. Formation of galaxies and large-scale structure with cold dark matter. *Nature*, 311(5986):517–525, 1984.

[12] Daniel Baumann, Horng Sheng Chia, and Rafael A Porto. Probing ultralight bosons with binary black holes. *Physical Review D*, 99(4):044001, 2019.

[13] Hector Masia-Roig, Nataniel L Figueroa, Ariday Bordon, Joseph A Smiga, Yevgeny V Stadnik, Dmitry Budker, Gary P Centers, Alexander V Gramolin, Paul S Hamilton, Sami Khamis, et al. Intensity interferometry for ultralight bosonic dark matter detection. *Physical Review D*, 108(1):015003, 2023.

[14] Shuailiang Ge, Kyle Lawson, and Ariel Zhitnitsky. Axion quark nugget dark matter model: size distribution and survival pattern. *Physical Review D*, 99(11):116017, 2019.

[15] Dmitry Budker, Peter W Graham, Micah Ledbetter, Surjeet Rajendran, and Alexander O Sushkov. Proposal for a cosmic axion spin precession experiment (casper). *Physical Review X*, 4(2):021030, 2014.

[16] MS Safronova, D Budker, D DeMille, Derek F Jackson Kimball, A Derevianko, and Charles W Clark. Search for new physics with atoms and molecules. *Reviews of Modern Physics*, 90(2):025008, 2018.

[17] Paul Langacker. The physics of heavy zâ$^2 gaugebosons$. *Reviews of Modern Physics*, 81(3):1199, 2009.

[18] Maxim Pospelov, Adam Ritz, and Mikhail Voloshin. Bosonic super-wimps as kev-scale dark matter. *Physical Review D*, 78(11):115012, 2008.

[19] Ann E Nelson and Jakub Scholtz. Dark light, dark matter, and the misalignment mechanism. *Physical Review D*, 84(10):103501, 2011.

[20] Nick E Mavromatos and Joan Sola Peracaula. Stringy-running-vacuum-model inflation: from primordial gravitational waves and stiff axion matter to dynamical dark energy. *The European Physical Journal Special Topics*, 230(9):2077–2110, 2021.

[21] Charles R. Harris and et al. Array programming with NumPy. *Nature*, 585(7825):357–362, 2020. DOI: 10.1038/s41586-020-2649-2. URL: https://doi.org/10.1038%2Fs41586-020-2649-2.

[22] Ellert van der Velden. CMasher: scientific colormaps for making accessible, informative and 'cmashing' plots. *Journal of Open Source Software*, 5(46):2004, 2020. DOI: 10.21105/joss.02004. URL: https://doi.org/10.21105%2Fjoss.02004.

[23] Bernard Carr, Florian Kühnel, and Marit Sandstad. Primordial black holes as dark matter. *Physical Review D*, 94(8):083504, 2016.

[24] Lars Bergström. Dark matter candidates. *New Journal of Physics*, 11(10):105006, 2009.

[25] Richard Hammond. *The Unknown Universe: The Origin of the Universe, Quantum Gravity, Wormholes, and Other Things Science Still Can't Explain*. Red Wheel/Weiser, 2008.

[26] Robert H Sanders and Stacy S McGaugh. Modified newtonian dynamics as an alternative to dark matter. *Annual Review of Astronomy and Astrophysics*, 40(1):263–317, 2002.

[27] Tom Lancaster and Stephen J Blundell. *Quantum field theory for the gifted amateur*. OUP Oxford, 2014.

[28] Anthony Zee. *Quantum field theory in a nutshell*, volume 7. Princeton university press, 2010.

[29] Georges Aad, Tatevik Abajyan, Brad Abbott, Jalal Abdallah, S Abdel Khalek, Rosemarie Aben, B Abi, M Abolins, OS AbouZeid, H Abramowicz, et al. Evidence for the spin-0 nature of the higgs boson using atlas data. *Physics Letters B*, 726(1-3):120–144, 2013.

[30] Gennadi Sardanashvily. Noetherâs theorems. *Applications in mechanics and field theory*, 2016.

[31] Cliff Peter Burgess. Goldstone and pseudo-goldstone bosons in nuclear, particle and condensed-matter physics. *Physics Reports*, 330(4):193–261, 2000.

[32] Akash Kumar Saha, Priyank Parashari, Tarak Nath Maity, Abhishek Dubey, Subhadip Bouri, and Ranjan Laha. Bounds on ultralight bosons from the event horizon telescope observation of sgr a

* . *arXiv preprint arXiv:2208.03530*, 2022.

[33] Alexander B Balakin, Vladimir V Bochkarev, and Nadezhda O Tarasova. Gradient models of the axion–photon coupling. *The European Physical Journal C*, 72:1–14, 2012.

[34] Pierre Sikivie. Experimental tests of the" invisible" axion. *Physical Review Letters*, 51(16):1415, 1983.

[35] Jonathan Ouellet and Zachary Bogorad. Solutions to axion electrodynamics in various geometries. *Physical Review D*, 99(5):055010, 2019.

[36] Pierre Fayet. U (1) a symmetry in two-doublet models, u bosons or light scalars, and ψ and Υ decays. *Physics Letters B*, 675(2):267–271, 2009.

[37] Aaron Pierce, Zhengkang Zhang, Yue Zhao, et al. Dark photon dark matter produced by axion oscillations. *Physical Review D*, 99(7):075002, 2019.

[38] Haipeng An, Shuailiang Ge, Wen-Qing Guo, Xiaoyuan Huang, Jia Liu, and Zhiyao Lu. Direct detection of dark photon dark matter using radio telescopes. *arXiv preprint arXiv:2207.05767*, 2022.

[39] William E East and Junwu Huang. Dark photon vortex formation and dynamics. *Journal of High Energy Physics*, 2022(12):1–44, 2022.

[40] Naoya Kitajima and Kazunori Nakayama. Nanohertz gravitational waves from cosmic strings and dark photon dark matter. *arXiv preprint arXiv:2306.17390*, 2023.

[41] Salvatore Capozziello and Mariafelicia De Laurentis. Extended theories of gravity. *Physics Reports*, 509(4-5):167–321, 2011.

[42] Edward Witten. Search for a realistic kaluza-klein theory. *Nuclear Physics B*, 186(3):412–428, 1981.

[43] Daniel Z Freedman and Antoine Van Proeyen. *Supergravity*. Cambridge university press, 2012.

[44] Derek F Jackson Kimball, Leanne D Duffy, and David JE Marsh. Ultralight bosonic dark matter theory. In *The Search for Ultralight Bosonic Dark Matter*, pages 31–72. Springer International Publishing Cham, 2022.

[45] Edward W Kolb and Michael S Turner. The early universe. *Nature*, 294(5841):521–526, 1981.

[46] John Preskill, Mark B Wise, and Frank Wilczek. Cosmology of the invisible axion. *Physics Letters B*, 120(1-3):127–132, 1983.

[47] Pieter G Van Dokkum, Marijn Franx, Mariska Kriek, Bradford Holden, Garth D Illingworth, Daniel Magee, Rychard Bouwens, Danilo Marchesini, Ryan Quadri, Greg Rudnick, et al. Confirmation of the remarkable compactness of massive quiescent galaxies at z$\tilde{2}$.3: early-type galaxies did not form in a simple monolithic collapse. *The Astrophysical Journal*, 677(1):L5, 2008.

[48] Yuichiro Nakai, Ryo Namba, and Ziwei Wang. Light dark photon dark matter from inflation. *Journal of High Energy Physics*, 2020(12):1–20, 2020.

[49] Wayne Hu, Rennan Barkana, and Andrei Gruzinov. Fuzzy cold dark matter: the wave properties of ultralight particles. *Phys. Rev. Lett.*, 85:1158–1161, 6, 2000. DOI: 10.1103/PhysRevLett.85.1158. URL: https://link.aps.org/doi/10.1103/PhysRevLett.85.1158.

[50] Hsi-Yu Schive, Tzihong Chiueh, and Tom Broadhurst. Cosmic structure as the quantum interference of a coherent dark wave. *Nature Physics*, 10(7):496–499, 2014. DOI: 10.1038/nphys2996. URL: https://doi.org/10.1038%2Fnphys2996.

[51] Peter Adshead and Kaloian D. Lozanov. Self-gravitating vector dark matter. *Phys. Rev. D*, 103:103501, 10, 2021. DOI: 10.1103/PhysRevD.103.103501. URL: https://link.aps.org/doi/10.1103/PhysRevD.103.103501.

[52] Mudit Jain and Mustafa A. Amin. Polarized solitons in higher-spin wave dark matter. *Phys. Rev. D*, 105:056019, 5, 2022. DOI: 10.1103/PhysRevD.105.056019. URL: https://link.aps.org/doi/10.1103/PhysRevD.105.056019.

[53] Hong-Yi Zhang, Mudit Jain, and Mustafa A. Amin. Polarized vector oscillons. *Phys. Rev. D*, 105:096037, 9, 2022. DOI: 10.1103/PhysRevD.105.096037. URL: https://link.aps.org/doi/10.1103/PhysRevD.105.096037.

[54] Marco Gorghetto, Edward Hardy, John March-Russell, Ningqiang Song, and Stephen M. West. Dark photon stars: formation and role as dark matter substructure. *Journal of Cosmology and Astroparticle Physics*, 2022(08):018, 2022. DOI: 10.1088/1475-7516/2022/08/018. URL: https://doi.org/10.1088%2F1475-7516%2F2022%2F08%2F018.

[55] Neal Dalal and Andrey Kravtsov. Excluding fuzzy dark matter with sizes and stellar kinematics of ultrafaint dwarf galaxies. *Phys. Rev. D*, 106:063517, 6, 2022. DOI: 10.1103/PhysRevD.106.063517. URL: https://link.aps.org/doi/10.1103/PhysRevD.106.063517.

[56] Mustafa A. Amin and Mehrdad Mirbabayi. A lower bound on dark matter mass, 2022. arXiv: 2211.09775 [hep-ph].

[57] Asimina Arvanitaki, Savas Dimopoulos, Sergei Dubovsky, Nemanja Kaloper, and John March-Russell. String axiverse. *Phys. Rev. D*, 81:123530, 12, 2010. DOI: 10.1103/PhysRevD.81.123530. URL: https://link.aps.org/doi/10.1103/PhysRevD.81.123530.

[58] Masha Baryakhtar, Robert Lasenby, and Mae Teo. Black hole superradiance signatures of ultralight vectors. *Phys. Rev. D*, 96:035019, 3, 2017. DOI: 10.1103/PhysRevD.96.035019. URL: https://link.aps.org/doi/10.1103/PhysRevD.96.035019.

[59] Ann E. Nelson and Jakub Scholtz. Dark light, dark matter, and the misalignment mechanism. *Phys. Rev. D*, 84:103501, 10, 2011. DOI: 10.1103/PhysRevD.84.103501. URL: https://link.aps.org/doi/10.1103/PhysRevD.84.103501.

[60] Fatemeh Elahi and Sara Khatibi. Light and feebly interacting non-abelian vector dark matter produced through vector misalignment. *Physics Letters B*, 843:138050, 2023. DOI: 10.1016/j.physletb.2023.138050. URL: https://doi.org/10.1016%2Fj.physletb.2023.138050.

[61] Yohei Ema, Kazunori Nakayama, and Yong Tang. Production of purely gravitational dark matter: the case of fermion and vector boson. *Journal of High Energy Physics*, 2019(7), 2019. DOI: 10.1007/jhep07(2019)060. URL: https://doi.org/10.1007%2Fjhep07%282019%29060.

[62] Prateek Agrawal, Naoya Kitajima, Matthew Reece, Toyokazu Sekiguchi, and Fuminobu Takahashi. Relic abundance of dark photon dark matter. *Physics Letters B*, 801:135136, 2020. DOI: 10.1016/j.physletb.2019.135136. URL: https://doi.org/10.1016%2Fj.physletb.2019.135136.

[63] Jeff A. Dror, Keisuke Harigaya, and Vijay Narayan. Parametric resonance production of ultralight vector dark matter. *Phys. Rev. D*, 99:035036, 3, 2019. DOI: 10.1103/

PhysRevD.99.035036. URL: https://link.aps.org/doi/10.1103/PhysRevD.99.035036.

[64] Yuichiro Nakai, Ryo Namba, and Ziwei Wang. Light dark photon dark matter from inflation. *Journal of High Energy Physics*, 2020(12), 2020. DOI: 10.1007/jhep12(2020)170. URL: https://doi.org/10.1007%2Fjhep12%282020%29170.

[65] Yuichiro Nakai, Ryo Namba, and Ippei Obata. Peaky production of light dark photon dark matter, 2022. arXiv: 2212.11516 [hep-ph].

[66] Peter Adshead, Kaloian D Lozanov, and Zachary J Weiner. Dark photon dark matter from an oscillating dilaton. *Physical Review D*, 107(8):083519, 2023.

[67] Mustafa A. Amin, Mark P. Hertzberg, David I. Kaiser, and Johanna Karouby. Nonperturbative dynamics of reheating after inflation: a review. *International Journal of Modern Physics D*, 24(01):1530003, 2014. DOI: 10.1142/s0218271815300037. URL: https://doi.org/10.1142%2Fs0218271815300037.

[68] David Cyncynates, Olivier Simon, Jedidiah O. Thompson, and Zachary J. Weiner. Nonperturbative structure in coupled axion sectors and implications for direct detection. *Phys. Rev. D*, 106:083503, 8, 2022. DOI: 10.1103/PhysRevD.106.083503. URL: https://link.aps.org/doi/10.1103/PhysRevD.106.083503.

[69] Mark Goodsell, Joerg Jaeckel, Javier Redondo, and Andreas Ringwald. Naturally light hidden photons in LARGE volume string compactifications. *Journal of High Energy Physics*, 2009(11):027–027, 2009. DOI: 10.1088/1126-6708/2009/11/027. URL: https://doi.org/10.1088%2F1126-6708%2F2009%2F11%2F027.